THESIS FOR THE DEGREE OF DOCTOR OF PHILOSOPHY (PHD)

Accessibility of DNA in chromatin: The role of constrained superhelicity

by Rosevalentine Bosire (M.Sc.)

UNIVERSITY OF DEBRECEN

DOCTORAL SCHOOL OF MOLECULAR CELL AND IMMUNE BIOLOGY

DEBRECEN, 2021

THESIS FOR THE DEGREE OF DOCTOR OF PHILOSOPHY (PHD)

Accessibility of DNA in chromatin: The role of constrained superhelicity

by Rosevalentine Bosire (M.Sc.)

Supervisor: Prof. Gábor Szabó, M.D., Ph.D., D.Sc.

UNIVERSITY OF DEBRECEN

DOCTORAL SCHOOL OF MOLECULAR CELL AND IMMUNE BIOLOGY

DEBRECEN, 2021

TABLE OF CONTENTS

LIST OF FIGURES

LIST OF ABBREVIATIONS

ATAC-seq:	Assay for transposase-accessible chromatin with sequencing
BME:	beta mercaptoethanol
bTMP:	biotynilated 4,5,8-trimethyl psoralen
CCC:	Covalently closed circular
CHEF:	Contour-clamped Homogenous Electric Field electrophoresis
ChIP:	Chromatin immunoprecipitation
DAPI:	4′,6-diamidino-2-phenylindole
DHS:	DNase I hypersensitive sites
DNase I:	Deoxyribonuclease I
DNase-seq:	DNase I hypersensitive sites sequencing
Dox:	Doxorubicin
dsRNA:	Double stranded ribonucleic acid
EBr:	Ethidium bromide
FACT:	FAcilitates Chromatin Transcription
FAIRE-seq:	Formaldehyde-assisted isolation of regulatory elements with sequencing
FCS:	Fluorescence correlation spectroscopy
FLIM:	Fluorescence lifetime imaging
FRAP:	Fluorescence recovery after photobleaching
GTF:	General transcription factor
HMGB1:	High mobility group box protein 1
HPBMCs:	HeLa and human peripheral blood mononuclear cells
LMP:	Low melting point
LSC:	Laser scanning cytometer
MNase-seq:	Micrococcal nuclease digestion with deep sequencing
NCP:	Nucleosome core particle
NFRs:	Nucleosome free regions
NGS:	Next generation sequencing
NHSs:	Nuclease hypersensitivity sites
PBM:	Protein binding microarray
PBS-EDTA:	Phosphate buffered saline with 5 mM EDTA

PTMs:	Posttranslational modifications
PWM:	Position weight matrices
RCS:	Remodeling the Structure of Chromatin
RNAP II:	RNA polymerase II
RNase A:	Ribonuclease A
RT:	Room temperature
rRNA:	Ribosomal RNA
SELEX:	Systematic evolution of ligands by exponential enrichment
SHL:	Superhelix location
Sox:	SRY-related HMG-box
SLO:	Streptolysin O
TAD:	Topologically associated domain
TBP:	TATA-box binding protein
TCF/LEF:	T-cell factor/lymphoid enhancer factor
TF:	Transcription factor
TFAM:	Mitochondrial transcription factor A
TFBM:	Transcription factor binding motifs
Tx-100:	Triton x-100
WAPL:	Wings apart-like
yNHP6A:	yeast non-histone chromosomal protein 6A

1. INTRODUCTION

1.1 ACCESSIBILITY AND TRANSCRIPTIONAL REGULATION

Regulation of gene transcription is important for cell differentiation and for maintaining cell-type specific phenotypes, and its disorders often lead to disease [1]. Transcription factors (TFs) recognize and bind to specific regulatory sequences in the genome to either activate or repress particular genes, in particular cells, at particular times [2]. In eukaryotes, activation of protein coding genes begins by recognition and binding of the general transcription factor (GTF) TFIID to the core promoter element and sequential recruitment of RNA polymerase II (RNAP II) and other GTFs [3]. Together, the GTFs and RNAP II form the pre-initiation complex (PIC) which unwinds about 12-14 bp of DNA (promoter melting) and loads the template strand into the active site of the RNAP II so as to begin transcription [4]. Although the GTFs and RNAP II suffice to initiate basal transcription, the binding of sequence-specific TFs to promoter-proximal and distal regulatory elements called enhancers helps to modulate the level of transcription [5].

Recognition and binding of regulatory factors to their cognate sites is preceded by access. In the cell, transcription takes place in the context of chromatin, of which ~70 % is bound by nucleosomes with the rest being made up of internucleosomal linker DNA and nucleosome free regions (NFR). The NFRs are defined as stretches of about 200 bp of DNA to which a nucleosome is not bound or is occupied by easily destabilized nucleosomes, what make up about 1% of the genome [6]. Whereas nucleosomes are refractory to factor binding, NFRs present "open windows" through which trans-acting factors can access their binding sites in chromatin [6]. NFRs exhibit a 100-fold higher sensitivity to nuclease cleavage than the rest of chromatin and are thus termed nuclease hypersensitivity sites (NHSs) [6]. All NHSs determined so far correspond to regulatory elements such as enhancers, promoters, insulators, silencers and locus control regions [6–8]. Consequently, nuclease hypersensitivity assays have been traditionally used to probe regulatory sequences in chromatin. Initially they were used together with Southern blotting hybridization [9,10], a low through-put method to identify regulatory regions in a given locus. Later they were used with tiled microarrays [11–13] and more recently next generation sequencing (NGS) that has enabled the mapping of accessible sites genome-wide with single

base-pair resolution. The commonly used genome wide accessibility assays based on nuclease hypersensitivity and their drawbacks are discussed below.

1.1.1 DNA accessibility assays

1.1.1.1 DNase I hypersensitive sites sequencing (DNase-seq)

DNase-seq (Fig.1a) relies on the use of deoxyribonuclease I (DNase I) coupled with sequencing to map regulatory sequences genome wide. The 30 kDa sequence-nonspecific endonuclease preferentially binds nucleosome free DNA in the minor groove and nicks the phosphate backbone in the presence of divalent cations Ca^{2+} and Mg^{2+} [14]. In the presence of transition metals such as manganese and cobalt, DNase I cleaves both strands at the same point or in close proximity resulting in DNA double strand breaks [15]. To determine DNase hypersensitive sites (DHS), isolated nuclei are digested with limiting DNase I concentration to preferentially cut at DHSs. In a typical experiment, cell nuclei are digested with a range of DNase I concentrations and the DNA fragments generated are separated on a gel to determine the fragment size. The DNase I concentration to cell number ratio has to be determined for each cell type and batch of DNase I [16]. Typically for mammalian cells 0.4-4 U/ $7x10^6$ nuclei generates fragments ranging from 50-1000 kb which are suitable for DNase-seq. 12 U/ $7x10^6$ nuclei generates fragment <50 kb while 40 U/ $7x10^6$ nuclei completely degrades the genome [17,18]. The ends of the generated fragments are then purified and identified by next-generation sequencing. Sites accessible in a large proportion of cells in a population are cleaved more often and appear as a peak of the sequenced reads. Sequencing reads from more than one DNase I concentration can further identify sites with varying degrees of hypersensitivity.

A major drawback of this technique is that, though DNase I cleavage is not sequence-specific, the enzyme exhibits an intrinsic sequence bias [19]. Cleavage rate has been shown to be significantly enhanced by a narrowed minor groove adjacent to the cleavage site [20] and by sequence dependent flexibility [21] facilitating its binding.

An alternative to DNase-seq is FAIRE-seq (formaldehyde-assisted isolation of regulatory elements with sequencing) which instead of digesting DNA, uses sonication to fragment formaldehyde crosslinked chromatin (Fig. 1b). Following sonication, DNA is isolated by phenol-chloroform extraction such that DNA not crosslinked to histone partitions into the

aqueous phase and the heavily crosslinked protein-DNA complexes remain in the organic phase. Sequencing reveals the map of accessible DNA [22]. A major drawback of this technique is that regulatory regions occupied by proteins such as TFs are also crosslinked and eliminated from reads. Hence this method is not widely used recently.

1.1.1.2 Micrococcal nuclease digestion with deep sequencing (MNase-seq)

MNase-seq (Fig. 1c) employs the use of micrococcal nuclease (MNase), a *Staphylococcus aureus* enzyme with both endonuclease and exonuclease activity. MNase preferentially cleaves linker DNA and processively digests the generated DNA ends when it doesn't disengage from the DNA in the course of its exonuclease activity. Prolonged digestion results in progressively shorter fragments and may lead to digestion of nucleosomal DNA too [23]. Subjecting the nucleosome protected fragments to high through-put sequencing gives an indication of the positions of nucleosomes in the given locus. Though all segments of DNA devoid of nucleosomes are susceptible to MNase, differential accessibility of the MNase-sensitive regions genome-wide can be deduced from a controlled titration of enzyme concentration or limiting digestion times [23,24]. It has been experimentally shown that different nucleosomes are released from chromatin during a partial digest (low MNase cc. or short digestion time) and during more complete digest (high MNase cc. or extended digestion time). This is because certain non-histone protein complexes offer less protection to DNA compared to nucleosomes [25] and nucleosomes in complex with remodelers (e.g. RSC) are partially destabilized exposing the DNA to MNase activity [26]. These nucleosome-RSC complexes have been mapped to regulatory regions. However, one has to also take into account the sequence bias exhibited by MNase when analysing sequence results. MNase cleaves A/T rich sequences up to 30x faster compared to G/C rich sequences [24]. Consequentially, A/T-rich nucleosomes are also released during a partial digest though they may not represent accessible DNA. As an example, A/T rich nucleosomes have been mapped to transcription termination sites in yeast [25].

1.1.1.3 Assay for transposase-accessible chromatin with sequencing (ATAC-seq)

ATAC-seq (Fig. 1d) probes DNA accessibility using Tn5, a hyperactive transposase which in nature excises a transposon from one genomic location and inserts it to a new genomic location in a "cut and paste fashion" [27]. In ATAC-seq, the transposase which is pre-bound with an

adapter DNA, cuts genomic DNA and simultaneously ligates adapters for sequencing, a process called tagmentation [28]. Following DNA extraction and sequencing, bioinformatics tools are used to classify ATAC-seq reads. Two categories are generated; a) those whose size corresponds to the length of nucleosomal DNA revealing nucleosome occupied regions, and b) those whose length is shorter than that of a canonical nucleosome. This second group is considered to be NFRs where transcription factors can bind. A limitation of this technique is that its reads are often contaminated with mitochondrial DNA.

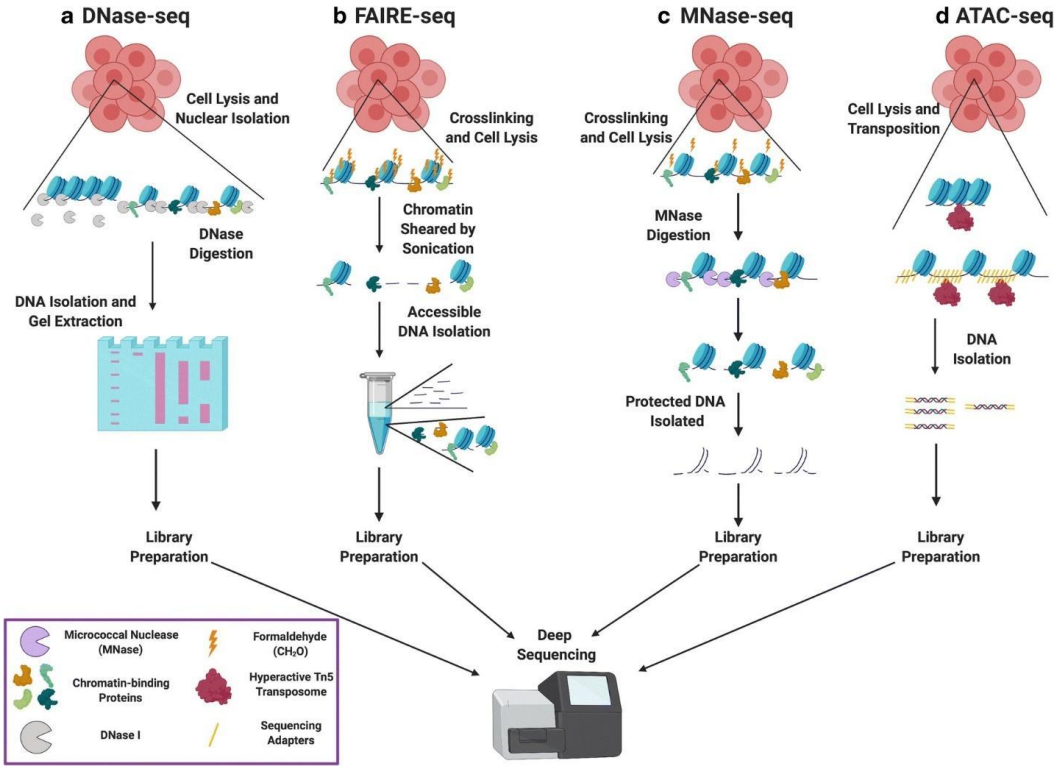

Figure 1: General outline of commonly used DNA accessibility assays. Figure reproduced from [29].

DNase-seq, FAIRE-seq, MNase-seq and ATAC-seq assays discussed above all rely on two principles; 1) that DNA sequences bound by protein are protected from digestion or resist sonication and 2) that the histones are the main molecular species in contact with DNA [29]. They thus provide a snapshot of the nucleosome occupancy and the accessible DNA genome-wide. This snapshot is a population average, since they use millions of cells and are only being adapted to single cell protocols recently. Nevertheless, there is a general overlap in the sequences identified as open across the assays.

The accessibility assays discussed above reveal accessible DNA on chromatin but do not characterize regulatory factor binding to these accessible sites. Characterization of protein-DNA interactions is instead achieved by ChIP assays, which are now also coupled to sequencing (ChIP-seq) for genome-wide characterization.

Chromatin immunoprecipitation (ChIP)-based techniques use antibodies raised against specific proteins to identify DNA sequences to which a particular protein of interest is bound *in vivo*. A typical experiment involves fixing cells with formaldehyde to crosslink proteins to DNA. The cells are then lysed and the chromatin sonicated to fragments of about 300-400 bp. A primary antibody which is immobilized on magnetic beads is then used to pull down a particular protein along with the DNA it is bound to. Extraction and sequencing of these DNA fragments then reveals where on the genome the particular protein binds to. This technique is applicable for all proteins to which ChIP-grade antibodies are available. Modifications to this technique, ChIP-exo [30] and ChIP-nexus [31] use exonucleases to digest the edges of the DNA fragments after sonication to further improve resolution.

More recently, protein binding characterization has also been investigated using CUT &RUN [32]. In this technique, an antibody to the protein of interest is used to tether MNase to particular loci *in situ*. Activation of MNase activity using Ca^{2+} causes the cleavage of DNA around where the MNase is tethered. This greatly increases the signal to noise ratio from sequencing results as only the cleaved chromatin fragments are released into solution while the rest remains in nuclei.

1.1.1.4 Microscopy-based techniques for studying DNA accessibility

In addition to the biochemical approaches discussed above, accessible DNA has also been studied by microscopy based techniques. The heterochromatin-euchromatin dichotomy discovered almost a century ago [33], was later to be interpreted in the context of transcriptional inactivity-activity determined by differential accessibility. A dense heterochromatin packaging would reduce the average pore of these nucleoprotein matrices hence limiting the size of proteins (including TFs) that can diffuse through it. Contrary to this notion, however, microscopy-based techniques tracking the distribution and/or mobility of fluorescent molecules found no differential access between heterochromatin and euchromatin regions to relatively large molecules. It was observed that a significant fraction of heterochromatin was accessible

even to 70 kDa fluorescent dextrans micro-injected into the nucleus of a live cell [34,35]. Similarly, eGFP oligomers up to 81 kDa [36] were shown to be equally distributed all over the nuclei except for the nucleoli. Grünwald and colleagues also observed that fluorescently labelled streptavidin microinjected into the nucleus rapidly diffused into the nucleus diffused through even heterochromatin unimpeded [37]. Though fluorescent microscopy resolution is limited to 250 nm, this and other similar observations show that gene-specific TFs which are about 50 kDa can easily access their promoters even in heterochromatin. Brownian motion [38] would then bring bound targets to the surface [39] allowing larger components of the transcription machinery to bind [40]. Binding of large transcription complexes to the exposed target sequences would then retain the segment on the domain surface where transcription occurs. Further, even heterochromatin is not static, single-nucleosome imaging reveals that even within heterochromatin fluctuations of about 50 nm/30 ms occur. This fluctuation would increase the actual pore sizes in heterochromatin or expose buried sequences to the surface to facilitate access of transcription complexes to their target DNA [39].

Enzymatic assays for DNA accessibility present the nucleosome as a physical barrier to TF binding. This is corroborated by biophysical studies which rule out dense packaging as a barrier. Except for pioneer TFs that can bind to nucleosomal DNA and recruit chromatin remodelers to open the chromatin [41], TFs generally bind to nucleosome free DNA. In agreement with this, the promoters of active genes are either nucleosome depleted or occupied by nucleosomes that are easily destabilized [42]. Considering that the DNA is wrapped around the nucleosome with at least 50% of its surface facing the outside, reduced accessibility to nucleosomal DNA cannot be fully explained by steric hindrance. This prompted us to look further for an explanation which may be found in the structural alteration chromatinized DNA undergoes as a consequence of packaging. I will next discuss the role DNA geometry plays in TF binding and specificity before looking into how the DNA geometry is altered during packaging into chromatin.

1.1.2 Transcription factor binding specificity

General and gene-specific TFs recognize and bind to specific DNA sequence motifs in the cis-regulatory elements through the establishment of hydrogen bonds between amino acids on the DNA binding domain of the TF and the DNA bases. The sequence motifs recognized by TFs are short, their length being about 6-10 bp, and exhibit great sequence degeneracy. Sequence

specificity for any particular TF can be determined by *in vitro* DNA binding assays. Traditionally, low throughput assays such as electrophoretic mobility shift assay, DNase I footprinting, surface plasmon resonance and southwestern blotting were used to characterize TF binding to distinct DNA sequences. Today, however, high throughput assays capable of characterizing binding to thousands of sequences in parallel are the methods of choice.

Two main high throughput techniques have been used to determine TF sequence specificity: protein binding microarray (PBM) assays and SELEX-based techniques. PBM assays quantify the binding of a TF to commercially synthesized, immobilized DNA sequences. The binding affinity to each of the sequences is directly inferred from the binding of a fluorescently labelled antibody [43]. SELEX-based techniques start with random DNA fragments and subject them to rounds of systematic enrichment for preferred sequences which are then subjected to sequencing. The sequences identified as high affinity by PBM assays and SELEX-based techniques are then subjected to computational algorithms to generate a sequence logo/sequence motif for a particular TF.

Sequence motifs are based on position weight matrices (PWM) and are a representation of the preference for a particular nucleotide at a particular position in a sequence motif. PWM assume that each nucleotide in a motif exerts an additive and independent effect to the recognition of the sequence. However, it is now apparent that, in certain cases, the presence of a particular nucleotide in one position determines the preferred nucleotide in another position. And this effect is more significant for adjacent nucleotides compared to nucleotides far apart.

The DNA structural features determined by the sequence of the motifs that play a role in TF binding specificity [44,45] are described below. To date a catalogue of 13 DNA structural features have been recognized to play a role in TF affinity and have been included in computational algorithms for TF binding motif prediction [46]. These include the shape of DNA grooves, DNA curvature and flexibility of DNA to bend or unwind. These are in turn dependent on the nucleotide sequence both within and in the regions flanking the motif. The effect of nucleotide sequence on DNA conformation is perhaps most evident in the DNA minor groove. Minor grooves with short A-tracts have a propensity to be narrow, with their width being < 5 Å compared to 5.8 Å of linear B-DNA. A narrowed minor groove reduces the distance between the phosphates on the backbone of both strands hence increasing the negative electrostatic

potential in the groove. DNA binding proteins with positively charged residues such as arginine and histidine on their surface are likely to be attracted to a narrowed minor groove [44].

1.1.3 Structural properties of DNA

The overall structure of DNA is described by the so-called translational & rotational parameters of its base pairs, the groove parameters and local helical parameters [47,48]. Three translational (shift, slide and rise) and three rotational (tilt, roll and helix twist) parameters are used to describe the position of one base pair relative to the next (Fig. 2C). Similarly, three translational (shear, stretch and stagger) and three rotational (buckle, opening and propeller twist) parameters are used to describe the position of one base relative to its partner in a base pair (Fig. 2D). It is important to note that the helix twist (HelT) between successive base pairs varies between 24º and 51º and is different from global Twist which is an average over the full helical turn of a DNA molecule and is about 34º for B-DNA [49]. These parameters are intrinsically dependent on the DNA sequence and have been experimentally determined using X-ray crystallography or computationally derived for various DNA sequences [48]. Importantly, these features are interdependent. For example untwisting DNA widens its grooves while decreasing the helical rise [50].

On the basis of the structural parameters DNA is classified as either A- or B- form. In nature, most DNA exists in the B-form, a right-handed helix of 10.5 bp per turn [49]. The base pairs are arranged almost perpendicularly to the helical axis, with a rise of 3.4 Å, an average helix twist of 34º and minor and major grooves of equal depth. Under high ionic conditions, the B-form DNA transitions to A-form which has characteristically deep major and shallow minor grooves. There are also several other alternative DNA conformations (Z-DNA, triple-triplexes, G-quadruplexes etc.) that are thought to have biological significance but have no direct relevance to the focus of this thesis and therefore are not discussed here.

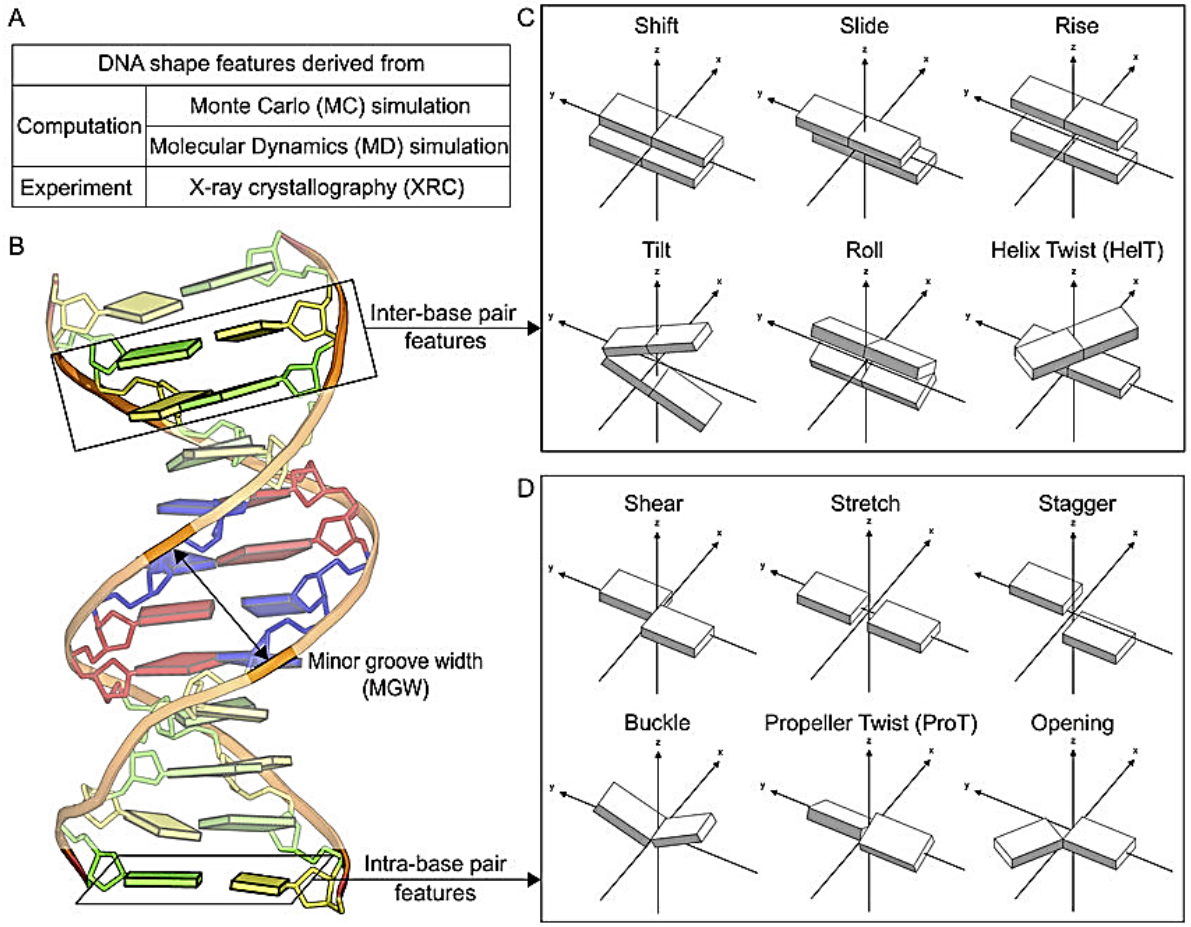

Figure 2: Translational and rotational parameters of DNA base pairs. A) The methods used to derive the parameters. B) Double stranded DNA molecule. C) Translational (shift, slide and rise) and rotational (tilt, roll and helix twist) parameters describing the degrees of freedom between two base pairs. D) Translational (shear, stretch and stagger) and rotational (buckle, propeller twist and opening) parameters describing the relative position of bases within a base pair. Figure reproduced from [46].

The structural parameters of DNA can be modulated by a number of factors including i) the binding of drugs such as DNA intercalators; ii) DNA supercoiling; iii) the binding of some structural proteins e.g. histones and structural proteins; and iv) DNA base mismatches. Pyrimidine-pyrimidine mismatches widen while purine-purine mismatches constrict the base pairs [51]. I will discuss the factors relevant to my research in the subsequent sections.

1.2 DNA INTERCALATORS

Small molecules that interact with DNA can either bind covalently (e.g. cisplatin binding to guanine) or non-covalently. The non-covalent interactions include binding to the phosphate backbone, the DNA grooves or reversible intercalation between base pairs [52]. Interactions that affect DNA processes have been exploited for therapeutic purposes.

Intercalating molecules possess a characteristic electron-deficient planar ring system termed chromophore, which inserts between adjacent DNA base pairs. While simple intercalators such as ethidium, propidium and proflavin consist of only the chromophore, other intercalators have in addition peptide groups or sugar moieties [53]. These additional groups non-covalently interact with bases in the DNA grooves and contribute to sequence specificity and the orientation of the bound ligand. Intercalation of the hydrophobic chromophores into DNA is energetically favoured since it removes the nonpolar ligand from the polar environment of water [54].

Studies on isolated DNA demonstrated that intercalation increase the distance between adjacent bases by 3.4 Å per mono-intercalator and 6.8 Å per bis-intercalator molecule, thus increasing the length of the DNA duplex. Further, intercalation causes unwinding of the DNA in the base pairs adjacent to the site of intercalation. The degree of unwinding is dependent on the nature of the intercalator. For example, EBr unwinds the DNA by 26° [55], YOYO-1 by ~ 24±8° [56] and anthracyclines by 11°. The local perturbation from intercalation however spreads along the DNA molecule.

Four DNA intercalators were used in the research described in this thesis. They are ethidium bromide and YOYO-1, both known as a useful DNA fluorescent probes, doxorubicin (Dox), a well-known antitumor antibiotic, and psoralen which is used in the treatment of some skin disorders. The structures of these molecules are shown below (Fig. 3).

Binding of ethidium anion and doxorubicin to naked DNA has been studied extensively [55,57–61]. The intercalation of ethidium is non-sequence specific. Following intercalation into dsDNA or dsRNA, ethidium absorbance is red-shifted and its fluorescence increases 20-fold most likely due to shielding from the water molecules [62]. The Dox chromophore preferentially intercalates between GC base pairs while the sugar moiety is positioned in the minor groove [61]. Upon

intercalation the Dox fluorescence is greatly quenched[63,64]. Whereas Dox readily enters live cells, ethidium has largely been considered cell impermeant.

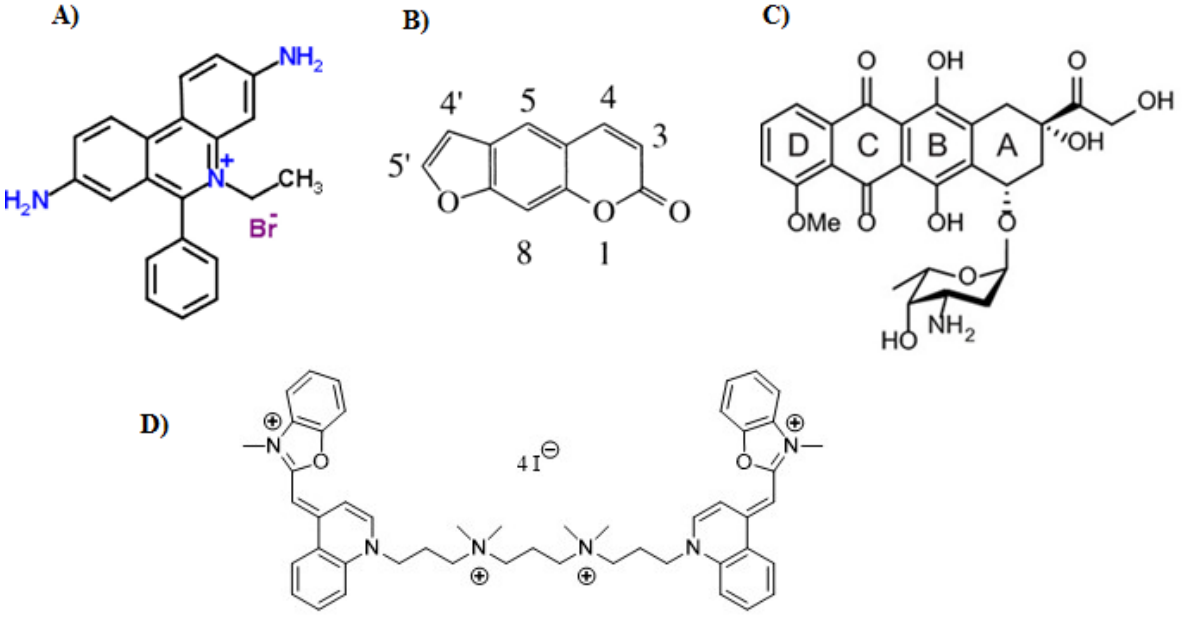

Figure 3: Intercalators: A) Ethidium bromide, **B)** Psoralen, **C)** Doxorubicin & **D)** YOYO-1.

YOYO-1, is a cell membrane impermeant molecule made up of two identical heterocyclic moieties connected by a linker. The length and flexibility of the linker allows both moieties to intercalate into DNA (bis-intercalation) [56]. Following intercalation its fluorescence undergoes > 1000-fold enhancement, a property that makes it suitable for single molecule studies.

Psoralen, a naturally occurring furanocoumarin has been shown to preferentially intercalate into negatively supercoiled DNA. When the intercalated molecule is exposed to UV, it forms covalent adducts with thymine [62], a property that has been exploited for medicinal purposes such as treatment of psoriasis [65] and cutaneous T cell lymphoma [66], as well as basic research into DNA damage and repair [67]. Psoralen absorbs in UV region and emits weak blue fluorescence. However, for laboratory use the psoralen is tagged with functional molecules such as biotin for easy detection.

In the subsequent section I will describe DNA supercoiling followed by a discussion of the superhelical properties of chromatinized DNA.

1.3 DNA SUPERCOILING AND CHROMATIN TOPOLOGY

1.3.1 DNA supercoiling

For linear B-DNA of length N base pairs, each strand winds about the other every 10.5 bp, this is its helical repeat length (*h*). If the ends of the linear molecule were ligated, a relaxed, covalently closed circular DNA molecule would be formed. For such a molecule, the DNA strands are permanently intertwined and can only be separated if one or both of the strands were cut and allowed to swivel about the other. The number of times one strand would have to rotate about the other in order to separate the two strands is referred to as the linking number (*Lk*) and it is always an integer as only opposite DNA ends (3' to 5') can be joined. The *Lk* for a relaxed molecule, i.e. one whose *h* =10.5 bp/turn, is denoted Lk_o. If the double helical linear molecule were first twisted around its axis before ligating its ends, its *Lk* would differ from its Lk_o, ($\Delta Lk = Lk - Lk_o$), and the molecule would be referred to as superhelical. The ΔLk would be positive if the DNA double helix is twisted in a right-handed direction (over-twisted), and negative if it is twisted in a left-handed direction (untwisted) before ligation. The extent to which ΔLk differs from the Lk_o, regardless of the size of the DNA molecule, is referred to as the superhelical density of a molecule (σ), $\sigma = \Delta Lk/Lk_o$.

The *Lk* is a geometrical parameter made up of two components; twist (*Tw*) and writhe (*Wr*), and changes in *Lk* are distributed between the two components, hence the formula $\Delta Lk = \Delta Tw + \Delta Wr$. *Tw* describes the number of times one DNA strand winds about the other in a duplex, while *Wr* is the number of times the duplex winds about its own axis. A relaxed covalently closed circular (CCC) DNA molecule has no writhe and therefore its *Lk* (Lk_o) is equal to the *Tw* and is directly derived from the formula N/*h*, *(*where N is the length of DNA bp and *h* is the helical repeat length in bp). *Wr* is a vector quantity of a positive sign if the helices cross each other in a left-handed direction or negative sign if the helices cross each other in a right-handed direction (Fig. 4). However, if the writhing occurs around an object such as a protein as is the case in nucleosomes, a left-handed turn is denoted a negative sign whereas a right-handed turn is denoted a positive sign. Writhes that form in space are referred to as plectonemes, whereas those occurring around an object are referred to as toroids.

In the following section, I will discuss DNA packaging into chromatin while highlighting how its structure deviates from that of B-DNA in solution.

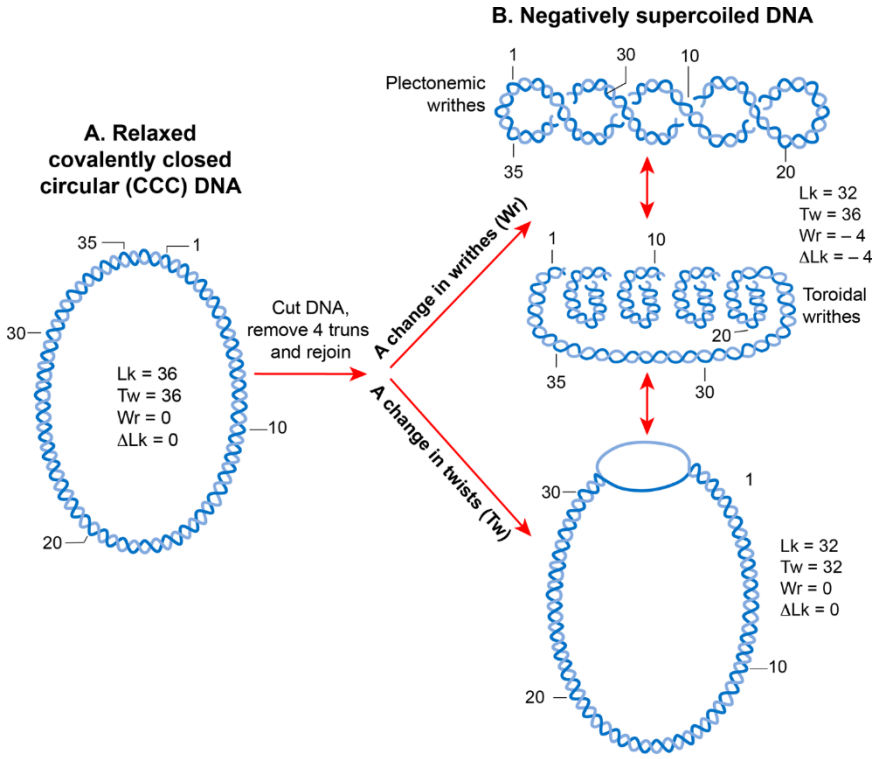

Figure 4: DNA supercoiling. A) A relaxed covalently closed circular DNA molecule formed by ligating the ends of a linear molecule (h=10.5 bp). **B**) The DNA in (A) was cut and four left handed turns were made about its axis before re-ligation to generate negative superhelical torsion which manifests as right handed plectonemic writhes (*top panel*) or left handed toroidal writhe (*middle panel*) or causes local strand separation (*bottom panel*). The double-head red arrows indicate that the molecules can interconvert between the three negatively superhelical states without nicking the DNA. Figure from [68].

1.3.2 DNA supercoiling at the nucleosomal level

The nucleosomal structure is the lowest level of eukaryotic DNA packaging. 145 to 147 bp of DNA is wrapped around a core histone octamer, forming nucleosome core particles (NCPs) which are interspersed with linker DNA. Linker DNA is bound by the linker histone H1 and the architectural proteins of the high mobility group. The DNA on each NCP makes 1.67 left-

handed superhelical turns around the histone octamer, an inner complete turn and two outer incomplete turns.

The ΔLk generated per nucleosome is determined by the seminal band counting technique developed by Keller [69]. In this technique, deproteinized, supercoiled plasmid DNA is relaxed using topoisomerase I in the presence of increasing amount of ethidium bromide (EBr) and the resulting covalently closed molecules are separated by gel electrophoresis after dye removal. Each sample yields a mixture of DNA molecules whose migration on the gel is dependent on the ΔLk of its constituent topoisomers, which is in turn dependent on the number of EBr molecules intercalated into the DNA molecule during relaxation. That is, when EBr binds to supercoiled CCC DNA, it causes the DNA to untwist and a compensatory positive writhe is formed ($\Delta Tw < 0$, $\Delta Wr > 0$). If the concentration of EBr in the solution is increased, more EBr molecules will intercalate into DNA and cause more untwisting. The positive writhe is relaxed by the topoisomerase. When EBr is removed, the DNA will again twist revealing the supercoils that were "trapped" by EBr ($\Delta Tw > 0$, $\Delta Wr < 0$). DNA molecules in consecutive bands in the same lane differ by $\Delta Lk = 1$, and molecules with equal ΔLk migrate together in the different lanes. Topoisomers on the same lane that co-migrate are further resolved by including EBr in the gels. By counting the overlapping bands between relaxed DNA samples and the untreated supercoiled control DNA under different electrophoresis conditions, the ΔLk of a given molecule can be determined. Using this technique, the ΔLk of the SV40 minichromosome was determined to be about -26 [69]. These translated to a ΔLk of about -1.0 per nucleosome since the SV40 minichromosome carries about 26 nucleosomes. Similarly, the ΔLk generated per nucleosome for reconstituted nucleosome arrays was determined to be about -1.0 [70].

The experimentally determined ΔLk per nucleosome ($\Delta Lk = -1.0$), however, differs from theoretically expected one ($\Delta Lk = -1.67$) owing to the 1.67 turns the DNA makes around the nucleosome, based on the X-ray crystallographic structure [71]. The difference between the theoretically expected and the experimentally measured ΔLk came to be known as the *Lk* paradox and has been the subject of much research. Two main hypotheses supported by experimental evidence, have been put forward to explain the *Lk* paradox. One hypothesis postulates that the DNA wrapped around the core nucleosome is over-twisted by about + 0.23 [72–74]. This is supported by the evidence from hydroxyl radical and DNase I footprinting

experiments that determined the helical repeat of nucleosomal DNA to be 10.2 bp compared to 10.5 for naked DNA [72,75]. This effectively increases the ΔLk per nucleosome to -1.44. The second hypothesis states that the length of the linker DNA determines its path which determines its contribution to the ΔLk. (The length of linker DNA occurring in nature was observed to be quantized and has been categorized as either 10n or 10n+5, where n is an integer. Thus 10n linkers are of a length in multiples of 10 bp, whereas the 10n+5 has multiples of 10 plus 5 bp). This is supported by recent modelling and experimental measurements involving positioned nucleosomes which found the ΔLk to range from – 0.8 to -1.4, with linkers of the 10n series constraining a higher ΔLk than linkers of the 10n + 5 series [76,77]. The 10n vs 10n +5 linker repeat length seem to correlate with the zigzag vs solenoid arrangement of nucleosomes in the 30 nm fibre determined *in vitro* and with the heterochromatic – euchromatic partitioning in cell [78,79]. Considering the experimental evidence supporting the two hypotheses, it is probable that the linking number paradox is only fully explained by taking into account both the twist changes in nucleosomal DNA as well as the contribution of the linker DNA length.

1.3.3 Constraint of DNA supercoiling by the nucleosome core particle

The altered structure discussed above is constrained on the histone octamer surface. I will briefly discuss the core octamer structure before highlighting the features of the DNA constraint. The histone octamer is formed of two of each of the core histones H2A, H2B, H3 and H4. Each of the core histones are composed of a structurally conserved motif named the histone-fold and unstructured positively charged N-terminal tails. In addition, each histone H2A has a C-terminal tail. Whereas the histone folds organize the 146 bp of DNA around the NCP, the histone tails interact with both nucleosomal & linker DNA [71,80]. The interactions between histone tails and the nucleosomal DNA, which are mainly governed by electrostatic interactions, contribute slightly to the thermal stability of mononucleosomes [81]. Tail removal was shown to mildly increase DNA unwrapping events in mononucleosomes which increased its access to other DNA-binding proteins [82]. The tails also project beyond the NCP mediating nucleosome-to-nucleosome interactions which are the basis of the higher order structure of chromatin [83]. Posttranslational modification occurring on the tails alter the charge or structure of the tail and are recognized by specific reader proteins. Such alterations ultimately affect the accessibility of the nucleosomal DNA as well as the stability of the chromatin fibres.

The histone-fold is made up of three alpha helices α1, α2 and α3, which are linked by the L1 and L2 loops, and are responsible for the heterodimeric interactions to form histone-fold pairs of H2A-H2B and H3-H4. The folds are organized so as to form a "handshake motif" in which the L1 loop of one histone is juxtaposed with the L2 loop of its pairing partner, as shown in Fig. 5 b & c. Each histone-fold pair forms a scaffold around which about 25 bp of DNA wraps, and carries three sites at which DNA-histone interactions are established; two L1L2 sites and one α1α1 site. In total, the histone folds are responsible for organizing the central 121 bp of NCP DNA whereas the 13 bp stretches of DNA on entry/exit sites are organized by the N-terminal α- helix of the H3 histone (αN) (Fig. 6).

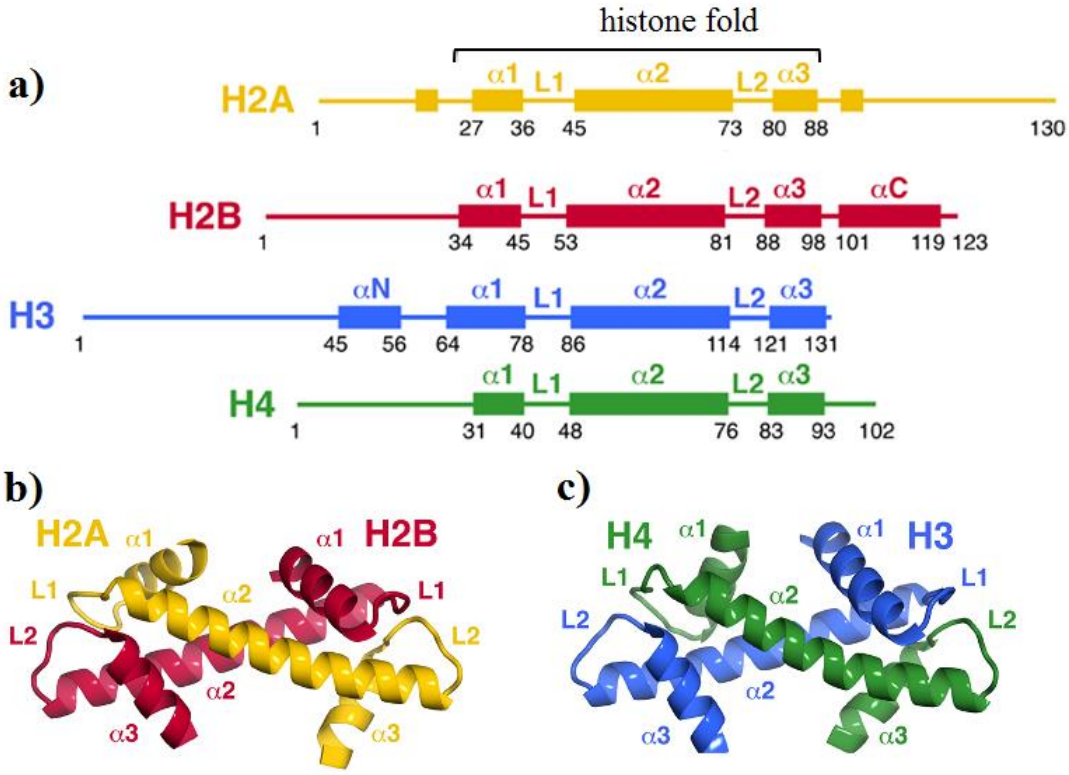

Figure 5: Histone fold and histone-fold heterodimers. Schematic representation of the core histone architecture and histone fold pairs. a) Histone architecture showing the conserved histone fold with 3 alpha helices α1, α2 and α3 joined by the L1 and L2 loops. The N-terminal tail of each histone and the C-terminal tail of H2A are shown as lines to the left and right of the histone fold, respectively. b) & c) Histone fold heterodimers H2A-H2B and H3-H4 showing the juxtaposed L1 and L2 loops on the ends. Figure adapted from [84].

The path that DNA follows on the NCP has been determined for core particles containing 146 and 147 bp of DNA, NCP146 and NCP147, respectively [85]. In this, it was determined that a single base pair lines up with the dyad (the central location of the nucleosome that divides the nucleosome to 2 symmetrical halves) dividing the DNA into two fragments, 72 bp and 73 bp long for NCP146 or two equal halves for NCP 147. The DNA winds around the histone octamer with its minor and major grooves alternately facing the octamer. The positions where the minor groove faces or looks away from the nucleosome core octamer are referred to as the superhelix locations (SHL) and they are numbered starting with the dyad position (SHL0) where the minor groove of DNA looks away (Fig. 6). The minor groove faces the nucleosome core at 14 different locations: SHL ±0.5, ±1.5, ± 2.5, ±3.5, ±4.5, ± 5.5 and ±6.5. Each inward facing minor groove lies adjacent to the DNA binding sites on the histone octamer. It is at these sites that histone-DNA contacts are established in a sequence-independent manner.

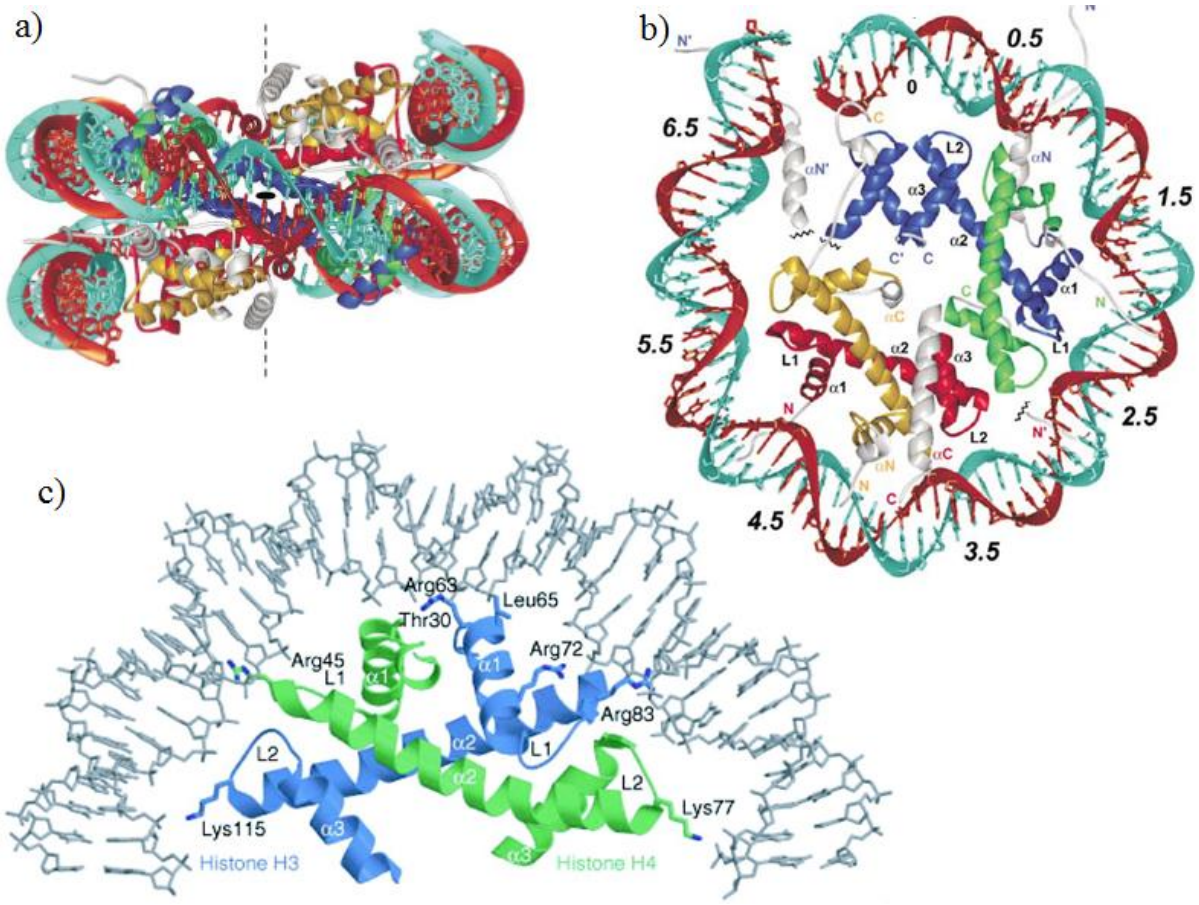

Figure 6: DNA path and DNA-histone contacts in the nucleosome core particle. a) Structure of the NCP viewed from the dyad axis (dotted vertical line). The DNA is shown in a ribbon structure with the two strands shown in red and cyan. The histones are shown in different colours: yellow H2A; red H2B; blue H3; green H4. The histone H3 N terminal alpha helices (H3 αN) and histone H2B C terminal alpha helices (H2B αC) are shown in grey. b) Half the NCP showing the organization of the histone folds and DNA. The terminal stretch of DNA around SHL 6.5 is organized by the H3αN; colour coding same as is (a). c) H3-H4 histone fold with the DNA. The amino acids involved in bond formation are labelled. There is an arginine residue protruding into each minor groove. Figure adapted from *panels a, b,* [86]; *panel c,* [87]

A total of 142 direct and at least 358 water mediated hydrogen bonds link the DNA to the histone octamer per NCP. Most of these bonds are formed between the phosphate backbone and arginine & lysine side chains (Table 1). In addition, electrostatic interactions between the

negatively charged phosphate DNA backbone and positively charged amino acids (Lys^+/Arg^+) in histones, as well as van der Waals interactions strengthen the grip on nucleosomal DNA. Though nucleosomal DNA undergoes spontaneous transient unwrapping from the ends [88], in steady state the DNA is largely constrained on the octamer by the large number of bonds. This constraint would be expected to greatly hamper the degrees of freedom for nucleosomal DNA.

Number of hydrogen bonds mediating histone protein–DNA interaction[a]

	Direct							Indirect (H_2O mediated)								
	Phosphodiester chains				Minor groove			Phosphodiester chains					Minor groove			
	Side-chain		Peptide		Side-chain			Side-chain		Peptide		DNA	Side-chain		DNA	
SHL of protein site	Arg, Lys	Ser, Thr	NH + [b]	NH	Arg	Tyr	Total	Arg, Lys	Other[c]	NH	CO		Arg	Tyr		Total[d]
−0.5	1	1	3	5	2		12	8[e]	4		7	15	5		12	51 (17)
0.5	2	1	3	5	3		14	10[e]	4		5	11	6		11	47 (15)
−1.5	3		2				5	3	0	1	1	5				10 (4)
1.5	6		2				8	3	1	1	1	8				14 (6)
−2.5	3	2	1	3	1		10	1	4	2	2	6	5		7	27 (9)
2.5	3	1	1	3	1		9	2	3	2	2	7	5		9	30 (9)
−3.5	3	1	1	3	1		9	6	0		3	8	2		5	24 (9)
3.5	3	2	1	3	1		10	3	2		2	8	2		4	21 (8)
−4.5	5		1	2	1		9	3	3	6	2	7	1		3	25 (8)
4.5	5		1	2	1		9	5	4	7	1	8	1		2	28 (7)
−5.5	0	1	1	2	1		5	2	3	3	3	9	3		7	30 (11)
5.5	1	3[f]	1	2	1		8	3	3	3	1	6	2		4	22 (8)
−6.5	1	1		1		1	4	0		1	2	4	1[g]	1	5	14 (5)
6.5	1	1		1		1	4	1		1	0	3	2[g]	2	6	15 (5)
Totals	37	14	18	32	13	2	116	50	31	27	32	105	35	3	75	358 (121)

[a] N-terminal tail regions (H3, 1–36; H4, 1–24; H2A, 1–15; H2B, 1–29) and C-terminal tail of H2A (121–128) are not included.
[b] Helix-dipole assisted: peptide amide group at N terminus of an α-helix.
[c] Gln/Glu/Ser/Thr/Tyr.
[d] Number of water molecules in parentheses.
[e] One hydrogen bond to His.
[f] One hydrogen bond to Tyr.
[g] Hydrogen bonds to His.

Table 1: Direct and water mediated hydrogen bonds in the nucleosome core particle. Table from [86].

In addition to the superhelical changes and the constrained conformation, the DNA in the NCP is greatly bent, such that 80 bp form a complete superhelical turn. This is a great deviation from the persistent length of linear B-DNA in solution which is 150 bp. This bending results in widening of both the minor and major grooves that face away from the octamer, while the minor grooves that face the octamer become narrow. Furthermore, an arginine residue penetrates into each of the inward facing minor grooves where it kinks the DNA.

1.3.4 Higher-order organization of chromatin

Early *in vitro* experiments suggested that the 10 nm fibre hierarchically folds into a 30 nm fibre in the presence of histone H1 or Mg^{2+}. In the 30 nm fibre, two models have been proposed for the arrangement of nucleosomes: the solenoid or one-start helix in which for a given nucleosome, the nearest neighbour is the ±1 nucleosome [89] and the zigzag or two-start helix in which the nearest neighbour is the ±2 nucleosome [90,91]. The arrangement partly relies on linker DNA length. For short linkers (18-30 bp), the 10n linker series favours the more compact zigzag helix whereas the 10n+5 series linkers form a more open solenoid helix, corresponding to the hetero- and euchromatin, respectively [79,92].

Nucleosome interactions within the 30 nm fibre are mediated by core histone tails [93], also see review [83]. Of the tail mediated interactions, those involving the H4 N terminal tail and the H2A-H2B acidic patch of the neighbouring nucleosome are the most important and deletion of this tail abolishes cation induced chromatin folding [94,95].

The rigid 30 nm fibre has, however, not been observed *in vivo*. This has been postulated to be due to i) the presence of architectural proteins such as the high mobility group proteins that bind and bend the linker DNA disrupting the regularity of the 30 nm fibre [96]; ii) the higher concentration of cations in the nuclei compared to 1-2 mM Mg^{2+} required to form the 30 nm fibre in solution [97]; iii) the high concentration of nucleosomes *in vivo* which favours inter-fibre nucleosomes association as opposed to the dilute *in vitro* conditions in which inter-fibre interactions are negligible. In contrast to the rigid structure observed *in vitro*, chromatin in the nuclei has been described to be flexible and follow a disordered "polymer-melt" model in which nucleosomes from adjacent fibres freely interdigitate [97].

As revealed by chromatin conformation capture (3C) techniques including its subsequent improvements especially Hi-C, chromatin is organized into compartments, topologically associated domains (TADs) and loops. There are two compartments: compartment A is enriched for highly expressed genes, carries activating chromatin marks such as H3K36me3, H3K79me2, H3K27ac and H3K4me1 and is replicated during early to mid S phase. Compartment B on the other hand, is gene poor, enriched for repressive chromatin marks such as H3K27me3 and is replicated during mid to end of S phase. The A and B compartments

correlate with the euchromatin and heterochromatin, identified earlier using electron microscopy.

Within each chromatin compartment DNA is organized in TADs and loops. The TADs are up to megabase size (880 kb) [98] and are defined as regions of increased contact frequency that are insulated from the neighbouring regions. That is, chromatin loci within a TAD interact more with each other but do not interact with loci in other TADs. Loops and possibly also TADs are formed by a mechanism referred to as loop extrusion and have CTCF binding motifs at the boundaries [99]. The CTCF binding motif is not palindromic and thus if its 5' to 3' orientation were to be considered forward, pairs of CTCF binding sites can be arranged in a forward, reverse, convergent or divergent manner. To initiate loop extrusion, cohesin is loaded onto a chromatin fibre by its loading factor NIPBL. Initially cohesin binds to two closely positioned sites on the fibre forming a small loop. The cohesin then slides along the chromatin fibre, partly pushed along by transcription-induced plectonemes [100], increasing the loop size until it reaches a properly oriented CTCF. The majority of the loops have convergent CTCF motifs at their boundaries [101]. The binding of CTCF to the CTCF binding site acts as a barrier preventing further extrusion. The size of the extruded loop is determined by the residence time of the cohesin on the chromatin fibre which is in turn influenced by its unloading protein called WAPL (Wings apart-like) [102]. WAPL releases cohesin from chromatin by opening its rings causing it to fall off; depletion of this protein leads to formation of long loops. In contact maps, TADs appear as triangles demarcating regions within which intra-TAD contacts are possible, while loops appear as punctate dots which represent enrichment of discrete contacts. Different laboratories have identified varying numbers of loops per eukaryotic genome. Differences in the number of loops identified apparently depend on the bioinformatics analyses: If the pixel density is compared with the local background one ends up with ~10,000 loops per genome [101] whereas if it is compared to the genome-wide background, one ends up with 10^5 to 10^6 loops per genome [103,104].

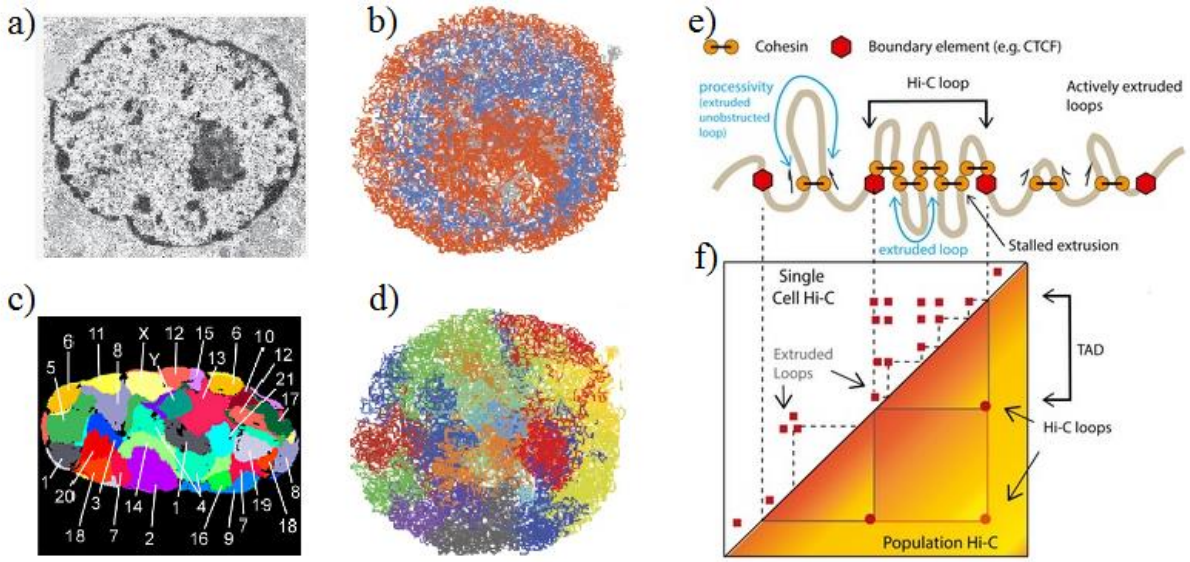

Figure 7*:* 3-D organization of chromatin in interphase nuclei. a) & b). Transcriptionally active and silent chromatin occupy distinct regions of the nucleus. The silent heterochromatin is mainly found associated with the nuclear lamina and around the nucleolus. It is densely packed as depicted by dark staining in the electron micrograph in a) and by reduced interactions in the Hi-C contact maps (red colour) in b). Euchromatin is found in the nucleoplasm lightly stained in a) and as regions of frequent contacts in Hi-C maps (blue colour) in b). c) &d). Chromosomes occupy distinct territories in the interphase nucleus as revealed by FISH in c) and contact mapping in d). e) & f). Cartoon presentation of loop extrusion by cohesin as observed in single cell and population Hi-C. Cohesin slides along the DNA until it encounters a properly oriented CTCF or an opposing cohesin which causes it to stall. Hi-C loops occur as dots and their boundaries are demarcated by CTCF. In single cell Hi-C, all loops including those not bound by CTCF are detected. Images panels adapted from panel a, [105]; panels b & d, [106]; panel c, [107]; panels e &f [108].

1.3.5 Chromatin topology

The topological state of the genome is established during replication as the DNA emerging from the replisome is promptly assembled into nucleosomes [109]. For both prokaryotes and eukaryotes, the superhelical density is about -0.06 [110]. Changes to this topological state are generated mainly by RNA polymerase (RNAP) during gene transcription. This is because the rotation of DNA is hampered by the viscous drag related to its length or by anchorage to elements of the nuclei

matrix. Consequently, the DNA ahead of the advancing RNAP becomes positively supercoiled and negatively supercoiled behind, according to the twin supercoiling domain model [111]. In similar fashion, positive supercoils form ahead of the replication machinery while negative supercoils form in the nascent duplex bearing the leading strand which is continuously synthesized [112].

A build-up of the locally generated topological changes can stall transcription [113] and compromise genome integrity, thus, cells contain topoisomerases to relax the supercoiling. Eukaryotic cells have two types of topoisomerases, TOPO I and TOPO II which can cleave one or both strands of a DNA duplex, respectively, to relax both + and – supercoiling. In addition, some of the torsional energy can dissipate by i) annihilation of oppositely supercoiled waves e.g. between two tandem transcribing RNAPs, the negative supercoiling behind the leading RNAP would neutralize the positive torsion ahead of the second RNAP; ii) absorption by DNA binding proteins e.g. nucleosomes which constrain negative supercoils; and iii) diffusion along the chromatin fibre in a gradient fashion. The extent of diffusion of torsional energy is limited by friction but has been detected up to 1.5 kb upstream of the TSS of a transcribed gene [114]. In principle, the net change in superhelicity emanating from transcription is zero as the number of positive and negative supercoils generated are equal. However, whether the supercoils are promptly, symmetrically and completely removed remains enigmatic mainly because of limited tools for measurement of supercoiling *in vivo*. So far this measurement has been made by measuring the crosslinking of DNA by the intercalating and strand-crosslinking molecule psoralen. Negative supercoiling is said to favour psoralen crosslinking, but so does the removal of histone proteins which increases the binding sites available for psoralen. A further factor could be the difference in linker length between heterochromatin (shorter) and euchromatin (longer).

1.3.6 Regulatory role of transcription-induced supercoiling

Supercoiling causes folding of chromatin in 3-dimension bringing distant domains elements such as enhancers and promoters into close proximity. Further, it affects DNA geometry which in turn alters its interaction with regulatory and structural proteins subsequently impacting transcription [110]. As such, supercoiling is considered an analogue code that controls how the digital code (nucleotide sequence) is accessed and read. Nucleosomes for example, readily form

on negatively but not positively supercoiled DNA *in vitro* [115]. *In vivo*, this may serve to destabilize nucleosomes ahead of the advancing RNAP [116,117], while facilitating their re-assembly behind the transcribing complex. However accumulation of torsion beyond a threshold value, results in reduced mRNA yield as seen in yeast mutants [113,118].

Negative supercoiling facilitates spontaneous strand separation at temperatures below the DNA melting point. The single stranded DNA thus formed, forms the basis of transitions to non B DNA structures and is required for binding of single-strand DNA-binding proteins.

Additionally, supercoiling generated in one gene alters the transcription of neighbouring genes depending on the orientation. For divergent genes, negative supercoils behind the RNAPII complex induces promoter melting of the neighbouring promoter and activating transcription also there. For convergent genes positive supercoils accumulate between the approaching RNAPs. In tandem genes, the negative and positive supercoils between advancing RNAPs cancel out; however, there is still accumulation of positive and negative supercoils ahead of the leading and behind the rear RNAP, respectively.

1.4 THE HMG-BOX DNA BINDING DOMAIN

The HMG-box is a 75 amino acid DNA-binding domain initially discovered in the architectural proteins HMGB in mammals, HMG-D in Drosophila [119] and yNHP6A in S. cerevisiae [120]. Later it was also found in chromatin remodelers such as BAF35 & BAF57, the nucleosome chaperone FACT [121], and transcription factors such as TFAM in the mitochondria [122], UBF1 in the nucleoli, the Sox family of developmental TFs [123], and the TCF/LEF-1 that regulate gene expression during differentiation, among others.

This domain has been shown to preferentially bind supercoiled, cisplatin damaged DNA, hemicatenanes and other non-B DNA structures. It binds to the DNA minor groove causing unwinding and widening of the minor groove as well as bending of DNA towards the major groove. The degree of bending caused by proteins that have the HMG-box domain varies from protein to protein; for example, the TATA binding protein (TBP) induces a 95^{o} bend [124], while HMGB1 causes a 77^{o} bend. The bending of DNA is brought about by partial intercalation of amino acid side chains[125]. Intercalating amino acids are core to the binding and bending of DNA and their substitution may result in a protein that cannot bind DNA as was observed in a

HMGB1 triple mutant, [125] or a protein with a reduced bend angle as observed in Sac7d double mutant [126]. DNA bending has two major outcomes of gene regulatory importance. It loops DNA, bringing distant regulatory sites such as enhancers and promoters into proximity and it locally facilitates the DNA binding of transcription factors [127].

1.4.1 The HMGB1 protein

HMGB1 is the most abundant non-histone architectural protein found in the cell nuclei, occurring at a density of one molecule per 10-15 nucleosomes [128]. In the nucleus it binds to linker DNA in competition with histone H1. While histone H1 stabilizes the nucleosome structure and facilitates higher order chromatin folding [129] binding of HMGB1 enhances nucleosome sliding and decompacts chromatin [130]. Following necrosis or activation of macrophages and monocytes, HMGB1 is release to the extracellular milieu where it acts as an alarmin [131–133]. In living cells, it is actively shuttled between the nucleus and cytoplasm

The protein consists of three domains; two HMG-box domains; box A and box B that bind DNA and an acidic C-terminal tail which interacts with histone H1 and also regulates DNA binding and bending (Fig. 8) [128,134–136]. Boxes A & B carry a total of three intercalating amino acids (Phe37 on box A and Ile121 and Phe102 on Box B) and three redox-sensitive cysteines (Cys23 and Cy45 on box A, and Cys106 on Box B). The redox state of these cysteins affects both the protein's nuclear interactions as well as its immunogenic properties. The all-thiol form has chemokine activity; the disulphide form has cytokine activity while the oxidized form has no immunogenic activity. Reduced HMGB1 exhibits higher affinity for DNA, causes greater DNA bending [137], and has greater ability to displace histone H1 from nucleosomes compared to the oxidized form [138]. Several of the HMGB1 residues also undergo post-translational modifications (PTMs) which affects its DNA binding and cellular localization; lysine acetylation [131], serine phosphorylation [137] and lysine methylation [137] reduce its binding to DNA, increase retention in the cytoplasm and redirect it towards secretion.

HMGB1 has been described as a jack of all trades due to its involvement in many cellular processes including transcription, DNA repair, DNA recombination, chromatin organization and inflammation, *see Reviews* [139,140]. It exerts its nuclear functions by i) directly restructuring the nucleosome or recruitment of nucleosome remodellers to make the DNA more accessible

[141,142]; ii) DNA bending to enhance binding of TFs that require pre-bent DNA such as p53 [143] and/or iii) directly interacting with TFs to increase their residence time on the promoters [144]. It has also been shown to be recruited to DNA damage sites where it either enhances or obstructs repair [145].

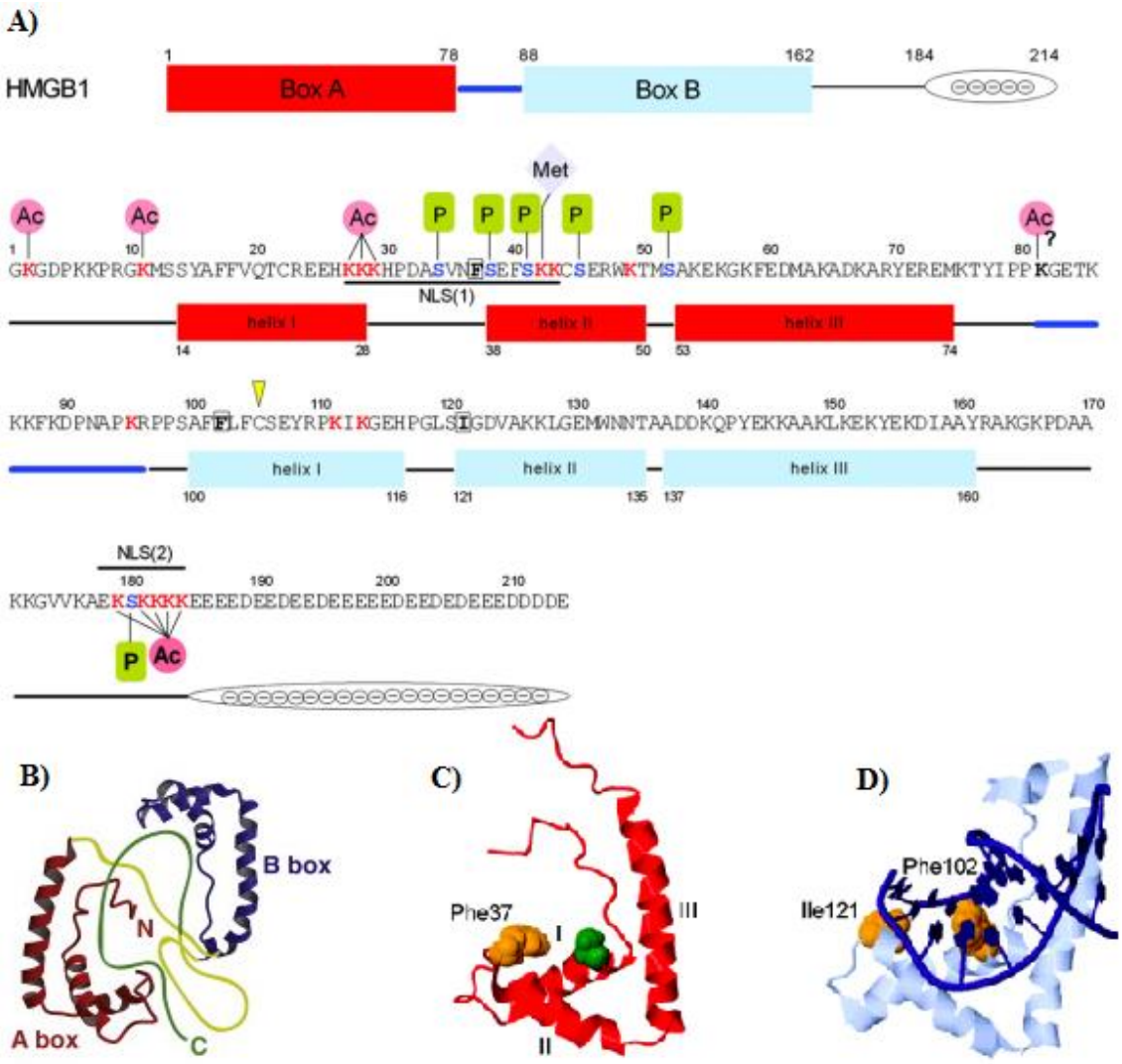

Figure 8: Structure and sequence of HMGB1: A) The domains and sequence of HMGB1. The amino acid sequence and the post translational modifications are also indicated. B) Tertiary structure of HMGB1, the linkers linking box A to box B and box B to the C-terminal tail are indicated in yellow. The C terminal tail shown in green can be seen interacting with the DNA binding surfaces of box A and box B. C) Box A showing the constituent alpha helices I, II & III and the intercalating amino acid in yellow. D) Box B (cyan) binding to DNA (blue), intercalating amino acids shown in yellow. NLS, nuclear localization signal .Figure adapted from [128]

2. JUSTIFICATION & OBJECTIVES

2.1 JUSTIFICATION

The nucleosome structure has long been known to be a barrier to regulatory factor binding *in vivo*, and this was generally assumed to be due to steric hindrance. This view is, however, challenged by the fact that DNA is wrapped on the outside of the nucleosome structure with one of its strands exposed at any one point. Further, biophysical studies have revealed that relatively large molecules can access even densely packaged chromatin areas and local chromatin Brownian motions can bring buried DNA targets for factor binging. Thus, there is need for further experiments to elucidate the mechanism by which the nucleosome structure inhibits binding.

The results obtained from my experiments with small molecule intercalators suggest that constrained superhelicity hampers intercalation into DNA in chromatin. Considering that some protein DNA interactions involve intercalating moieties, I wondered if superhelicity would equally affect their binding. HMGB1 is an example for such a protein, containing an HMG-box domain what has been identified in various proteins involved in transcription, chromatin remodelling and even DNA repair. The binding of this domain to naked DNA in solution has been extensively studied but information is rather scanty regarding its binding features in the cell's inner environment, *in vivo*, warranting further investigation.

2.2 OBJECTIVES

2.2.1 General objective

To determine the mechanism by which chromatin packaging regulates access to DNA *in vivo*.

2.2.2 Specific objectives

1. To develop an assay to evaluate the binding of small molecule intercalators *in situ*.
2. To determine the factors regulating intercalation of small molecules *in situ*.
3. To assess the influence of factors affecting DNA supercoiling on the binding of HMGB1, a protein with intercalating moieties, to DNA *in vivo*.

3. MATERIALS & METHODS

3.1 MATERIALS

All materials were obtained from Sigma Aldrich Hungary unless where otherwise stated.

Cells and lines used:

i) HPBMCs from healthy donors
ii) Wildtype HeLa
iii) HeLa cell line stably expressing GFP tagged histone H1c ($HeLa^{H1c\text{-}GFP}$)
iv) HeLa cell line stably expressing GFP tagged histone H2B ($HeLa^{H2B\text{-}GFP}$)
v) HeLa cell line stably expressing GFP tagged histone H3 ($HeLa^{H3\text{-}GFP}$)
vi) Human osteosarcorma cell line, U2OS expressing H2B-RFP and GFP-HMGB1 ($U2OS^{2FP}$) (this cell line was kindly provided by Guido Kroemer

3.2 METHODS

3.2.1 Cells and cell culture

HeLa cells were maintained in RPMI-1640 medium. $HeLa^{H1c\text{-}GFP}$, $HeLa^{H2B\text{-}GFP}$ $HeLa^{H3\text{-}GFP}$ and $U2OS^{2FP}$ were maintained in DMEM medium (Gibco). Both RPMI and DMEM used in culture were supplemented with 10% FBS, 1x Glutamax, 100 U/ml penicillin, 100 µl/ml streptomycin and phenol red. In addition, media for $U2OS^{2FP}$ cells was suplemented with G418 0.5 mg/mL for continous selection of transformed cells. All cells were cultured at 37°C in a humidified, 5% CO2 incubator and passaged every two days.

HPBMCs were separated from whole human blood obtained from healthy donors. The blood was drawn at the regional Blood Center of the Hungarian National Blood Transfusion Service (HNBTS), (Debrecen, Hungary). Ethical approval for use of these samples was sought and obtained from the Director of the HNBTS and the Regional and Institutional research ethical committee of the University of Debrecen, Faculty of Medicine, (Debrecen, Hungary). Prior to blood donation, written, informed consent was obtained from the donors, and their data was processed according to the regulations of the European Union. HPBMCs were separated from

whole blood following the density gradient centrifugation technique developed by Böyum [146]. Briefly, whole human blood was mixed with an equal volume of PBS. The mixture was gently layered over Ficoll-Paque plus (Amersham Biosciences, Uppsala, Sweden) in the ratio of 2:1(blood mixture: Ficoll solution) and centrifuged for 20 minutes. The Puffy coat was carefully collected by a Pasteur pipette and transferred into a new tube. The mononuclear cells were washed twice PBS and used immediately or incubated in RPMI-1640 medium supplemented with 10% FCS (Gibco, Paisley, Scotland) and 1% antibiotic/antimycotic solution (Hyclone, South Logan, Utah).

3.2.2 Harvesting cells from culture flasks

1x Trypsin–EDTA was used to detach HeLa cells from culture flasks. First the culture media was completely aspirated from the culture flask. For a T-25 culture flask, the cells were rinsed 2x with 1ml of 1x Trypsin–EDTA to remove any traces of culture media. 1ml of Trypsin–EDTA was then added and the flask transferred to a 37°C water bath for 3 minutes. Detachment of cells was confirmed by gently tapping the side of the flask. 3 ml of culture media was added to the detached cells to stop the action of trypsin and the cells were transferred into a 15 ml centrifuge tube, centrifuged at 1250 RPM for 5 minutes. The supernatant was discarded and the cells were washed 1x using PBS and then resuspended in PBS at the required concentration.

3.2.3 Live cell microscopy

To study the uptake and intercalation of EBr in live cells, $HeLa^{GFP}$ cells were seeded at the rate of 30,000 cells per well onto the wells of an 8- well chamber (Ibidi, Martinstried, Germany) and allowed to attach overnight. Once removed from the incubator, cells were rinsed 3x with PBS pH 7.4 (150 mM NaCl, 3.3 mM KCl, 8.6 mM disodium phosphate dodecahydrate (Na2HPO4.12H2O) and 1.69 mM potassium dihydrogen phosphate (KH2PO4)) to remove medium. Cells were then stained with 300µl of 10 µM EBr in PBS-glucose (PBS + 7mM) glucose for 30 minutes at 37 °C and then imaged using the Olympus FV-1000 confocal laser scanning microscope. For experiments carried out under the microscope (Fig. 9), immediately after addition of the staining solution, the sample was transferred onto a pre-warmed (37°C) chamber on the microscope. For the microinjection experiment (Fig. 10), once the staining solution was added to the cells, the 8-well chamber was transferred to a Zeiss LSM 5 Live (Carl

Zeiss, Oberkochen, Germany) confocal laser scanning microscope coupled with a patch clamp apparatus. Individual cells were microinjected in a whole-cell patch clamp set-up with a dye solution equivalent to that in the bathing solution. Patched cells were imaged for 20 minutes, every 30 seconds for the first 5 minutes and then every 2 minutes for the remaining time.

3.2.4 NaCl-induced histone elution

To study the effect of the nucleosome structure on intercalation of EBr in situ, histones were sequentially evicted from agarose embedded nuclei using varying concentrations of NaCl before addition of 10 µM EBr. First, 8-well chambers were coated with 1% low melting point agarose dissolved in water (1% LMP-w) as follows: 150 µl of molten 1% LMP-w was dispensed onto each well of the chamber to coat the bottom of the well. During the dispensing, the chamber was kept on hot plate maintained at 42°C. The molten 1% LMP-w was then quickly removed from the wells and the chamber transferred to a metal plate on ice for 2 minutes to allow the agarose to gel, and then back to 42°C for 30 minutes until the agarose dried. The procedure was repeated one more time to apply a second layer of agarose.

Next cells were embedded into the pre-coated wells. Pre-warmed 50 µl of 6 x 106cells/ml suspension was added to 150 µl molten 1% LMP-PBS at 37°C and gently mixed to create a homogeneous suspension. 22 µl of this suspension was dispensed into each well and quickly covered with a coverslip to allow the cells to spread. The 8-well chambers were kept at 37°C for a further 2 minutes to allow the cells to sediment and then on ice to allow the agarose to gel. The coverslips were detached from the agarose by adding 300 µl of cold PBS to the wells and carefully removed using a hooked needle.

The cells were washed 3x for 3 min using 300 µl/well of PBS and then permeabilized using 400 µl/well of 1% Triton-x-100/PBS-EDTA applied 2x for 10 min each. Nuclei were washed 3x for 3 min using 400 µl/well of PBS-EDTA to remove residual Tx-100. RNA was digested by incubating nuclei with 150 µl/well of 100 µg/ml RNase A (Thermo Scientific, Waltham, Massachusetts, USA) dissolved in PBS-EDTA for 2 hr at 37°C. After RNA digestion, nuclei were subjected to 400 µl/well of varying cc. of NaCl (as indicated on the x-axis) for 1 hr, with solution change every 10 minutes. NaCl was washed from the wells using 400 µl /well of PBS-EDTA 3 x for 10 minutes each before addition of intercalators.

The nuclei were then stained with either 300 µl/well of 10 µM EBr or 150 µ/well of 40 nM YOYO-1 for 2 hrs on ice. The staining solution was then replaced with 300 µl/ well of 1 µg/ml (3.6 µM) DAPI and incubated for a further 2 hrs on ice before imaging with the laser scanning cytometer. In the case of psoralen, 150 µl/ well of 1 mg/ml biotinylated 4,5',8-trimethyl psoralen (bTMP) (kindly provided by Nick Gilbert) was added to the nuclei and incubated on ice for 2 hrs. Unbound bTMP was removed by briefly rinsing the nuclei with PBS-EDTA. To induce bTMP-DNA cross links, the samples were exposed to UVA (365 nm) on ice for 10 min at a distance of 5 cm from the lamp. The samples were washed once more with PBS-EDTA and blocked with 1% w/v BSA in EDTA for 45 minutes. For detection of bound bTMP, nuclei were incubated with 150 µl/well of 1 µg/ml mouse anti-biotin antibody overnight at 4 °C. Unbound primary antibody was removed by 3 washes with PBS-EDTA before a 2 hr incubation on ice with 1µg/ml Alexa 633 conjugated anti-mouse antibody (Thermo Scientific, Waltham, Massachusetts, USA) 200 µl/well. Nuclei were counter stained with 1 µg/ml DAPI and imaged with LSC.

3.2.5 DNase I hypersensitivity assay

DNase hypersensitivity assay is routinely used to map accessible DNA in chromatin [17]. To test whether the increased binding of intercalators upon histone elution reflected increased access to DNA, a DNase hypersensitivity assay was carried out. Following the protocol described above, agarose embedded nuclei were depleted of RNA and of varying amounts of nucleosomes. The nuclei were then equilibrated with 400 µl/well of DNase I buffer (10 mM Tris pH 8, 0.1 mM CaCl2 and 2.5 mM MgCl2) then the DNA nicked by DNase I digestion for 10 min at 37°C (300 µl/well of 0.1 µg/ml DNase I). Residual enzyme was removed or its activity inhibited by three washes with PBS-EDTA. The samples were then equilibrated with DNA polymerase I buffer (50 mM Tris-HCl, pH 7.2, and 10 mM MgSO4). Nicks generated by DNase I were labelled by *in situ* nick translation in a reaction volume of 120 µl/well consisting of 0.5 U of DNA polymerase I, 5 nmol of dATP, dCTP, dGTP and biotin-dUTP for 10 min at room temperature. The biotin-dUTP was labelled with anti-biotin and fluorophore conjugated secondary antibody as described above, nuclei counter stained with DAPI and imaging done by LSC.

3.2.6 MNase Digestion

In live cells and in isolated nuclei, EBr was hypothesized to bind mainly to the linker DNA. To substantiate this hypothesis, agarose embedded, RNA-depleted nuclei (prepared as described above), were fixed with 300 µl/well of 4%formaldehyde for 20 min on ice. The nuclei were then washed 3x to remove residual formaldehyde and equilibrated with MNase buffer (50 mM Tris, pH 7.5, 1 mM $CaCl_2$). Next, 150 µl/well of varying amounts of MNase as indicated on the x-axis (Fig. 13A) were added to each well and the samples incubated at 37°C for 7 minutes. MNase activity was stopped by 3 washes with PBS-EDTA. The nuclei were stained with 10 µM EBr and counterstained with 1 µg/ml DAPI and fluorescence of each nucleus measured by the LSC.

3.2.7 EBr staining of nicked, linear and native plasmid DNA

To ascertain the effect of topology on EBr uptake by naked DNA, native pcDNA3-EGFP (6159 bp), was linearized or nicked using 1 U of ECoRI or 1 U of Nb.BsmI respectively following the manufacturer's instructions (Thermo Scientific, Waltham, Massachusetts, USA). Next, 0.5 µg of each plasmid form; linear, native and nicked were mixed and separated on 1% agarose gel (TAE buffer). After electrophoresis, the lanes were cut and stained with different cc. of EBr as indicated on the x-axis (Fig. 17a). The gel was reassembled, imaged by FluorChem Q (Alpha Innotech and the image processed using Fiji ImageJ to determine the fluorescence intensity of each DNA band.

3.2.8 In-gel cell irradiation and determination of nick incidence

To evaluate the effect of topology on EBr binding to DNA in situ, live cells were irradiated with x-rays and dye uptake by the nuclei prepared thereof, measured by LSC. First, however, it was necessary to determine the dosage of x-rays sufficient to cause 1 nick per chromatin loop (~50 kb DNA). To determine this, live $HeLa^{H3\text{-}GFP}$, were harvested and embedded into agarose plugs by the method described by Varga et al. [147]. Briefly, cells were resuspended in PBS at a cc. of 1.3x107/ml and brought to 37°C. The suspension was added to an equal volume of pre-warmed 1.5% LMP-PBS-EDTA and mixed to create a homogenous suspension. 90 µl of the mixture was distributed into CHEF moulds and allowed to gel at 4°C for 20 min. The resulting agarose plugs were transferred into the wells of an 8-well chamber containing DMEM. The

cells in the plugs were irradiated with varying doses (25-300 Gy) of X-ray radiation at a distance of 57.2 cm from the 6 MeV linear accelerator.

Next the plugs were washed with cold PBS-EDTA on ice 3x for 30 minutes each time and then submerged in lysis buffer (0.4325 M EDTA, 1% N-Lauroylsarcosine, 10 mM Tris, pH 8, and 0.5 mg/ml proteinase K (Thermo Scientific, Waltham, Massachusetts, USA) and transferred to a heating block set to 55°C. 24 hours later, the lysis buffer was replenished with a new batch and incubated for a further 24 hrs. At the end of the 48 hrs, proteinase K was inactivated using 1 mM PMSF (phenylmethylsulfanylfluoride) for 10 min at room temperature followed by washing the plugs 3x in cold Tris-EDTA (10 mM Tris HCl, 1 mM EDTA, pH 8.0).

To map the single stranded DNA breaks, the nicks on the genomic DNA were converted to double strand DNA breaks using S1 nuclease before electrophoresis. Briefly, once the proteinase K activity was stopped and the agarose plugs with genomic DNA washed, the plugs were equilibrated 3x with S1 nuclease buffer (250 mM NaCl, 49.5 mM Na-acetate, 0.36% ZnSO4, and 1% BSA, pH 4.4) for 10, 30 and 60 minutes in that order. Nicks were then converted to ds DNA breaks by submerging the plugs in 1000 U/ml S1 nuclease (Thermo scientific, Waltham, Massachusetts, USA) and incubating at 37°C for 1 hr. The plugs were then loaded into the wells of a 1% agarose gel in 0.5x TBE ds DNA fragments, 3-300 kb were separated by the CHEF mapper (Bio RAD). The gel was stained with 0.5 μg/ml EBr and imaged using FluorChem Q (Alpha Innotech, San Leandro, California, USA) gel documentation system. Fragment size was identified using a pulse marker (Midrange PFG marker New England Biolabs N0342S) that was run alongside the samples.

3.2.9 Salt extraction of histones

Salt extraction of histones was carried out using the technique described by Shechter et al. [66]. Briefly, $1x10^7$ HeLa cells were resuspended in 1 ml of extraction buffer (10 mM HEPES, pH 7.7, 10 mM KCl, 1.5 mM $MgCl_2$, 0.34 M sucrose, 10% glycerol, 20x dilution protease inhibitor cocktail and 0.2% NP-40) and incubated on ice for 10 min. Nuclei were recovered by centrifugation at 6,500g for 5 min and then washed in extraction buffer without detergent. Nuclei were then lysed by incubating with Tris-EDTA for 30 min on a rotator, at low speed. Chromatin was recovered by centrifugation at 6,500g for 5 min. Histones were then extracted

using 400 µl of high-salt buffer (50 mM Tris-HCl pH 8.0, 2.5 M NaCl, 0.05% NP40), by slowly rotating the samples for 30 min at 4°C. The solution was then centrifuged at 16,000g and the supernatant filtered through a 3,500 MWCO spin column (Sartorius AG, Göttingen, Germany). Samples were washed twice with PBS then quantified by measuring absorption at 280 nm.

3.2.10 Microscopy

An Olympus FlouView 1000 confocal laser scanning microscope fitted with 3 lasers was used. GFP was excited using the 488 nm laser line, the 543 nm line was used for EBr, and the 633 nm line for excitation of Alexa Fluor 633. Microscopy images were taken using the 60x oil immersion objective (NA = 1.35) analysed using Fiji ImageJ.

3.2.11 Automated microscopy

Automated microscopy was done using an iCys Research Imaging Cytometer (CompuCyte Corporation, Westwood, MA). The instrument is based on an Olympus IX-71 inverted microscope equipped with four lasers, photodiodes (detecting light loss and scatter) and four photomultiplier tubes (PMTs). A 405 nm solid state laser was used for the excitation of DAPI and Hoechst, the 488 nm Argon laser line was used to excite GFP and EBr, and a 633 nm HeNe laser for Alexa 633. For each salt treatment, 1500–2000 events were measured. The nuclei were contoured/identified by their DAPI fluorescence. No further masking of nucleoli was done as the samples were already digested with RNase A. Data analysis was performed using the iCys 7.0 software, and graphs were prepared using SigmaPlot 14.0.

3.2.12 Spectrofluorimetry

Quantification of EBr concentration remaining in the supernatant following staining of nuclei was carried out using a Fluorolog-3 spectrofluorimeter (Horiba Jobin Vyon, Edison, NJ). EBr was excited at 300 nm and the emission fluorescence measured at 590 nm. To prepare the EBr titration curve solution concentrations ranging from 0.5–4 µg/ml were used.

3.2.13 Fluorescence lifetime imaging and data analysis

The fluorescence decay dynamics were acquired using a Nikon A1 laser scanning microscope with a PicoQuant time-correlated single photon counting module. EBr was excited by a 510 nm

pulsed laser at 4 MHz repetition frequency. Laser power was 1,891 µW as measured at the back aperture of the objective. Emitted fluorescence photons were collected using a 60x water immersion objective (NA = 1.27) and directed to an avalanche photo detector (Excelitas Technologies), using a 594 long pass filter. An average of 2,000 counts were collected for every sample. Data was analysed using SymPhoTime 64 software and fitted using n-Exponential reconvolution module for 2 lifetime components. Lifetime component plots were prepared using SigmaPlot 14.

3.2.14 Cell fixation and immunofluorescence labelling

U2OS^{2RFP} cells grown on an 8 well chamber were fixed with one of the following fixatives for 30 min on ice and a further 30 minutes at RT. i) 4% formaldehyde in PBS-EDTA; ii) 0.003% glyoxal pH 5 (containing 20% ethanol and $7.5x10^{-6}$ % acetic acid); iii) 4% formaldehyde mixed with 2% glutaraldehyde and iv) 70% chilled ethanol in PBS. The fixative volume used was 300 µl/well. Formaldehyde was quenched by incubating the sample with 100 mM glycin for 20 min at room temperature. Fixed cells were then permeabilized using 0.5% Tx-100/PBS-EDTA for 10 min at RT. This was followed by washing 3 times using PBS-EDTA at a volume of 300 µl/well.

To prevent non-specific antibody binding, samples were blocked with 0.5% BSA/PBS-EDTA for 30 min. 200 µl of 1 µg/ml anti-HMGB1 polyclonal antibody produced in rabbit (FineTest, Wuhan, Cat # FNab10218) was added to each well and samples incubated overnight at 4°C. Samples were then washed 3x with 300 µl/well of PBAS-EDTA to remove unbound primary antibody before adding 200 µl/well of Alexa-647 conjugated goat anti-rabbit antibody and incubating on ice 2 hrs. Unbound secondary antibody was removed by 2 brief washes with 300 before imaging µl/well of PBAS-EDTA and the samples imaged on the Olympus FluoView 1000 confocal microscope

3.2.15 Cell treatment

HeLa$^{H1c\text{-}GFP}$ and U2OS^{2FP} cells were seeded on an 8 well chamber (Ibidi Manstried,Germany) at a cell number of 30,000 per well and allowed to attach overnight. Cells were treated with the indicated concentrations of either doxorubicin for 2 hrs (sigma Aldrich), EBr for 1 hr, bleomycin for 2 hrs or H_2O_2 for 20 min at 37°C in phenol red-free medium. Irradiation with x-

rays was done at room temperature at a distance of 57.6 cm from the window of a 6 MeV linear accelerator (irradiation was done by Attila Kovács at the Radiolotherapy Department, University of Debrecen).

3.2.16 Strip FRAP

To assess the mobility of histone H1-GFP, strip FRAP measurements were carried out as described previously with minor modification [148]. In brief, FRAP measurements were performed on FV1000 Olympus confocal microscope using a 60x, 1.2 numeric aperture oil immersion objective. The 488 nm laser line was used to excite GFP with a laser power of 4.45 μW at the objective (8%), and emission was detected through a 500 to 520 nm band pass filter. For quantitative analysis, a 512x512-pixel area was selected and scanned with an open pinhole (5.56 Airy units) and 9.1x zoom (pixel size: 0.045 μm), with a pixel dwell time of 0.664 μs. A strip region was illuminated with 100% of the 488 nm laser to bleach the EGFP molecules at a selected strip-shaped region of interest (FRAP ROI) having an area of 256 x12 pixels, a laser power of 55.6 μW at the objective, and a pixel dwell time of 20 μs. Before bleaching, 10 images were collected at intervals of 1.74 s followed by one bleach period at the FRAP ROI, and then collecting 80 post-bleach images for a total time of 139.5 s. To standardize the geometry of the measurement, the strip-shaped FRAP ROI (bleached area) was positioned horizontally at one third of the vertical extension of the nucleus, avoiding nucleoli. Image fluorescence was analysed in Fiji ImageJ. Recovery of fluorescence in the ROI was normalized to the total fluorescence of the nuclei at each time point to take care of photobleaching. Recovery data was fitted in GraphPad Prism version 8.02 using a one phase decay. Analysis of variance was performed with One-way Anova.

3.2.17 Point FRAP

For measurement of GFP-HMGB1 mobility, point FRAP measurements were performed on Olympus FluoView 1000 confocal microscope based on an inverted IX-81 stand with an UPlanAPo 60x NA 1.2 oil immersion objective. EGFP was excited by the 488 nm line of an Ar ion laser, and emission was detected through a 500–520 nm band-pass filter by PMT. The measurement for point FRAP data acquisition started with a confocal image of a cell (512×512-pixel, pixel size: 0.103 μm), followed by the selection of a laser spot at which the laser beam

was focused. Before bleaching, 5120 pre-bleach pixels were collected with a pixel dwell time of 10 µs (51.2 ms) with 8.84 µW laser power followed by bleach period for 51.2 ms with 100% laser power 55.6 µW and then collecting 40,000 post-bleach pixels from the same spot for a total time of 297.59 ms.

In order to change the laser power of the Ar-ion laser shorter than pixel dwell time, a dedicated LabVIEW program was developed (by Gábor Mocsár). The analogue output of a NI 7833 field programmable gate array (FPGA) card (National Instruments, Austin, TX) was fed into the laser power controller input pin of the acousto-optic tunable filter (AOTF, AA Opto electronic MOD.NC) of the laser combiner unit, allowing fast (~1 µs) voltage driven laser power switching by FPGA card. The operating of the FPGA card was initiated by TTL output of the trigger port of the FV1000 system, thus the controlling the laser power and collecting the fluorescent data were synchronized.

The model function fitting of the recovery post-bleach data was performed by a custom written Matlab (The Math Works, Natick, MA) program (by Gábor Mocsár). Data were fitted assuming a one-component exponential recovery with the following equation:

$$I_{(t)} = I_1\left(1^{(-t/\tau 1)}\right) + I_{bg} \qquad \text{(eq. 1)}$$

Where $I_{(t)}$ is intensity at a given time point; t, time; I_1, amplitude of the intensity; τ1, recovery time; I_{bg}, background intensity.

3.2.18 Fluorescence correlation spectroscopy (FCS)

For FCS measurements, 1 µg of native pEGFP-C3 plasmid DNA and 945 ng of Alexa labelled rHMGB1 was used per well in a volume of 300 µl of protein binding buffer with or without doxorubicin. The mixture was allowed to equilibrate at RT for 1 hr before measurement.

FCS measurements were carried out on a Nikon A1 Eclipse Ti2 confocal laser-scanning microscope (Nikon, Tokyo, Japan), equipped with a Plan Apo 60× water objective [NA=1.27] and PicoQuant - TCSPC-FCS upgrade kit (PicoQuant, Berlin, Germany). FCS measurements involving Alexa 647 conjugated rHMGB1 and plasmid DNA were carried out in 8-well chambers. All measurements were made at room temperature. Alexa 647 was excited by the

633 nm laser. Fluorescence emission was filtered through a 650-700 nm band width filter and detected with single photon counting detectors (PicoQuant, Berlin, Germany). Measurements of 10x10 s runs were taken at a point in the solution. Fluorescence autocorrelation curves were calculated SymPhoTime64 software (PicoQuant, Berlin, Germany) at 200 time points from 300 ns to 1 s with quasi-logarithmic time scale. Autocorrelation curves were fitted to a model with triplet state and two diffusion components to account for DNA bound HMGB1 (slow component) and free 3D-diffusion of HMGB1 (fast component).

$$G(\tau) = \frac{1-T+Te^{-\frac{\tau}{\tau_{trip}}}}{N(1-T)} \left(\rho \frac{1}{1+\frac{\tau}{\tau_{D1}}} \frac{1}{\sqrt{1+\frac{\tau}{S^2\tau_{D1}}}} + (1-\rho) \frac{1}{\sqrt{1+\frac{\tau}{\tau_{D2}}}} \frac{1}{\sqrt{1+\frac{\tau}{S^2\tau_{D2}}}}\right) \qquad \text{(eq. 2)}$$

Where: N is the average number of fluorescent molecules in the detection volume, T is the fraction of molecules in the triplet state, τ_{tr} is the triplet correlation time. The rate of diffusion is characterized by the diffusion time, τ_d, which is the average time that a molecule spends in the illuminated volume. τ_{D1} and τ_{D2} are the diffusion times of the fast and slow component, ρ is the fraction of the first component and 1- ρ is the fraction of the second component. Diffusion coefficients (D) of the fast and slow component were determined from the following equation:

$$D = \frac{\omega_{xy}^2}{4\tau_d} \qquad \text{(eq. 3)}$$

Where ω_{xy} is the lateral e^{-2} radius of the detection volume. ω_{xy} was measured by determining the diffusion time of 100 nM Alexa 647 dye (dissolved in 10 mM Tris-EDTA buffer, pH 7.4) with a known diffusion coefficient (D_{A647} = 330 $\mu m^2/s$, at T = 22.5°C) and substituting them into eq. 3. All correlation curves were fitted using the free online QuickFit 3.0 software. FRAP and FCS data were plotted using GraphPad Prism version 8.0.2.

3.2.19 Expression and purification of rHMGB1

The pET19b expression vector carrying the full length human HMGB1 gene with C23S, C45S, C106S and E204C mutations (kindly provided by Jennifer Kugel at University of Colorado

Boulder, USA) was transformed into Rossetta (DE3)pLysS and grown overnight at 37°C incubator on LB agar plates containing 100 µg/ml ampicililin and 37.4 µg/ml chloramphenicol. A single transformed colony from the plate was used to inoculate 5 ml LB with antibiotic. The small culture was incubated overnight at 37 °C with shaking. The small culture was used to inoculate 100 ml of LB containing D glucose (100 ml LB, 2.4 mM NaOH, 0.2 g D-glucose) and antibiotic in a 500 ml culture flask. The culture was grown at 37°C with shaking until an OD_{600} of 0.5 was attained upon which expression was induced using 0.5 mM IPTG and the cells were grown for a further 3 hours. The culture was transferred into 50 ml centrifuge tubes and pelleted at 5000 RPM for 15 min. The supernatant was discarded leaving a small volume to resuspend the pellet in. The cells were then transferred into a 1.5 ml Eppendorf tube and pelleted again. The supernatant was discarded, the pellet flash-frozen and stored at -80°C.

To extract the protein, 2 ml of lysis buffer (20 mM Tris pH 7.9, 500 ml NaCl, 10% glycerol, 5mM imidazole, 5 mM beta mercaptoethanol (BME) and 0.2 mM PMSF) was added to a thawed pellet from 100 ml culture, the pellet was resuspended then the cells sonicated 5x on ice (30 s on /30 s off). The lysate was then centrifuged for 15 min at 4°C at 15000 RPM. The supernatant containing the protein was transferred into a packed Nickel column and then kept at 4°C for 1 hr with rocking motion. The supernatant was allowed to flow through, then the resin washed with 1 ml of lysis buffer followed by 3 ml of lysis buffer containing 50 mM imidazole. The protein was eluted using lysis buffer containing 250 mM imidazole. The column was stripped with lysis buffer supplemented with 1 M imidazole.

Following elution from the nickel column, the buffer was exchanged using a 10K MWCO spin column and 50 ml degassed dialysis buffer (20 mM Tris pH 7.9, 50 mM KCL, 10% glycerol, 100 mM PMSF, 100 mM $MgCl_2$ and 1 mM DTT). After buffer exchange the protein sample in about 250 µl was centrifuged at 18,000 RPM for 30 min at 4°C and the supernatant transferred to a dsDNA cellulose column and incubated for 1 hr at 4°C with rocking motion. The supernatant was allowed to flow through, the resin washed 3x with 3 ml wash buffer (20 mM Tris pH 7.9, 50 mM NaCl, 10 % glycerol, 5mM $MgCl_2$ and 1mM DTT) and the protein eluted using wash buffer with 500 mM NaCl. The column was stripped with wash buffer containing 1 M KCl. The protein was then desalted using 10K MWCO spin column and degassed dialysis buffer as above without DTT. Purification was confirmed using a 12% SDS PAGE gel

electrophoresed for 1 hr at 150V. Samples were centrifuged at 18,000 RPM for 30 min at 4°C, aliquoted, flash frozen and stored at -80°C. Quantification was carried out using Lowry assay and known amounts of BSA controls. Measurements were also made on the Nanodrop.

3.2.20 Fluorescence labelling of rHMGB1

Labelling of rHMGB1 with Alexa 647 C2 maleimide (Thermo scientific) was done following the manufacturer's instructions. To reduce the disulphide bonds in the protein, 750 µg of rHMGB1 in degassed buffer A (100mM Tris pH 7.1, 50 mM KCl, 10% glycerol, 0.2 mM PMSF and 5 mM $MgCl_2$) was mixed with DTT to a final concentration of 10 mM and incubated at 4°C for 2 hrs. DTT was removed using a spin column and 20 ml buffer A. 1.5 µl of 8 mM Alexa 647 C2 maleimide was added to the sample and incubated in the dark at 4°C overnight. Unbound dye was removed using 10K MWCO microfuge spin column and sample washed with column wash buffer (20 mM Tris pH 7.9, 50 mM KCl and 5 mM $MgCl_2$). Samples were quantified by measuring absorbance at 280 nm and compared to a standard curve prepared from known amounts of BSA. Glycerol was added to a final cc of 10 % and samples stored at either -20°C for short term or -80°C for long-term storage.

3.2.21 Electrophoretic mobility shift assay (EMSA)

To determine the binding affinity of the labelled rHMGB1 to various topological forms of plasmid DNA, gel electrophoresis was carried out. Native pEGFP C3 plasmid DNA was either nicked or linearized using Nb.Mva1269I and ECoRI (Thermo scientific), respectively, using the manufacturer's instructions. The DNA samples were then cleaned using gel cleaning kit (QIAGEN) following the manufacturer's instructions. DNA was quantified by measuring the absorbance at 260 nm on the Nanodrop. An equal amount (0.5 µg) of linear, nicked and native plasmid DNA was mixed in 20 µl of protein binding buffer (50mM NaCl, 20 mM Tris HCl pH7.5 and 0.2 mM EDTA). To this DNA mixture, varying amounts of rHMGB1 was added per sample as indicated on the gel (Fig. 23a) and incubated on ice for 40 min on ice. The samples were then loaded to a 1% agarose gel in 0.5x TBE and run for at 36 V for 15 hours at 4°C. The gel was stained with 0.5 µg/ml EBr and then imaged. The image was processed using Fiji ImageJ.

4. RESULTS

PART 1

4.1 INTERCALATION OF SMALL MOLECULES *IN SITU*

4.1.1 The cell membrane is not the only barrier to EBr staining *in vivo*

To evaluate the accessibility of DNA in native chromatin to small molecule intercalators, I utilized the classical intercalating dye EBr. Live cells incubated with 10 μM EBr rapidly took up the dye and its fluorescence could be observed in the cytoplasm and the nucleoli (Fig. 9b, c). The cytoplasmic fluorescence was likely due to dye intercalation into mitochondrial DNA and double-stranded RNA (dsRNA). The nucleolar signal was likely due to double-stranded RNA in ribosomal subunits as it was significantly diminished or eliminated when fixed nuclei were treated with RNase A. There was, however, minimal EBr fluorescence observed from the chromatin even after prolonged incubation with the dye. Following cell permeabilization with either Streptolysin O toxin (Fig. 9f, g) or Tx-100 (Fig. 9i, j), there was a somewhat elevated chromatin staining and a conspicuous increase in nucleoli fluorescence. This indicates that following permeabilization, a higher concentration of EBr is attained in the cell, staining the chromatin only moderately, however.

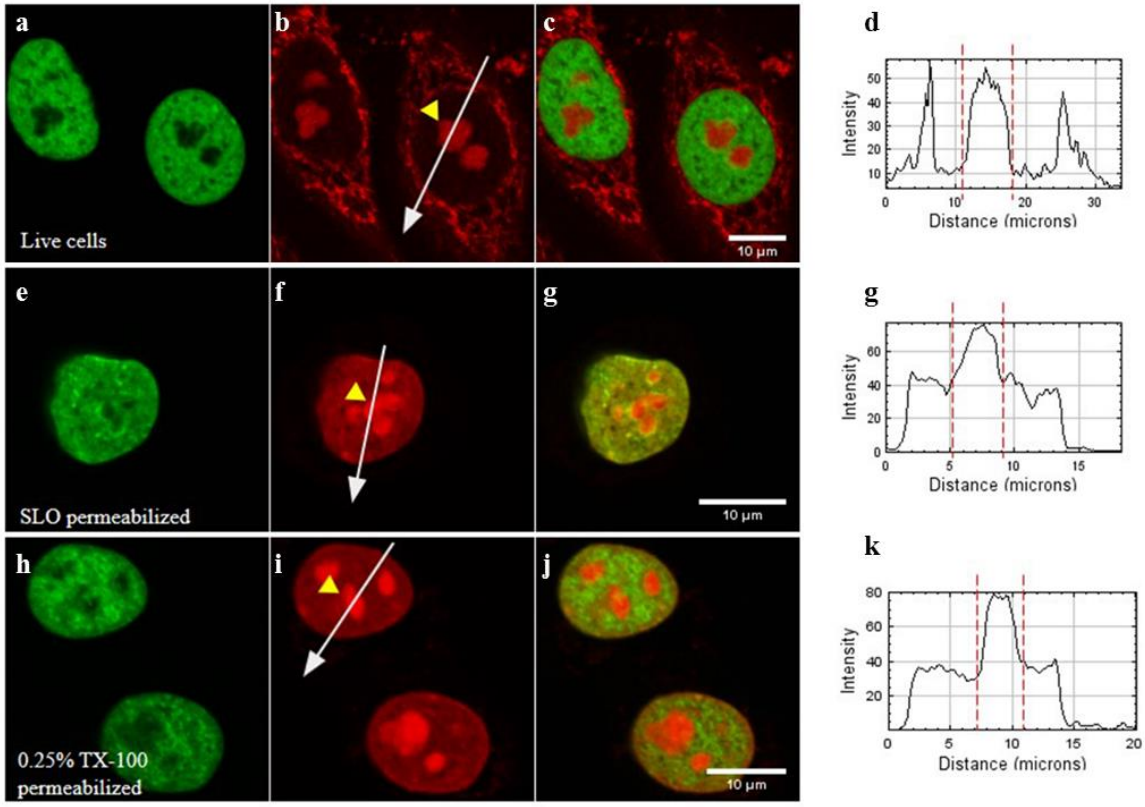

Figure 9: Uptake of EBr and chromatin staining by live and permeabilized HeLa cells expressing GFP tagged histone H3. Representative nuclei are shown here. (a-d) live cells, e-g) SLO permeabilized cells and (h-k) Tx-100 permeabilized cells. Line scans on the right show EBr fluorescence along the white arrow. Green, H3-GFP; red, EBr fluorescence; yellow arrowhead, nucleoli.

To investigate further the possibility that low levels of chromatin fluorescence was due to a limited amount of dye permeating the cell membrane, we incubated live cells with 10 µM EBr and then in a whole-cell patch-clamp setup, directly microinjected a single cell with the same dye concentration. The patch-clamp apparatus used was coupled with a confocal microscope which allowed us to monitor staining in real-time. We observed that the dye gradually spread across the cytoplasm from the point of microinjection and into the nucleus where it stained the nucleoli first. EBr fluorescence in the chromatin was only observed after about 5 minutes and it took about 15 minutes before the chromatin was fully stained (Fig. 10i). During the whole observation period, the spatial distribution and level of EBr fluorescence in the neighbouring cells did not change and was much less compared to that of the microinjected cell.

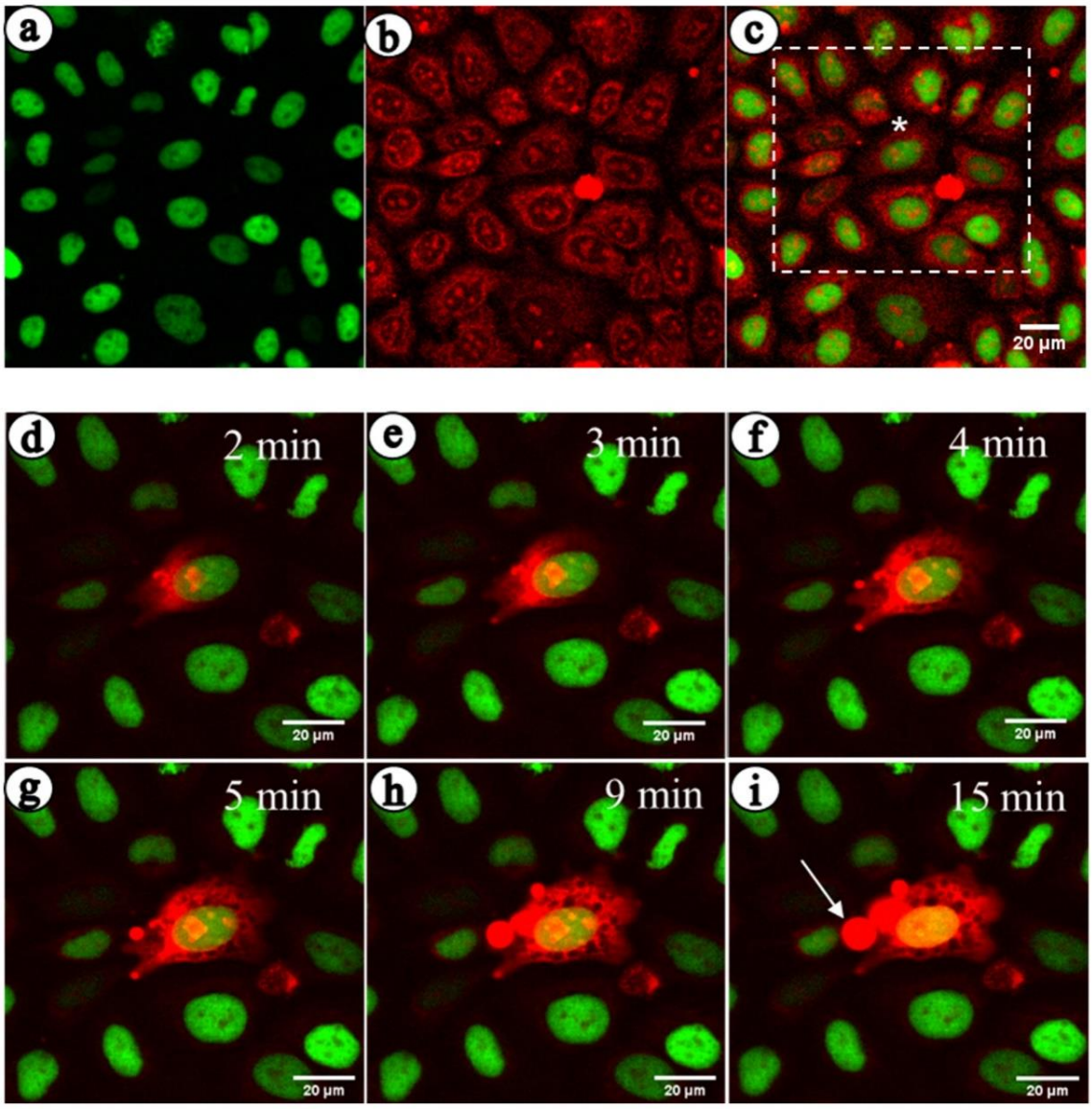

Figure 10: Native chromatin does not readily allow intercalation of EBr. a - c) Live HeLa cells expressing GFP tagged histone H3 were incubated with 10 µM EBr then imaged by a confocal microscope, a) H3-GFP b) EBr, c) merged image. The cell marked with a white asterisk (*) in image c) was microinjected with the same concentration of EBr and its fluorescence followed for a period of 20 mins. The white arrow points to a cytoplasmic bleb filled with EBr likely binding to lipid micelles.

This confirmed that, though EBr is a small molecule, only a limited fraction of the dye in solution diffuses across the cell membrane. However, even when the cell membrane barrier is overcome as in the patch-clamp setup, DNA in chromatin does not readily take up the intercalator. This suggests that intercalation into chromatin in a live cell is hindered to a considerable extent, whereas it is freely permitted to bind dsRNA and mitochondrial DNA.

4.1.2 Intercalation into nucleosomal DNA closely correlates with nucleosome core particle disassembly

The nucleosomal structure is known to inhibit the binding of regulatory factors to DNA *in vivo*. To determine whether it would equally affect the binding of a small molecule, I quantified EBr binding to DNA *in situ* following salt extraction of fractions of the histone compliment. Treatment of nuclei with salt elutes histones from chromatin in a concentration dependent manner [149]. Linker histones are the first to be eluted by about 0.35 M NaCl, followed by the H2A-H2B histone dimers eluted at 1.2 M NaCl and lastly the H3-H4 histone tetramers at about 1.55 M NaCl. Recently, Imre and colleagues [150] developed an assay to monitor salt-induced histone elution on a cell-by-cell basis. Based on this approach, I developed an assay to study intercalation with minimal perturbation to the native chromatin structure. Since EBr also binds to dsRNA, I included an RNase A digestion step to eliminate the contribution of dsRNA to the EBr fluorescence measured. This allowed me to evaluate the effect of each of the histone proteins in limiting EBr intercalation, in a large number of cells still on a cell-by-cell basis. I observed that the mean EBr fluorescence per nuclei was unchanged up to pre-treatment with 0.75 M NaCl. Above this salt concentration, the EBr fluorescence gradually increased up to about 3-fold relative to the initial staining at 1.55 M NaCl. This increase was observed in both HeLa and human peripheral blood mononuclear cells (HPBMCs). Remarkably, EBr fluorescence started to rise when core histones were also beginning to be released, at around 0.75 M NaCl (Fig. 11 a, b).

To ascertain whether the binding of other intercalating agents would be similarly affected by the presence of nucleosomes, the binding of the bis-intercalating dye YOYO-1 and psoralen were also measured. Similar to EBr, both bTMP binding and YOYO-1 fluorescence began to increase concurrently with core histone elution (Fig. 11 c, d).

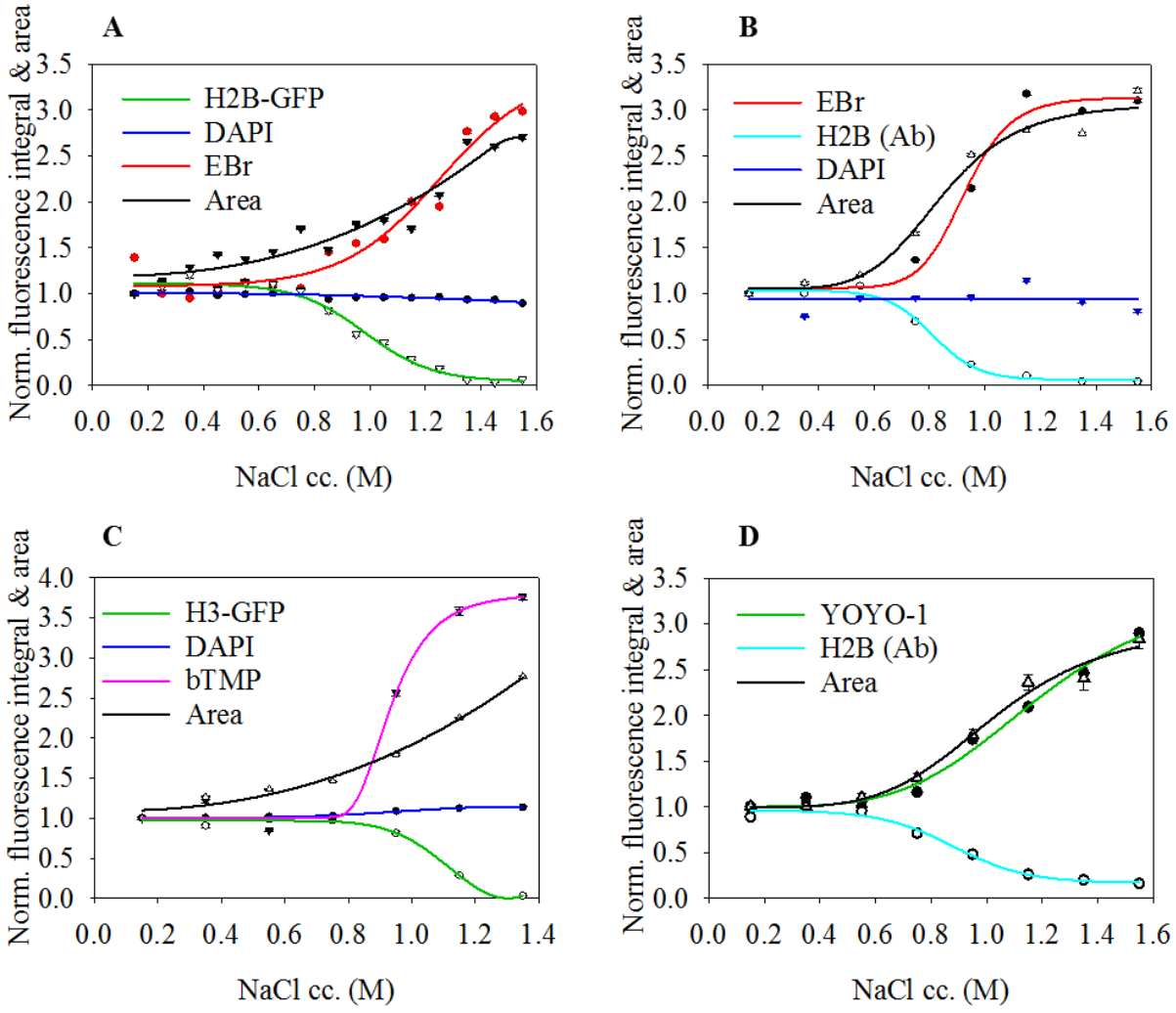

Figure 11: Increase in intercalator binding closely correlates with core histone elution: Changes in intercalator binding and nuclear area following histone elution. Following salt-induced histone elution, the remaining histones were detected by the GFP tag (A & C) or by immunofluorescence labelling (B & D). A) EBr intercalation in HeLa H2B-GFP cells. B) EBr intercalation into HPBMCs, C) Biotinylated trimethylpsoralen (bTMP) binding to HeLa H3-GFP cells. D) YOYO-1 binding in HeLa cells. Plots show a representative experiment of three replicates. Mean and SEM of ≥750 nuclei in G1 phase cells normalized to control samples maintained in PBS-EDTA.

Remarkably, salt-induced histone elution was accompanied by an increase in the cross-sectional area of individual nuclei (Fig. 11 a-d) confirming the role of nucleosomal packaging in DNA compaction. Furthermore, the nuclear area starts to enlarge even before the core histones would be evicted. As seen in Fig. 12, the nuclei remain intact, with most of the chromatin still within the confines of the nuclear lamina even for samples treated with 1.35 M NaCl.

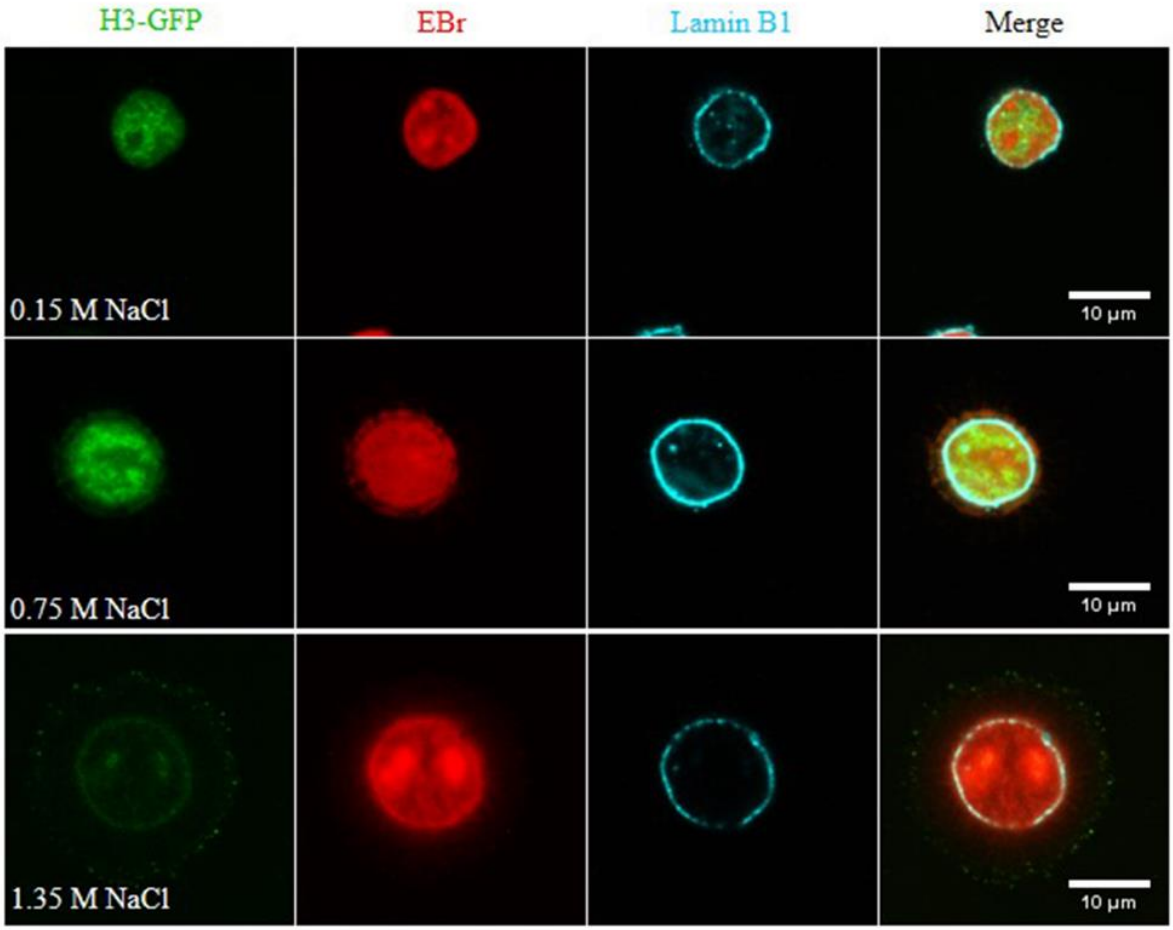

Figure 12: Chromatin remains within the confines of the nuclear lamina even after salt treatment. Representative images of agarose embedded, salt treated nuclei stained with EBr. Green, H3-GFP; red, EBr fluorescence; cyan, lamin B1 immunofluorescence.

4.1.3 Initial intercalator binding is largely limited to the linker and nucleosome free regions

The findings above (Fig. 11) suggest that intercalation occurs in regions not bound to nucleosomes, which comprises the linker DNA and NFRs. Intercalation into the 147 bp of DNA wrapped around each octamer appears to occur only when the core nucleosome particle is disassembled. To learn if the initial binding involved mainly the linker DNA only, formaldehyde fixed nuclei were digested using varying cc. of MNase. This resulted in a spectacular decrease of EBr staining without a similar loss of mononucleosomes as deduced from the H2B-GFP fluorescence (Fig. 13a). This indicates that the region initially stained by EBr is sensitive to MNase confirming it to be linker DNA. Similarly, this region was found to be hypersensitive to DNase I digestion as determined by *in situ* nick labelling (Fig. 13b). Above 1.05 M NaCl, there was a reduction in the number of nicks detected which was accompanied by a reduction in the DAPI fluorescence. This indicates loss of DNA as the DNase I digestion is enhanced in the absence of nucleosomes.

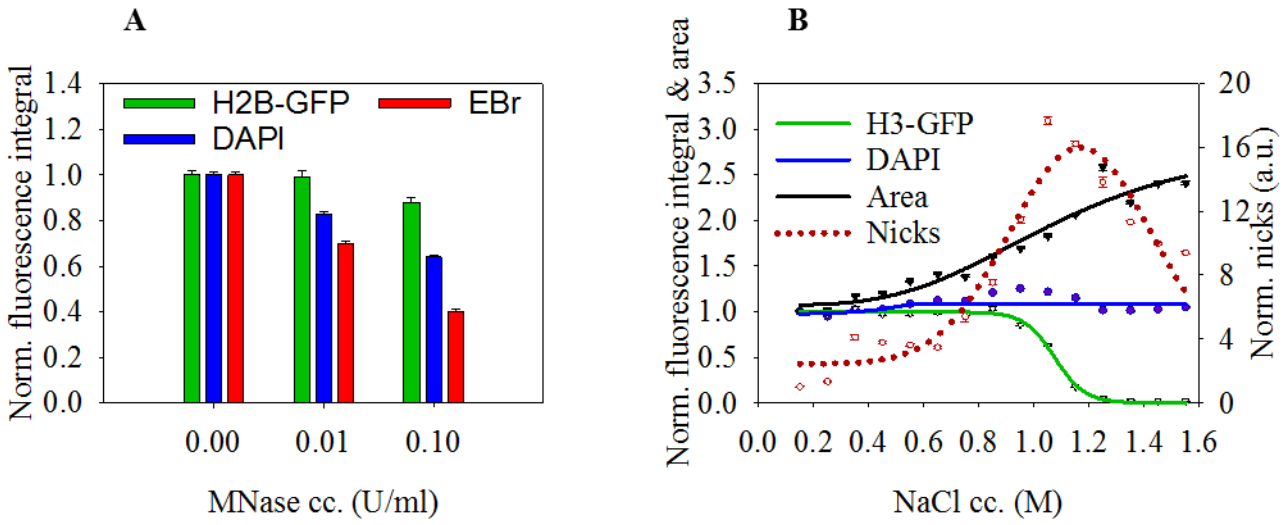

Figure 13: Initial intercalator binding in nuclei is limited to linker DNA. A) Reduction in EBr fluorescence following a brief MNase digestion of formaldehyde fixed, HeLa H2B-GFP nuclei. **B)** Marked increase in DNase sensitivity following core nucleosome destabilization as indicated by number of nicks (right Y-axis). The graphs show the results of one representative experiment of three independent replicates. Mean ± SEM of G1 phase cells normalized to the control, n ≥750.

By comparison, binding of DAPI, a minor groove binding dye which is of similar size as EBr, was unaffected by the elution of histones either when applied to nuclei already stained with EBr as in Fig. 11 or when applied to nuclei in its absence (Fig. 14). This confirms that a small molecule can freely access the DNA *in situ*, and thus the lack of EBr intercalation into chromatinized DNA was not due to limited access.

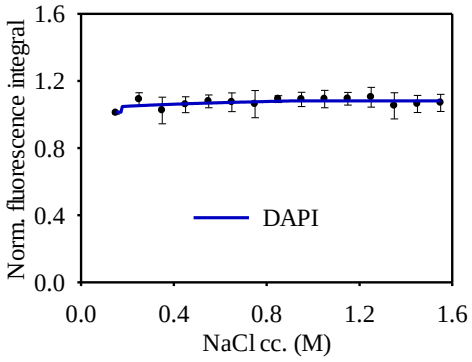

Figure 14: DAPI staining of DNA in chromatin is unaffected by the presence of histones. Fluorescence profile of HeLa nuclei treated with varying concentration of NaCl. Plot shows mean and SEM of ≥750 G1 nuclei, normalized to the control nuclei maintained in PBS-EDTA.

It has been previously suggested that DNA binding molecules may also bind to histone proteins [151]. If the histones bind a relatively large fraction of the available intercalator molecules, then there would be a limited number of molecules available to bind DNA. To rule this out, I measured the amount of dye left in the supernatant after staining nuclei. I found that about 75% of applied EBr was left in the supernatant. Furthermore, there was no difference in the amount of EBr left in the supernatant from wells where nuclei were treated with low salt (histones present) and those treated with high salt (histones absent). This means that even if the histones were to bind EBr, there was still a sufficiently high amount of EBr available to intercalate into DNA (Fig. 15a). Besides, using fluorescence lifetime imaging (FLIM), I detected only one fluorescence component in the agarose embedded, RNA depleted nuclei. The lifetime of this component was 22.6 ns which corresponds to EBr intercalated into DNA (Fig. 15b). Applying the same concentration of EBr to histones in solution yielded only one life time component corresponding to that of EBr in solution i.e. 1.8 ns. These FLIM measurements confirm that the

increase in fluorescence recorded in my experiments was indeed originating from increased intercalation of EBr into DNA.

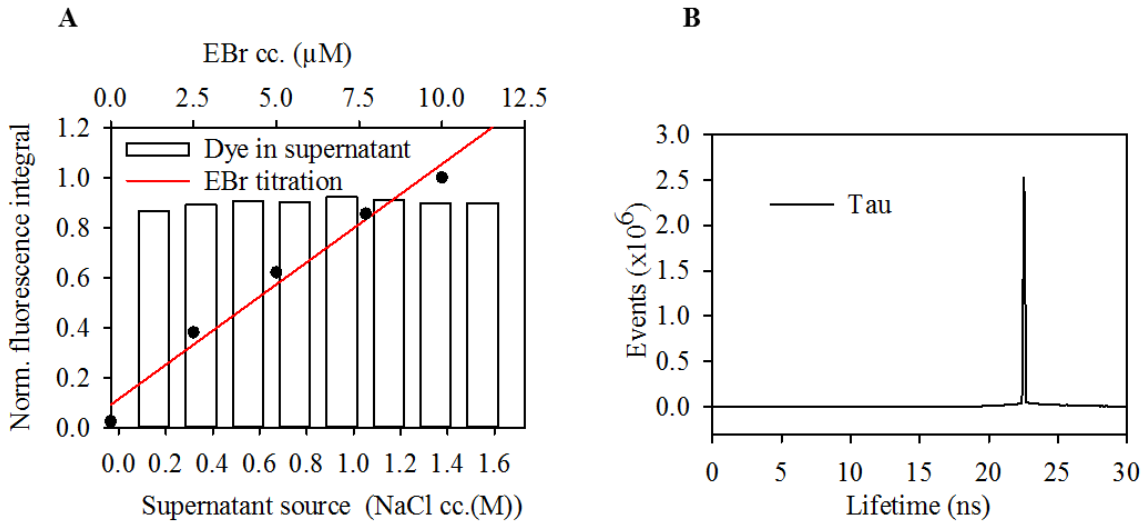

Figure 15: EBr fluorescence reflects the amount of DNA not bound to nucleosomes A) The amount of dye remaining in the supernatant after staining of the nuclei. The fluorescence of EBr in solution was determined by spectrofluorimetry. Bars were normalized to the fluorescence of 10 µM EBr in PBS-EDTA. The red line shows the EBr titration curve (upper axis). **B)** EBr fluorescence lifetime of agarose embedded, RNA-depleted, salt treated nuclei stained with the dye. At every salt pre-treatment a single component of ~ 22.6 ns was detected.

Having ruled out limited access as well as binding of EBr by histones from among the possible mechanisms by which the nucleosome structure could inhibit intercalation, I investigated the possible role of the topological constraint exerted on the DNA by the nucleosomal structure. The DNA wrapped around the histone octamer is held in place by several hydrogen and electrostatic bonds which severely limit its degree of freedom, as described in Introduction. Removal of these bonds as it occurs when histones are eluted by salt, may then increase the ability of DNA to deform to accommodate an intercalator. To assess the effect of constraint, I fixed salt pre-treated nuclei with either formaldehyde or ethanol then stained them with EBr and DAPI. In control experiments, the fixation was done post staining. The results showed that whereas ethanol had no effect on EBr intercalation (Fig. 16a), formaldehyde fixation negatively affected EBr intercalation (Fig. 16b). The effect of formaldehyde was much more pronounced in nuclei treated with a low NaCl cc. (0.35 M) when all the core histones were still present.

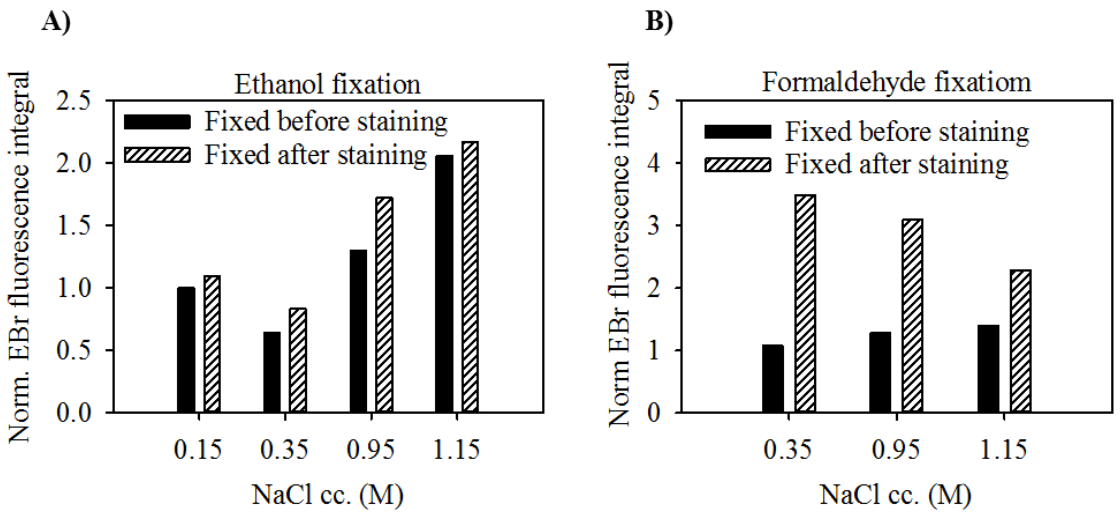

Figure 16: Crosslinking of DNA to histones by formaldehyde negatively affects EBr intercalation, as opposed to the lack of effect of ethanol fixation. EBr staining of agarose embedded, RNA-depleted, salt treated nuclei fixed with 70% ethanol (**A)** or 4% formaldehyde (**B)** before or after staining.

4.1.4 Enhancement of EBr intercalation by nicking of the DNA

Linker DNA is free of nucleosomes and its twist and writhe can freely interconvert however its ends are not free to rotate. To assess whether this would limit the level of intercalation, I compared the intercalation of EBr into supercoiled, linear and relaxed plasmid DNA. I observed that covalently closed supercoiled plasmids took up less EBr compared to an equal amount of linear and relaxed forms, and the difference was more pronounced at high EBr concentration (Fig. 17a). Similarly, nuclei obtained from cells exposed to 300 Gy of X-ray irradiation took up more EBr when compared to nuclei from control cells (Fig 17 c, d). 300 Gy X-ray radiation is sufficient to induce just a single nick within a 50 kb loop (Fig. 17b). The increase in EBr fluorescence of nicked vs control samples is present even at low salt (<0.75 M NaCl), where intercalation is limited to the linker and NFR regions and the nucleosomes are in place. In other words, this increase was not due to more DNA becoming available for EBr intercalation as it would happen when core histones are eluted. As shown in Fig. 17 c, d, the amount of core histones remaining in the nuclei derived from irradiated and non-irradiated cells below 0.75 M NaCl was equal. Above this salt concentration, irradiation sensitized the core histones H2B-GFP to salt elution.

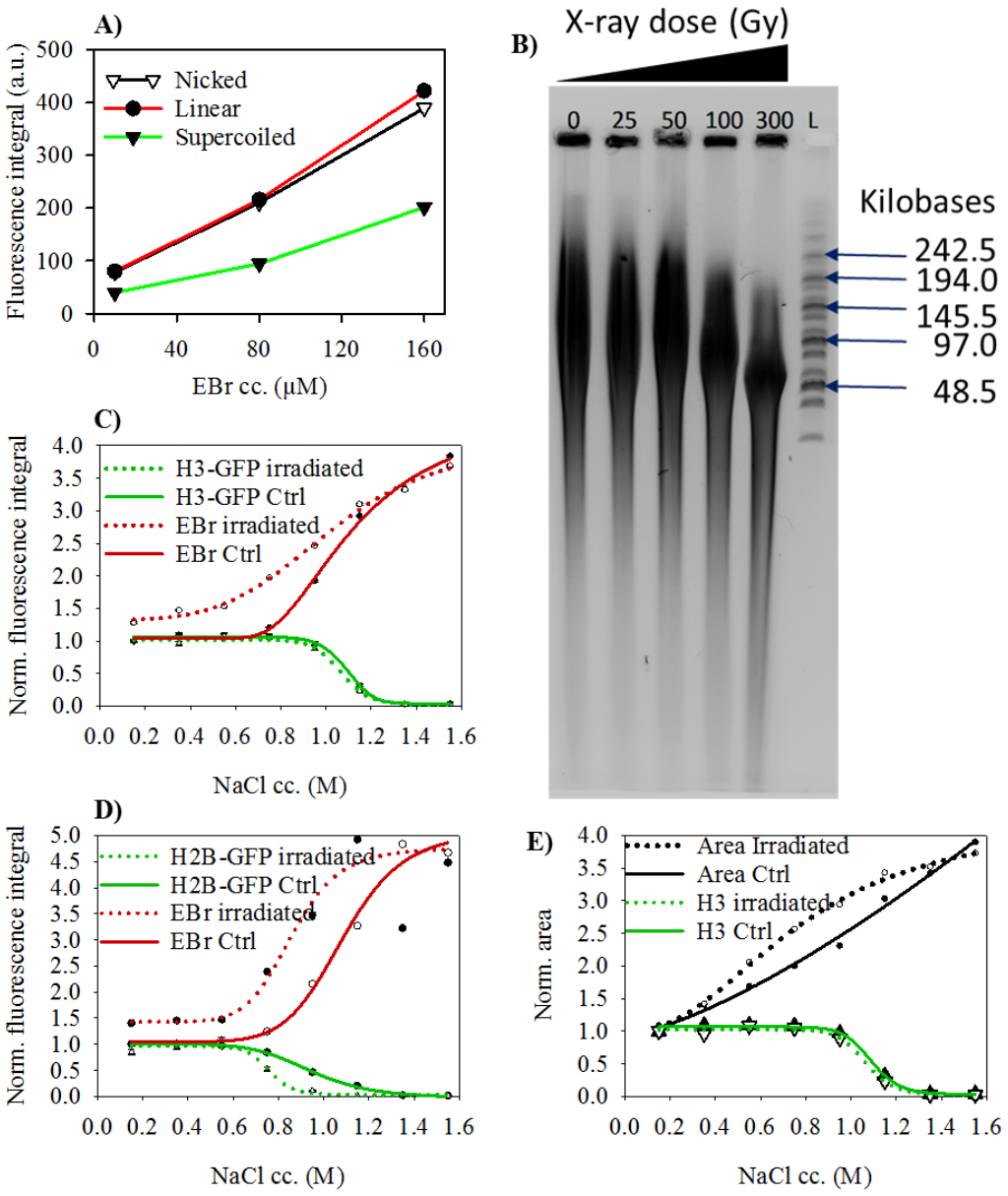

Figure 17: Relaxation of extranucleosomal torsion increases EBr intercalation. A) EBr fluorescence profile of linear, nicked and supercoiled plasmid DNA as a function of EBr concentration. **B)** Nick frequency as a function of X-ray dose. Nicks generated by irradiation were converted to double-strand breaks using S1-nuclease and the fragments separated by CHEF. **C** & **D**) EBr intercalation and histones remaining in the nuclei. H3-GFP (**C**) or H2B-GFP (**D**) in agarose embedded, RNA-depleted, salt-treated HeLa nuclei prepared from cells irradiated with 300 Gy or from un-irradiated cells (Ctrl). **E**) Change in area shown together with the H3-GFP data of panel C. Plots shows one representative experiment of three replicates. Mean ±SEM values of G1 phase nuclei normalized to control, n ≥ 750.

Transcription is expected to be an important determinant of the supercoiling state *in vivo*, so to check if it affects the binding of EBr *in situ*, I evaluated the binding of EBr to nuclei from transcription inhibited cells and compared it with the control. I observed a minimal increase in EBr binding in actinomycin D or α-amanitin treated cells (Fig. 18).

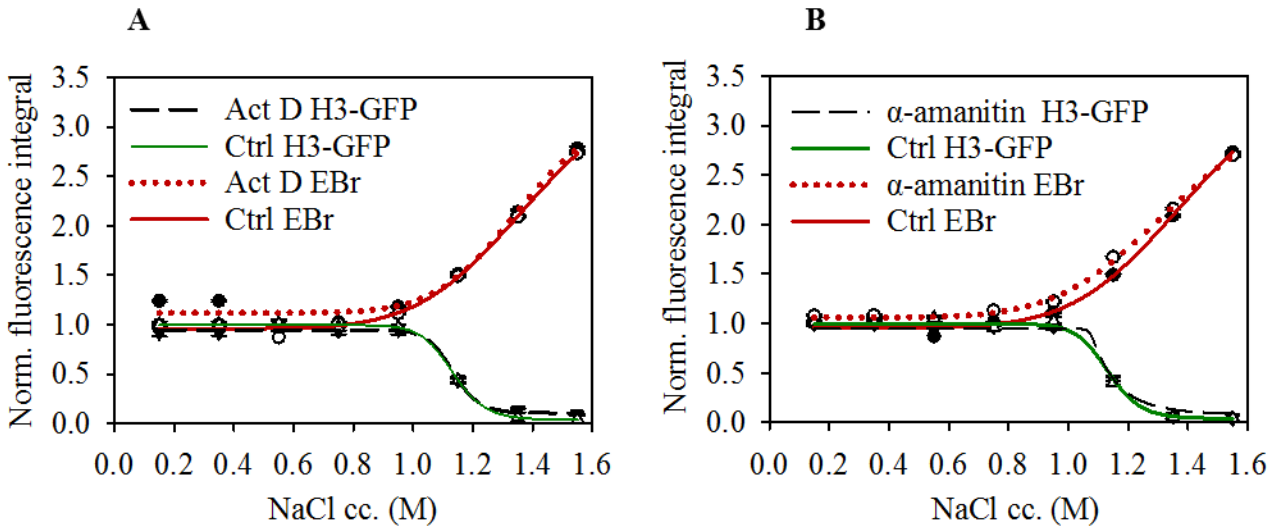

Figure 18: Transcription inhibition slightly increased EBr interaction. EBr fluorescence and remaining H3-GFP histones in nuclei derived from cells treated with either 10 µg/ml actinomycin D (**A**) or 50 µg/ml α-amanitin (**B**), compared with nuclei from untreated cells (Ctrl). Plots show one representative experiment of three replicates. Mean ±SEM of fluorescence and area of ≥750 G1 phase nuclei were normalized to the control values.

The results above demonstrate that the intercalation of a small molecule to DNA *in situ* can be increased by relieving the topological strain imposed by packaging of DNA into chromatin. Salt-induced elution of histones (Fig. 11), which perhaps mimics the nucleosome destabilization achieved by chromatin remodellers *in vivo*, converts the DNA around the NCP from a stiff toroid to a flexible plectoneme which is deformable and whose twist and writhe can easily interconvert. Additionally, nicking of the DNA increased binding of the intercalator to the extranucleosomal DNA even in the presence of nucleosomes (Fig. 17).

PART 2

4.2 FACTORS DETERMINING HMGB1 BINDING TO CHROMATIN

Next, I asked if the rules governing small molecule intercalation would hold true for a DNA binding protein whose binding involves intercalating moieties. To evaluate this, I have studied the binding of HMGB1 to DNA *in vivo* in response to changes in DNA supercoiling. *In vitro*, HMGB1 has previously been shown to preferentially bind supercoiled DNA over linear and relaxed forms [128].

PART 2/A

4.2A HMGB1 BINDING TO CHROMATIN IS AFFECTED BY INTERCALATORS

4.2.1 EBr causes recruitment of HMGB1 to binding sites on chromatin

To evaluate the effect of changes in supercoiling and DNA helical properties on HMGB1 binding, live U2OS^{2FP} cells were treated with varying concentrations of EBr and binding of HMGB1 was assessed by confocal microscopy. Uptake of EBr by the cells was evident from the appearance of red fluorescence in the cytoplasm and an increase in the red fluorescence in the nuclei (Fig. 19a). Intensive EBr staining was observed in the nucleoli indicating the ease with which an intercalator binds to double stranded RNA in ribosomal subunits compared to the DNA in chromatin. In chromatin, EBr intercalation is largely limited to the linker DNA [152]. Though the cells used here also express H2B-RFP, increase in EBr intercalation into DNA is evident from the increase in red fluorescence in the nuclei. EBr also induced chromatin condensation, most evident at the highest cc. of EBr used here (Fig. 19a panel j).

In the presence of EBr, GFP-HMGB1 was gradually reduced and eventually lost from the nucleoli, what can be attributed to either displacement of HMGB1 from its binding sites in the nucleoli or loss of fluorescence due to energy transfer to the EBr bound to double-stranded

RNA in ribosomal subunits there. In the rest of the nucleus, the GFP signal became structured, implying that it became more chromatin bound. To confirm this impression, point FRAP measurements were made. The fluorescence recovery time increased with increasing concentration of EBr, from 25 ms for the control samples up to about 60 ms for samples treated with 50 µM EBr (Fig. 19b). A further increase of EBr concentration from 50 to 100 µM yielded a reduction in recovery time.

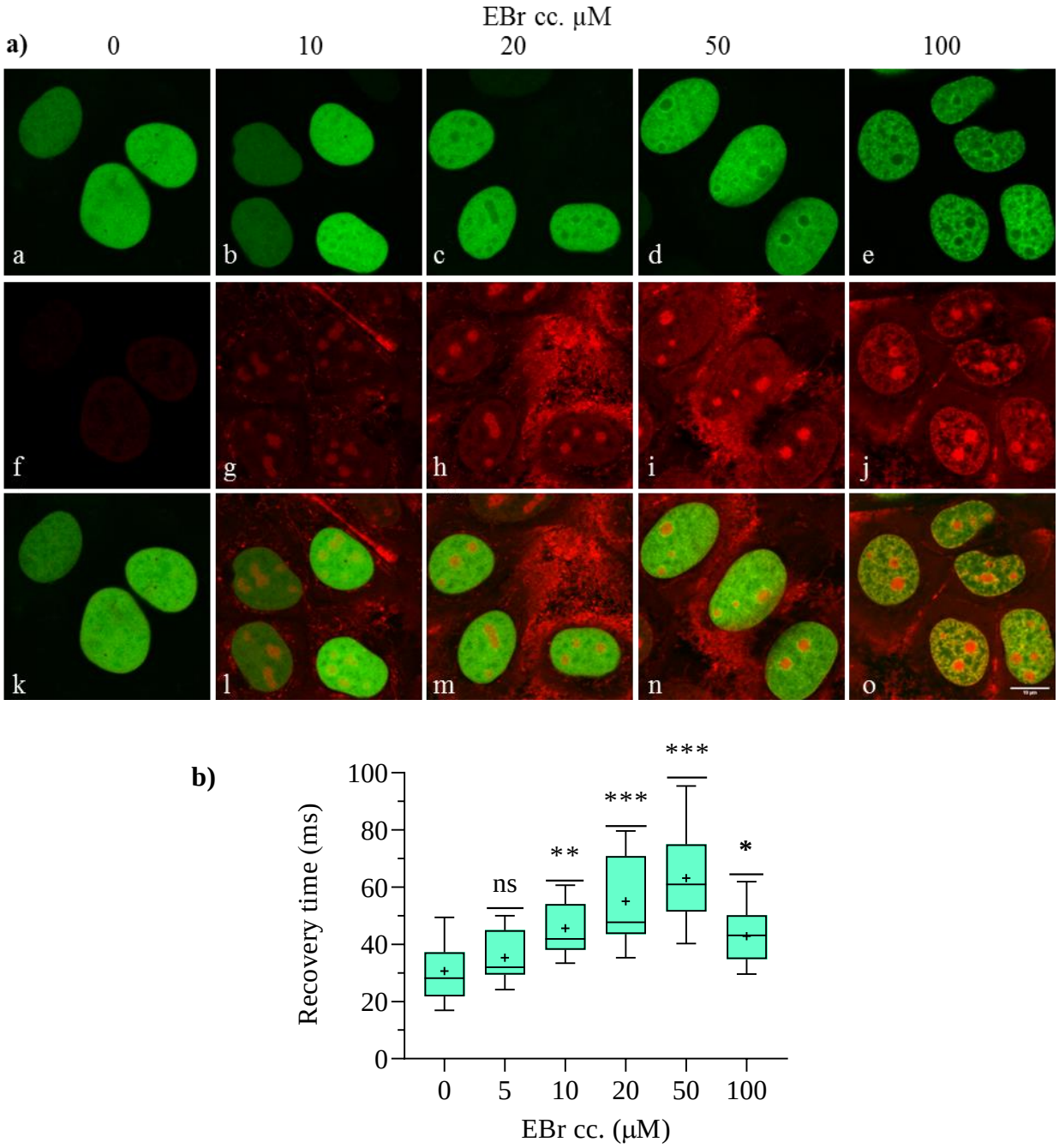

Figure 19: EBr increases the binding of HMGB1 to chromatin in a dose dependent manner. U2OS^{2FP} were incubated with 0, 10, 20, 50 and 100 µM EBr for 1 hr and then imaged by confocal microscopy. **a**) Representative nuclei showing GFP-HMGB1 (panel a-e), EBr and H2B-RFP (panel f-j) and the merged images (panel k-o). The fluorescence gain of the red channel in the control sample (panel f) was increased on the image to make it visible. **b**) Fluorescence recovery time of GFP-HMGB1 in EBr treated cells as measured by point FRAP. Very similar results were obtained when EBr was allowed to enter the cells by electroporation (not shown). *P*, * = 0.022; **<0.0047; *** < 0.0001; +, mean. Green, GFP-HMGB1; Red, Dox and H2B-RFP.

4.2.2 Dox exerts a biphasic effect on HMGB1 mobility *in vivo*

To check whether these observations were unique to EBr or could apply to other intercalating drugs, another intercalator, the anticancer anthracycline Doxorubicin (Dox) was tested. Similar to EBr, Dox caused GFP-HMGB1 loss from the nucleoli and a more structured distribution in the chromatin suggesting that the protein was becoming more chromatin bound (Fig. 20a). However, at Dox cc. > 9 µM, the GFP-HMGB1 signal again became diffuse suggesting that at higher cc., Dox caused the protein to become more mobile. This was also confirmed by point FRAP, the recovery time increased with increasing Dox cc. peaking at 50 ms for samples treated with 4.5 µM and then declined with further increase in Dox cc. (Fig. 20b).

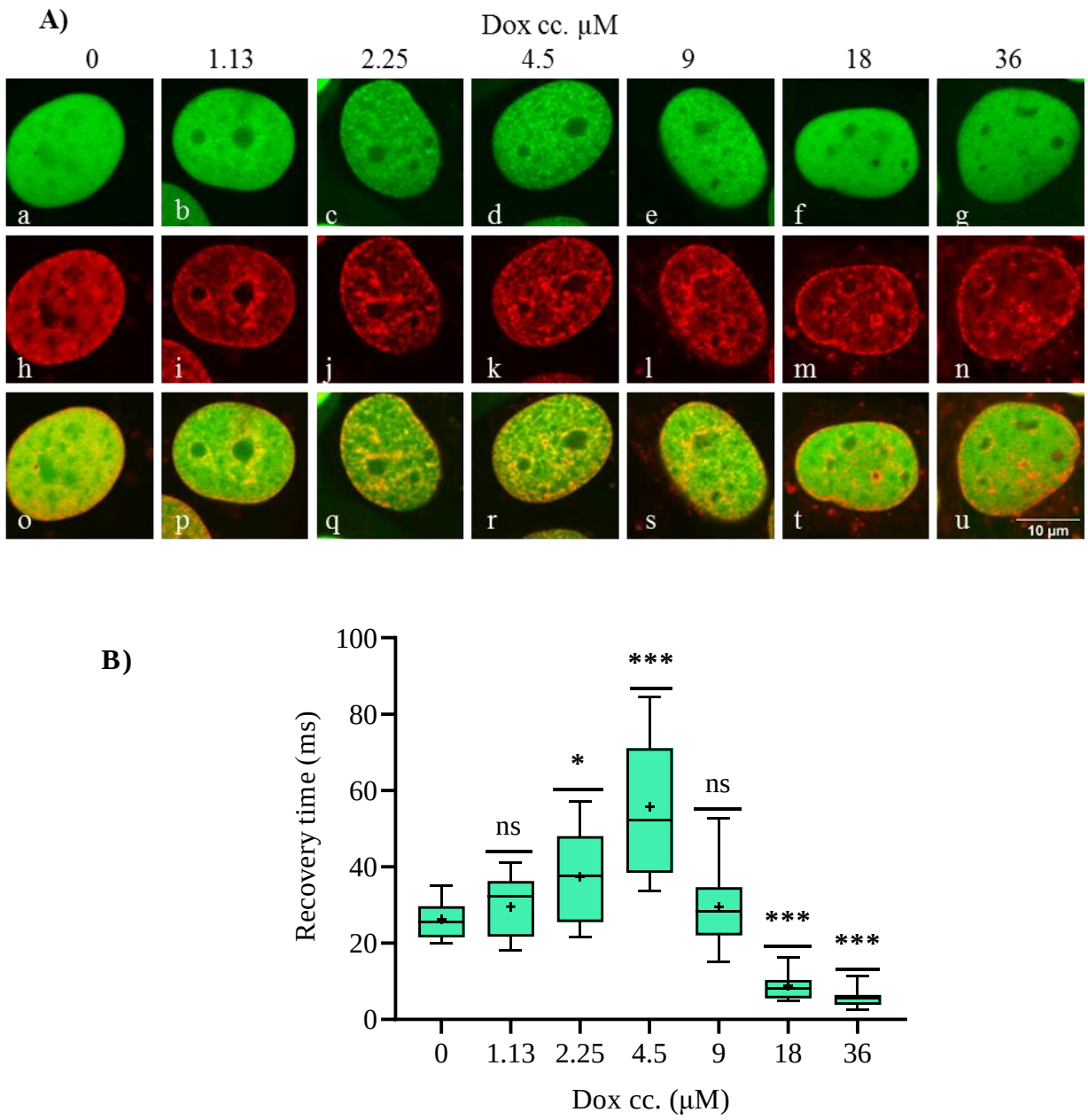

Figure 20: Doxorubicin affects HMGB1 dynamics in a concentration dependent manner. **A)** Representative nuclei of U2OS cells treated with the indicated concentration of Dox for 2 hrs. GFP-HMGB1 (panel a-g), Dox and H2B-RFP (panel h-n) and the merged images (panel o-u). **B)** GFP-HMGB1 recovery time of Dox treated cells as measured by point FRAP. The graph shows one representative experiment of three repeats. *P*, * =0.0295 *** < 0.0001; +, mean.

Drug intercalation to DNA increases the base pair rise while reducing the helix twist by an angle dependent on the intercalator molecule. This decrease in helix twist translates to an overall reduction in DNA twist, which is compensated by an increase in writhe within the chromatin loops. To elucidate the contribution of superhelicity to the recovery profiles generated above (Figs. 19b & 20b), I carried out further experiments as outlined below.

4.2.3 DNA nicking had no effect on HMGB1 binding *in vivo*

To test the possible role of writhe in HMGB1 binding *in vivo*, DNA writhe was relaxed by exposing live U2OS^{2FP} cells to DNA nicking agents: H_2O_2, bleomycin or x-ray irradiation, and GFP-HMGB1 binding to DNA was evaluated by point FRAP. Given the short time interval between nicking and measurement, it was expected that the breaks would still be unrepaired and if they are at all repaired, the original levels of internucleosomal superhelicity, as established in S phase, would not have been regenerated. Thus, if HMGB1 binding is sensitive to negative writhe, its relaxation would reduce its binding. Surprisingly, none of these agents caused a change in the recovery rate (Fig. 21).

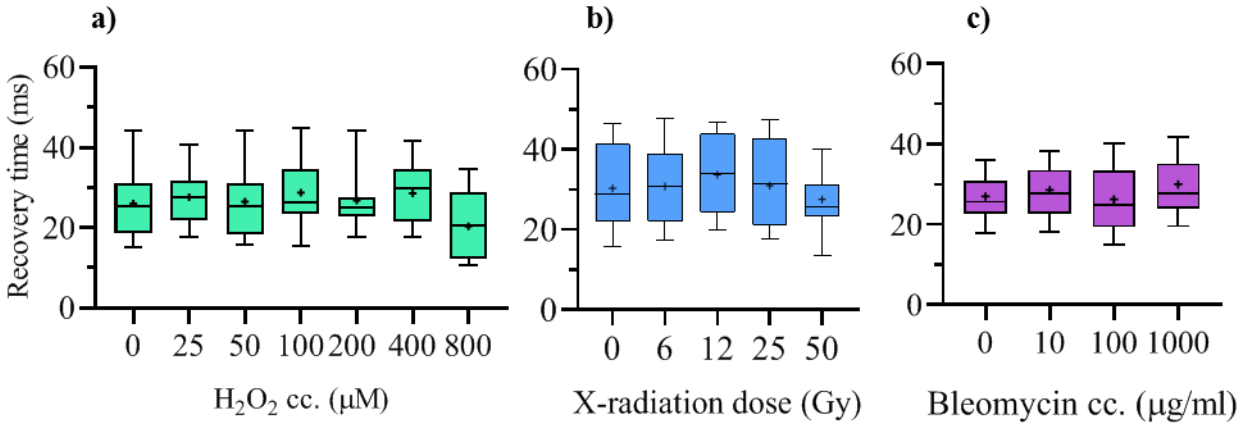

Figure 21*:* Relaxation of supercoiling by nicking doesn't affect chromatin binding of HMGB1. U2OS^{2FP} cells were treated with **a)** 25, 50,100, 200 400 and 800 μM H_2O_2 for 20 minutes or **b)** 6, 12, 25 and 50 Gy of X-ray radiation or **c)** 10, 100 and 1,000 μg/ml bleomycin for 2 hrs, then the mobility of GFP-HMGB1 was measured by point FRAP. Graphs show one representative experiment of three repeats.

To further test the effect of writhe, I evaluated the binding rHMGB1 to CCC plasmid DNA in the presence of varying cc. of Dox by FCS. The recombinant, fluorescently labelled HMGB1 used in this experiment behaved just as expected for the native protein [153]; preferential binding to supercoiled DNA was detected (Fig. 22A). As seen on the gel (Fig. 22A), the migration of supercoiled plasmid DNA was retarded by as low as to 60 rHMGB1 molecules per plasmid molecule and the retardation became more pronounced with increasing amounts of rHMGB1. Migration of the linear DNA was not affected until there was 100 rHMGB1 molecules per plasmid molecule and even then the retardation was only minute compared to supercoiled DNA. The nicked DNA band was not shifted at all for the protein concentration used in this experiment.

4.2.4 Dox decreases the binding of HMGB1 to CCC plasmid DNA

The diffusion constant (D) of rHMGB1 in solution as determined by FCS was 86 $\mu m^2/s$. In the presence of native plasmid DNA, two diffusing components were observed: a fast component corresponding to freely diffusing rHMGB1 (mean D = 90 $\mu m^2/s$) and a slow component (mean D = 5 $\mu m^2/s$) which was interpreted to be DNA-bound HMGB1 (Fig. 22b). Addition of increasing cc. of Dox led to a monotonous decrease in the fraction of HMGB1 bound to plasmid DNA (Fig 22c). This finding suggests that Dox may directly compete with HMGB1 binding or the positive plectonemic writhe it induces, negatively affects the binding of HMGB1 to DNA. Though the DNA: Dox ratios used in the FCS experiment may not directly compare to those of the *in vivo* experiment, however, the monotonous decrease in HMGB1 binding suggests that factors other than the overall DNA twist & writhe partitioning may be responsible for the initial increase in HMGB1 binding to DNA in the presence of an intercalator *in vivo*.

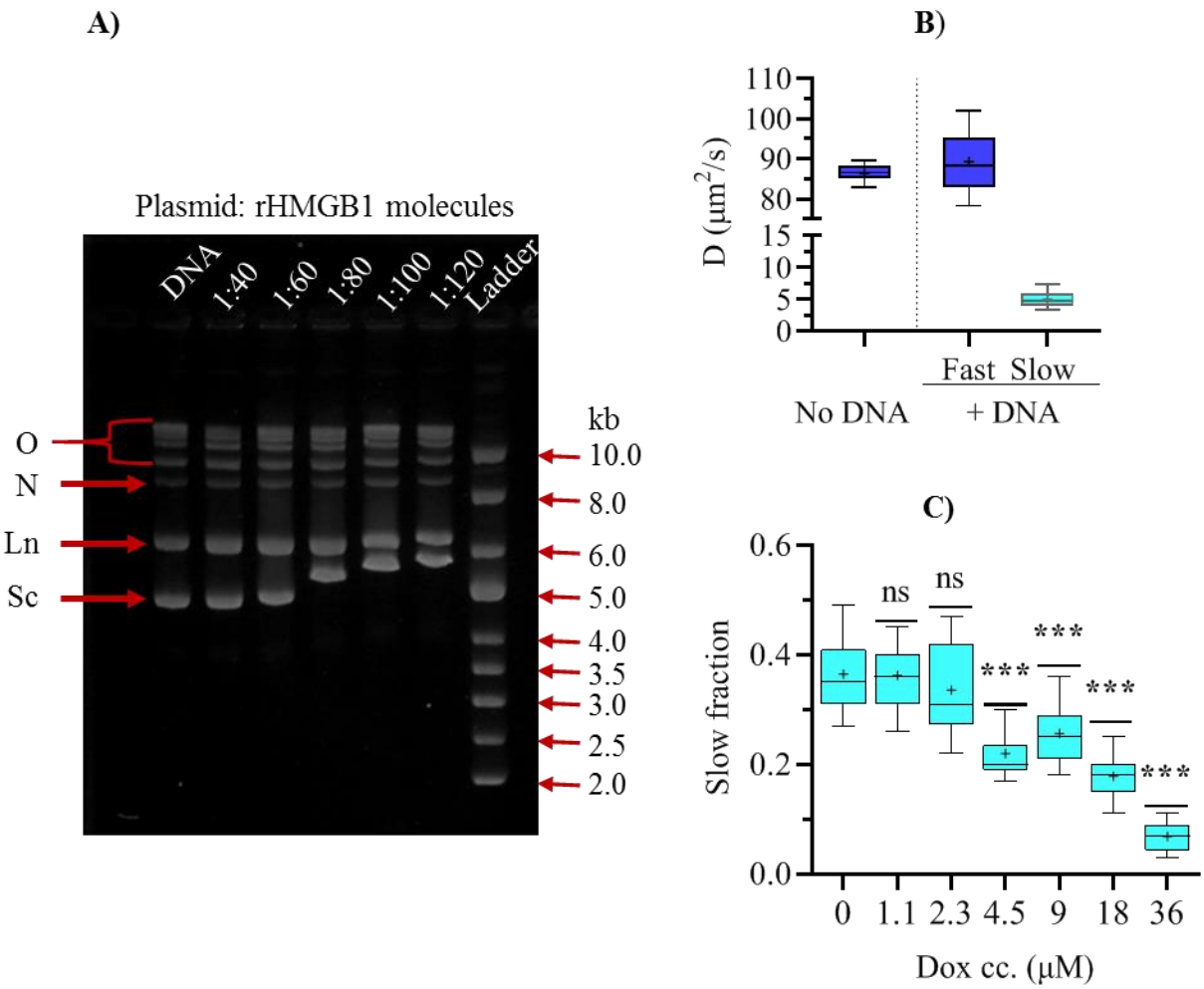

Figure 22: Doxorubicin displaces rHMGB1 from plasmid DNA in solution. **A)** Varying amounts of rHMGB1 were added and allowed to bind 1.5 µg of plasmid DNA mixture (equal amounts of nicked, linear and supercoiled) before being separated by gel elecrophoresis. At the end of electrophoresis the gel was stained with 0.5 µg/ml EBr before imaging. **B**) Diffussion coefficient of Alexa-647 labelled rHMGB1 in solution and in the presence of supercoiled plasmid DNA as measured by fluorescence correlation spectroscopy (FCS). **C)** Fraction of rHMGB1 bound to covalently closed plasmid DNA in the presence of varying concentrations of Dox. O, oligomers; N, nicked; Ln, linear and Sc, supercoiled plasmid DNA.

4.2.5 Dox and EBr displace histone H1 from chromatin in live cells

Previous studies have shown that HMGB1 competes with histone H1 for binding to the linker DNA near the nucleosome dyad [154]. Further, daunomycin, a drug structurally similar to Dox

was shown to evict the linker histone variant H1.1 from the chromatin [155]. To check whether the changes in recovery rate upon intercalator treatment observed here are related to their effect on histone H1 acting as a competitor of HMGB1, HeLa cells expressing GFP tagged H1c were treated with increasing cc. of Dox and its effect on histone H1c was assessed. The effect of Dox on H1c binding *in viv*o was both time and cc. dependent. Within 30 min, large-scale Dox-induced eviction of H1c-GFP from chromatin and its deposition in the nucleoli was observed (Fig. 23a). This was also reflected in its increased mobility as measured by strip FRAP (Fig. 23b). After 120 min of Dox treatment, the nucleolar component disappeared and there was a generalized loss of H1c-GFP from the cell (Fig. 23a). Similarly, EBr caused displacement of H1c-GFP from chromatin (Fig. 24). The displacement of histone H1 from DNA likely increases the number of available binding sites in the genomic DNA for HMGB1 which can explain its recruitment to chromatin and the slow recovery rate at low intercalator cc.

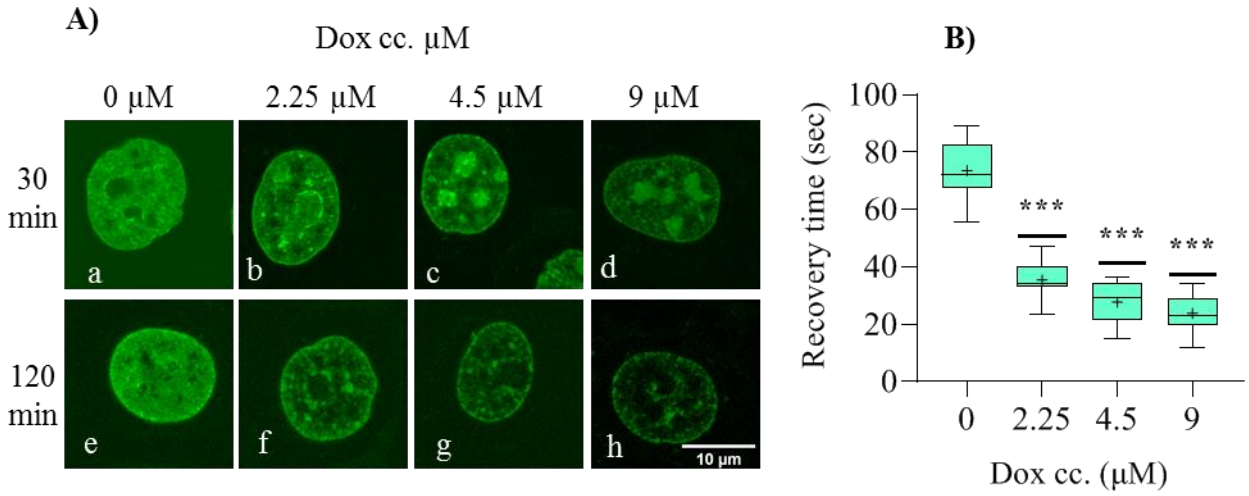

Figure 23*:* Doxorubicin affects histone H1c binding to DNA in a dose- and time-dependent manner. **A)** Representative images of HeLa cells expressing histone H1c-GFP treated with Dox **a)** for 30 minutes (top row) or 2 hrs (bottom row). **B)** FRAP analyses of H1c-GFP intranuclear mobility without Dox treatment and after for 30 minutes treatment with different cc of the drug. *P*, ***<0.0001)

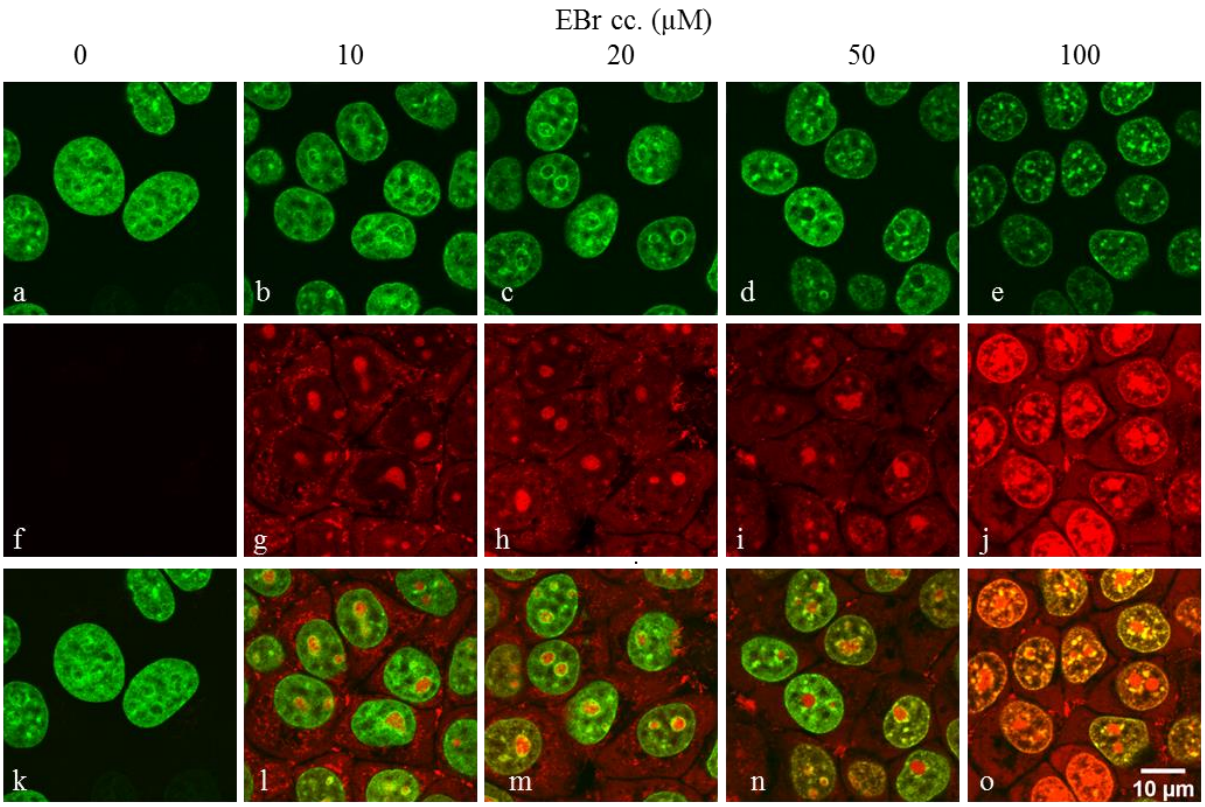

Figure 24: EBr displaces histone H1c from chromatin. Live HeLa cells expressing GFP tagged histone H1c were treated for 1 hr with varying concentrations of EBr. This figure shows representative nuclei from EBr treated cells. HMGB1-GFP, green; EBr, red; bottom row, merged images.

PART 2/B

4.2B METHODICAL ASPECTS OF HMGB1 NUCLEAR LOCALIZATION

Before assessing the effect of superhelicity on HMGB1 binding *in vivo*, I first carried out experiments to ascertain the cellular distribution and DNA binding properties of HMGB1. In the course of these experiments I noticed phenomena that have led to a shared publication with Zarębski and colleagues [156]. These studies do not belong to the line of main reasoning of my thesis, so I will summarize them under the subtitle below, in PART2/B.

4.2.6 Translocation of HMGB1 to the nucleoli during fixation

In live U2OS cells expressing GFP-tagged HMGB1 and RFP-tagged H2B, GFP-HMGB1 was distributed throughout the nucleus including the nucleoli (Fig. 25 a, c). Following cell membrane permeabilization by either Tx-100 or SLO, all the HMGB1 was lost from the cell. This was the case even when the permeabilization was carried out in a low salt, sucrose-based osmotic buffer indicating that this protein was weakly bound to the DNA.

When cells were fixed with a crosslinking fixative such as formaldehyde (Fig. 25 d, g) or glyoxal (Fig. 25 h, k), I observed a reduction of the green fluorescence in the nucleoplasm and an increase in the nucleoli, signifying a nucleoplasm to nucleoli translocation of GFP-HMGB1. This indicates that GFP-HMGB1 was able to escape crosslinking to its primary binding sites in chromatinized DNA what may be explained by its weak binding to the DNA allowing for a fast dissociation. The formation of formaldehyde crosslinks takes several minutes (~20 mins), during which the protein may dissociate and relocate to nucleoli. In support of this notion, fixation of cells using a formaldehyde/glutaraldehyde mixture, which increases the rate of fixation by up to 5x compared to formaldehyde alone [157], markedly reduced the translocation of HMGB (Fig. 25 l)

Fixation with ethanol (Fig. 25 p, r), which does not form crosslinks, led to loss of the protein from the chromatin, while a small amount translocated to the nucleoli. Subsequent steps in IF labelling led to the loss of all the HMGB1 from the ethanol fixed cells.

Interestingly, IF was unable to detect the large amount of HMGB1 in the nucleoli of formaldehyde fixed cells. This may be due to tight crosslinking caused by formaldehyde which hinders antibody access or masks the epitopes. The inhibition was more pronounced in samples fixed with a mixture of formaldehyde and glutaraldehyde; in these samples IF labelling was completely inhibited in the nuclei (Fig. 25 l & o). From these observations, I concluded that the GFP-tagged form better reflects the physiological behaviour of HMGB1, the tag notwithstanding.

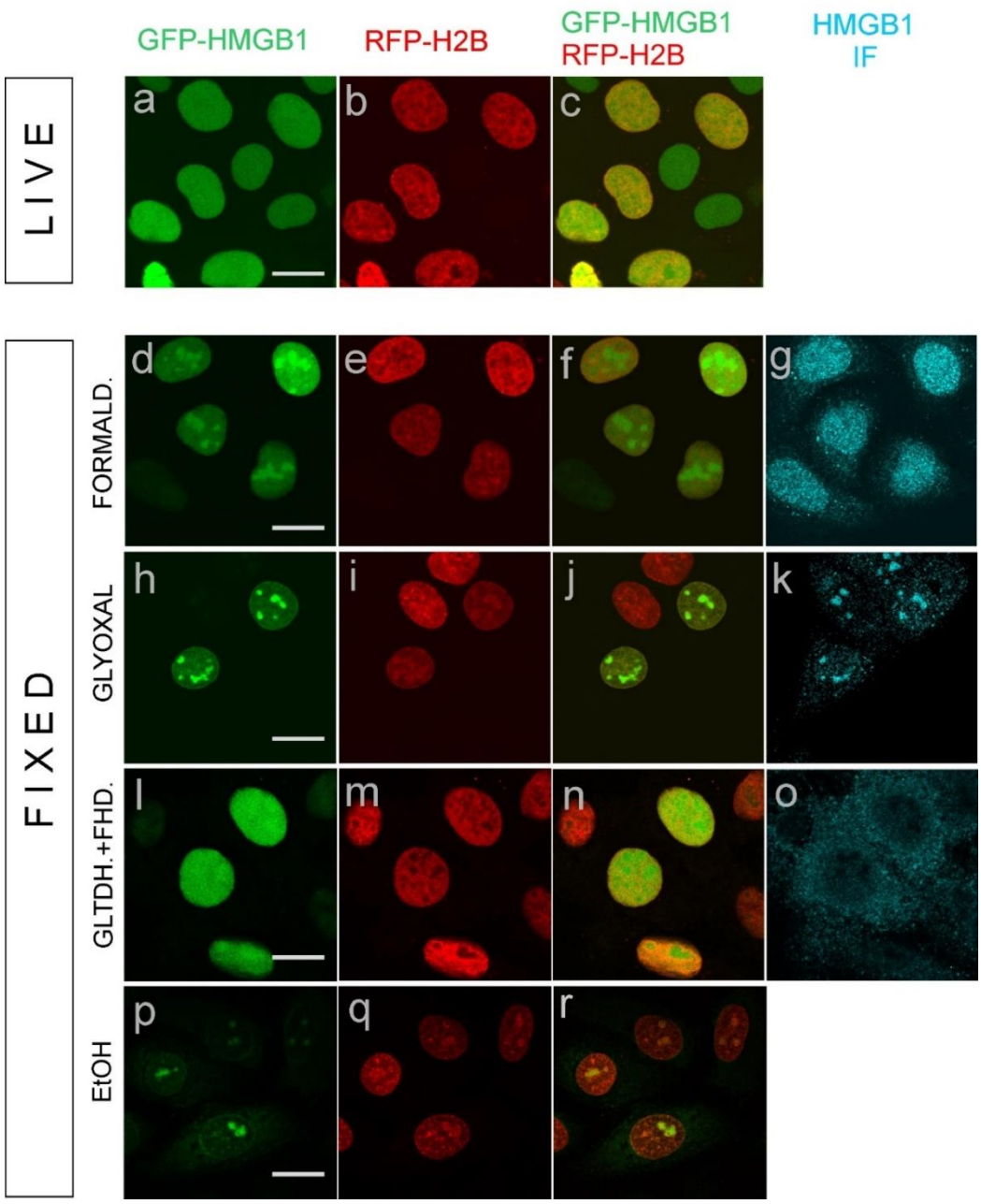

Figure 25: Relocation of HMGB1 during fixation. Representative nuclei of live and fixed U2OS^{2FP} cells showing relocation of GFP-HMGB1 during fixation. (a-c) live cells, (d-g) formaldehyde-fixed cells, (h-k) glyoxal-fixed cells, (l-o) glutaraldehyde + formaldehyde-fixed cells and (p-r) ethanol-fixed cells. Note that in the glyoxal-fixed sample, cells that express GFP-HMGB1 and those that have the endogenously expressed protein alone, have the same HMGB1 distribution as detected by IF (h vs k). Green, GFP-HMGB1; Red, H2B-RFP; Cyan, HMGB1 IF. Scale bar =10 µm

5. DISCUSSION

PART 1

EBr intercalation into genomic DNA in live cells is generally thought to be solely inhibited by the cell membrane, and as such this dye has been used as a marker of cell viability [158–160]. However, results presented herein reveal that a small amount of EBr does indeed traverse the cell membrane, apparently staining the mitochondrial DNA, and ds RNA in the ribosomal subunits present in the nucleoli (Fig. 9). However, even when the dye is introduced into the cytoplasm and then enters the nuclei, as obvious from the ready staining the nucleoli, its intercalation into nuclear DNA is still delayed (Fig. 10). Similarly to my observations, [161] failed to detect steady-state EBr fluorescence from the nuclei (nucleoli exempted) even though its presence could be detected through time correlated photon counting. These observations raise the possibility that there may exist stages in different forms of cell death when the membrane is permeable but the chromatin still resists intercalation.

Early studies investigating the intercalation of EBr into chromatinized DNA using isolated mononucleosomes [162,163] or chromatin fibres DNA [163–165], revealed that the nucleosome structure impeded intercalation into nucleosomal DNA. Whether this impediment manifests i*n situ*, has not been studied before. To evaluate this, I developed an assay based on salt-induced destabilization of nucleosomes [150,166], to sequentially elute histone proteins from agarose-embedded nuclei and assess their effect on EBr intercalation. Embedding cells into agarose prior to nuclei preparation ensures minimal perturbation to the chromatin. In this assay, the histone dimers H2A-H2B are eluted beginning at 0.75 M NaCl, whereas elution of the tetramers $(H3\text{-}H4)_2$ ensues at about 1.2 M NaCl. In agreement with those early findings, I found that the intercalation of EBr, YOYO-1 and psoralen into chromatinized DNA, at the conditions used, is limited to the linker regions (Fig. 11) and intercalation into nucleosomal DNA only occurs after nucleosome destabilization. The region that was initially stained by EBr in the presence of nucleosomes was found to be sensitive to MNase and hypersensitive to DNase I (Fig.13), which is characteristic of linker DNA. The fact that MNase digestion did not completely eliminate the EBr fluorescence from fixed nuclei indicates that when the ends of nucleosomal DNA become

free upon digestion of linker DNA, intercalation into the DNA wrapped around the NCP becomes possible, probably starting from the ends.

The increase in EBr fluorescence coincides with disassembly of the NCPs (Fig. 11) indicating that the nucleosome structure does indeed inhibit the intercalation of even a small molecule. The final fluorescence of EBr in nucleosome depleted nuclei is about three-fold higher than the initial fluorescence. Given that the EBr fluorescence measured in agarose-embedded nuclei is a reflection of intercalated EBr (Fig. 15b), it can be extrapolated that a third of the genome is nucleosome free while two-thirds is bound to nucleosomes. This is in agreement with the ratio of the total length of all the linker DNA to that of the nucleosome-constrained DNA.

I have ruled out the diminishing binding of EBr to histones in the wake of nucleosome eviction as the reason for increased dye binding to DNA. EBr binding to histone proteins has been previously reported before [151,167]. Even if such binding occurred in my experiments, there was still a large amount of dye left in the supernatant after staining the nuclei even in the presence of all the histones (Fig. 15a).

The fact that DAPI, another small molecule which binds to the DNA minor groove was not affected by the presence of histones (Figs. 11 and 14) is evidence against limited access as the means by which intercalation is inhibited. Thus, I hypothesized that intercalation, a step that follows access of EBr to DNA, is what is inhibited in chromatinized DNA. Inhibition is likely due to the tight grip of histones on DNA that greatly hinders its deformation to accommodate an intercalator.

During intercalation, a planar molecule is inserted between adjacent base pairs on a DNA molecule, which consequently affects the helix twist and rise to a degree dependent on the intercalator [168]. YOYO-1 untwists the DNA by ~24±8^{o} and increases the rise by 6.8 Å per molecule [56], while EBr untwists the DNA by ~26^{o} and increases the rise by 3.4 Å [55]. Such DNA distortion would be disfavoured in a molecule of DNA that is constrained when wrapped around the NCP.

The 147 bp of DNA wrapped around the NCP is bound to the histone core by several direct and water mediated hydrogen bonds, van der Waals bonds and electrostatic bridges [71,86,169]. Although histone-DNA interactions are highly dynamic, with the DNA spontaneously

unwrapping from the nucleosomal ends, such events are transient and involve only a few base pairs (~ 10 bp) [170,171]. Thus, a large fraction of the nucleosomal DNA still remains constrained [172,173]. This interpretation is in agreement with the finding that cross-linking the DNA to the nucleosome using formaldehyde further inhibits EBr intercalation unlike ethanol fixation which does not cause crosslinking and has no effect on EBr staining of nuclei (Fig. 16). Following salt-induced eviction of histones, the constrained toroidal structures are converted to flexible plectonemes capable of altering their twist and writhe to accommodate intercalator molecules.

The NCP organizes 147 bp of DNA in 1.67 left handed superhelical turns around the histone octamer. The experimentally determined ΔLk of about -1.0 per nucleosome is in a stark contrast with the theoretically expected -1.67. This discrepancy, which came to be known as the linking number paradox, is only solved if one considers the contribution of linker DNA to the generated ΔLk per nucleosome (as described in the Introduction). The fact that linker DNA contributes to the generated ΔLk implies that the linker DNA is itself supercoiled, suggesting the existence of net supercoiling in the extranucleosomal regions. In apparent support of this scenario, I observed an increase in EBr intercalation to the extranucleosomal DNA following nicking (Fig. 17 C & D). This increase was not related to histone eviction as there was no difference in the remaining H2B-GFP between nuclei from irradiated vs control cells, in samples treated with up to 0.75 M NaCl (Fig. 17 C & D).

The increase in intercalation, also observed when plasmid DNA was linearized or nicked, can alternatively be explained by topological constraint alone without existence of net torsion. That is, since intercalation causes DNA untwisting with a compensatory increase in writhe in a covalently closed DNA molecule, the build-up of positive writhe, which can occur even in a relaxed molecule, is what limits the extent of intercalation. Positive writhe possibly increases the dissociation constant of EBr from DNA [57]. In case of an initial negative superhelicity, which favours intercalation compared to relaxed DNA, the resulting positive supercoiling would still greatly limit intercalation compared to the nicked molecules in which there is no positive writhe build-up. Though topological constraint can fully explain the increase in EBr intercalation, existence of net torsion may still be supported by the following argument.

Following salt treatment of nuclei, there was a modest increase in the size of the nuclei before eviction of core histones (Fig. 11). This suggests that chromatin loops are confined to a small

volume by interactions that are more sensitive to salt than nucleosomes are. These possibly involve histone H1, which is evicted at ≥ 0.35 M NaCl. At moderate salt concentrations, the chromatin/DNA loops possibly undergo changes in writhe thus pushing against the nuclear lamina (Fig. 12). At high salt concentration, when much or all the nucleosomes have been evicted, the DNA loops can be seen projecting between the gaps in the nuclear lamina. Further increase in nuclear area following X-ray irradiation beyond that of control samples (Fig. 17 E), even at concentrations where the nucleosomes are still present, is additional evidence for the existence of extranucleosomal torsion. Since X-ray irradiation creates mostly nicks [174], the increase cannot be due to conversion of a chromatin loop into double stranded DNA anchored to the nuclei matrix at one end. This is in agreement with the fact that in the absence of nucleosomes the area of nuclei from irradiated and control cells was comparable.

The evidence presented above in support of the existence of net extranucleosomal torsion in the eukaryotic genome is at variance with some earlier conclusions [175] [176]. In those early experiments, the authors observed no difference in psoralen photo-binding to the whole genome, between gamma or X-ray irradiated cells and control cells, which led to the conclusion that there is no net extranucleosomal torsion in eukaryotic cells. Recently however, Naughton and colleagues demonstrated a reduction in psoralen binding following treatment of cells with bleomycin, a DNA nicking agent [177]. This discrepancy may arise from a number of factors; i) the results presented herein, as well as the immunofluorescence measurement referred to in Naughton *et al*, were obtained on a cell-by-cell basis as opposed to the population average in those early experiments. ii) The low concentration of psoralen used in the early experiments may have been a limiting factor[177]. iii) Upon UVA-illumination, psoralen forms just 1 crosslink for every 15 mono-adducts formed. Quantification of psoralen intercalation based on detection of double stranded DNA resistant to denaturation or exonuclease digestion only captures a small fraction of bound psoralen as opposed to the immunofluorescence utilized by Naughton *et al*.

The global increase in EBr binding to the extranucleosomal regions (Fig. 17C & D) was caused by a single nick per 50 kb chromatin loop (Fig. 17B). This implies that binding of torsion-sensitive regulatory factors would simultaneously be affected within a particular loop following local topoisomerase activity. In the cell, transient DNA breaks are generated during transcription elongation and during replication to resolve torsional stress. Such breaks are

expected to occur at random locations within the gene. Topoisomerase induced DNA breaks have also been detected at promoters of neuronal genes [178], promoters of androgen & oestrogen target genes [179] as well as at androgen regulated enhancers [180] where they facilitate transcriptional activation (also see reviews [181,182]. Some of the DNA breaks may not be repaired and have been detected as persistent DNA breaks. Given that a single nick causes the relaxation of the whole chromatin loop, the persistent DNA breaks and superhelical domains must be somehow separated in the genome.

In vivo, transcription is the main cause of superhelical changes, generating positive supercoils ahead and negative supercoils behind of the transcription machinery. Whether these changes induce any net change in the superhelical state of the chromatin is dependent on the efficiency with which topoisomerases acting ahead and behind of the transcription machinery relax the torsion. Following transcription inhibition by either actinomycin D or α-amanitin, EBr intercalation in the presence of nucleosomes was only slightly increased (Fig. 18). This implies that transcription generates minimal net change in the overall supercoiling of the cell, hence the effect of transcription inhibitors is not detectable. This could be due to symmetrical resolution of transcription induced torsional stress ahead and behind of the transcription machinery *in vivo.* Alternatively, it has before been observed that following transcription inhibition, chromatin domain that were initially negatively supercoiled became negatively supercoiled and vice versa, while others were unaffected [177]. Such dynamic changes at domain level may cancel out.

DNA intercalators such as doxorubicin and daunomycin form a major class of cancer chemotherapeutic agents. The success of these agents depends on their functional interaction with DNA. The fact that *in vivo* nicking increased the binding of EBr to DNA (Fig. 17C & D), implies that radiotherapy or chemotherapeutical agents that induce DNA breaks such as bleomycin and topoisomerase inhibitors may synergize with anthracycline therapy when used concurrently.

PART 2/A

I have shown that drug intercalation into DNA *in vivo* affects HMGB1 binding to DNA in a manner dependent on the concentration and the drug itself. By increasing the intercalator concentration, both EBr and Dox lead to recruitment and binding of HMGB1 to sites on chromatin as shown by the structured distribution (Figs. 19a and 20a). This is also reflected in the increase in recovery time following photobleaching (Figs. 19b & 20b). At high concentration, > 9 µM Dox caused a drastic reduction in the binding of GFP-HMGB1 to DNA.

The initial increase in HMGB1 binding was found to be the result of increased number of binding sites following histone H1 displacement from DNA. Both H1 and HMGB1 compete for the linker DNA near the nucleosome dyad [154]. However, histone H1 demonstrated higher sensitivity to intercalator binding than HMGB1 as it was readily displaced from chromatin by both EBr and Dox at concentrations where HMGB1 was clearly bound to DNA (Figs. 23 and 24).

The reduction in HMGB1 binding to DNA at high Dox concentrations (Fig. 20b) could be due to intercalator induced DNA distortion or competition between Dox and HMGB1 for binding sites on DNA. Dox carries two DNA binding moieties; the anthraquinone moiety which intercalates between adjacent G-C base pair steps and the amino sugar which is positioned in the DNA minor groove [61]. Intercalation of the anthraquinone moiety increases the base pair rise to 5.2 Å and reduces the helical twist at the site of intercalation. *In vivo,* untwisting of the DNA due to intercalation would be compensated for by positive writhing within the closed chromatin loops without change in the linking number, in line with the equation $\Delta Lk = \Delta Tw + \Delta Wr$. The level of the compensatory positive torsion would increase with increase in the number of intercalated molecules. This intercalator-induced change in torsion together with that induced by ongoing replication and transcription would trigger topoisomerase activity to resolve it, as reviewed in [181,183]. However, at the high concentrations (>9 µM) Dox would inhibit topoisomerase binding to DNA (as reviewed in [184]), thus leading to accumulation of positive torsion. Though some of the negative toroidal superhelicity constrained around the nucleosomes would be converted to plectonemic negative torsion due to Dox induced histone eviction [185,186], this may reduce but not completely annihilate the positive torsion. The positive writhe would thus hinder the binding of HMGB1 because it involves intercalation. This

argument is supported by the monotonous reduction in HMGB1 binding to covalently closed plasmid DNA in the presence of Dox (Fig. 22c).

The binding of Dox and HMGB1 to DNA overlap in two aspects: both involve intercalation into DNA and minor groove binding. HMGB1 consists of two DNA binding domains, box A and B, which are connected by a short linker to an intrinsically disordered, acidic C-terminal tail [187]. The A and B domains form an "L"-shape with a concave DNA binding surface. The binding of HMGB1 to DNA occurs through the DNA minor groove and induces a bend towards the major groove. Additionally, hydrophobic amino acids phenylalanine (Phe38) on box A, phenylalanine (Phe1103) and isoleucine (Ile122) on box B partially intercalate between base pairs following DNA binding, and unwind the DNA [128]. This overlap in the Dox and HMGB1 binding to DNA is bound to create grounds for competition and as the drug concentration is increased beyond 9 µM, HMGB1 seems to be the weaker competitor. Hence, HMGB1 binding is reduced at high Dox cc. The Dox amino sugar has also been shown to sterically obstructs interactions between histones and DNA and is responsible for histone displacement from DNA [185].

Even at the highest concentration of EBr used (100 µM), HMGB1 binding to DNA was markedly increased beyond that of the control both as seen in the microscopy images and through the point FRAP profiles (Fig. 19). This is a sharp contrast from the observation with Dox were at drug concentrations above 9 µM HMGB1 (Fig. 20) binding to DNA was markedly reduced. This could be attributed to the lower uptake of EBr by live cells due to its positive charge, which means that the amount intercalated in DNA is much lower than that in the extracellular milieu. Doxorubicin on the other hand, is known to accumulate in the cells attaining higher intracellular concentration compared to the extracellular milieu. It may also be that the drastic reduction in GFP-HMGB1 binding at high Dox concentration is solely due to the presence of the amino sugar positioned in the DNA minor groove.

Relaxing the DNA writhe in chromatin loops by use of DNA nicking agents like X-ray irradiation, H_2O_2 or bleomycin, did not yield any observable effect on the binding of HMGB1 binding *in vivo* (Fig. 21). This is despite the well documented preference of HMGB1 binding to supercoiled over relaxed DNA *in vitro* (Fig. 22a; see also [128]). At the dosage used in these experiments, X-ray irradiation would cause 6,000 -50,000, while H_2O_2 would cause 15,000 -

36,000 single strand breaks per nucleus [174,188]. Despite the rapid repair of single strand breaks occurring in a matter of minutes [189], many of the breaks would still be unrepaired given the short time interval between nicking the DNA and measurement. And even if a large fraction were repaired it is unlikely that the level of supercoiling that could be re-established in S-phase would have been restored in the absence of DNA replication in these circumstances. The fact that HMGB1 binding *in vivo* was not affected by DNA nicking means that the protein does bind to linear or relaxed DNA equally well when it is the only form available.

Other groups have observed nuclear to cytoplasmic translocation or extracellular secretion of HMGB1 from immune cells following ionizing radiation or H_2O_2 peroxide treatment and x-ray radiation, at doses lower than those used here [138,190,191]. This, however, occurred 3-24 hours after exposure, i.e. long after most of the single strand breaks would have been repaired and thus cannot be directly related to changes in superhelicity or H1 binding.

The evidence presented here suggests that supercoiling may not affect HMGB1 binding *in vivo*. To put it more accurately, any effect of supercoiling may be overshadowed by interactions involving the chromatin environment.

The concentration dependent influence of Dox on HMGB1 binding has not been recognized before and may contribute to the effects and side-effects of this anthracycline of medical significance.

The findings presented herein suggest that, the constraint of nucleosome-bound DNA imposed by the numerous histone-DNA bonds inhibits ligand binding to the DNA. An exception to this may be the pioneer TF which are able to bind DNA at the nucleosome entry/exit points during spontaneous unwrapping events or bind partial motifs and induce local release or distortion of DNA [192]. Though the binding of the small molecule minor groove binder, DAPI, used in my experiments was unaffected by presence of nucleosomes, it may not be so for larger ligands that may require larger deformation. Further, due to the interrelated character of the DNA-shape features [50], the constraint imposed by the nucleosomes is expected to affect ligands with or without intercalating moieties that bind to DNA grooves or backbone. A number of TF that establish hydrogen bonds with DNA in the major groove also have moieties that extend to the minor groove.

On the other hand, the DNA devoid of nucleosomes encompassing linker DNA and NFR is flexible enough to allow deformation and ligand binding. For these regions, ligand binding appears to be strongly influenced, perhaps also regulated by competition between ligands.

PART 2/B

Sample fixation and subsequent permeabilization are important steps in the immunofluorescence detection of intracellular components. Fixation is expected to preserve the spatial distribution of the components of interest. Contrary to this expectation, results presented here (Fig. 25) reveal that HMGB1 may escape crosslinking to its binding sites on chromatin and be subsequently relocated to the nucleoli. The escape is probably made possible by the weak binding of the protein to DNA, allowing it to detach and move to another location during the process of fixation which may take several minutes [157,193]. Similar relocation has been observed for histone H1 following ethanol fixation or anthracycline treatment [156]. It is therefore important to always optimize fixation protocols to the component of interest. The observation also raises the intriguing question why nucleoli which excludes many proteins under normal circumstances behave as depots of the protein released from chromatin.

6. SUMMARY

Transcriptional regulation plays an important role in cell differentiation and in maintaining cell phenotypes, and misregulation often leads to disease. In eukaryotes, chromatin is maintained in a repressive state by the nucleosomal structure. Consequently, transcription activation requires creation of nucleosome free regions for regulatory factor binding. Similarly, transcription elongation requires destabilization of the nucleosomes ahead of the transcribing machinery. The mechanism by which the nucleosome structure inhibits regulatory factor binding has, however, not been fully elucidated. Current knowledge from biophysical experiments challenges the possibility of limited access as the mechanism of inhibition. This is especially obvious considering that the DNA winds on the exterior surface of the core histone octamer being continuously exposed toward the surroundings. Further, it has been shown that even regions of dense chromatin packaging are freely accessible to relatively large ligands partly due to the relatively large pore-size in the chromatin matrix and to the local Brownian motion occasionally bringing sites buried in chromatin domains to the surface where large TF would bind. Therefore, the question how access to DNA in chromatin is regulated remains unanswered.

I have considered the possible role of alteration of DNA structure that results from packaging of DNA into chromatin as a mechanism of controlled access. This is bearing in mind the important contribution that DNA shape makes to TF binding specificity. Further, it is well known that TF binding to DNA results in deformation of both the DNA and protein so as to form a proper fit between the macromolecules. However, such a plasticity may not be allowed in view of the limited degrees of freedom that DNA in chromatin has.

In my work, I evaluated the binding of fluorescent, small molecule intercalators to DNA *in situ*. Intercalation requires deformation of DNA akin to that of TF binding. Given their low molecular weight, small molecules would be expected to easily access the DNA in all chromatin domains and there intercalation could be easily quantified from their fluorescence. My results revealed that intercalation was limited to extranucleosomal DNA, while intercalation into the nucleosomal DNA only became possible after histone eviction. Intercalation into extranucleosomal DNA could be moderately enhanced by topological relaxation in the wake of nicking the DNA. A single nick per 50 kbp loop was sufficient to achieve this increment revealing that the conformational change elicited readily spreads along the chromatin. Staining

with DAPI, which binds to the minor groove without intercalation, was unimpeded by the presence of nucleosomes. These data have led me to conclude that the conformational constraint imposed on DNA by the several chemical bonds linking the DNA to the nucleosome core are likely responsible for this shielding of the DNA to particular small molecules from inside, while the internucleosomal DNA can adapt to bind the ligand.

Next, I evaluated the effect of supercoil relaxation on the binding of HMGB1, a protein whose binding to DNA partly involves intercalation. These measurements have yielded a complex picture. Relaxation of supercoiling by using DNA nicking agents had no effect of HMGB1 binding *in vivo*. However, binding of Dox, a membrane permeable DNA intercalator, led to an initial increase in HMGB1 binding *in vivo*, followed by decreased binding at higher concentrations. In solution, intercalator binding caused a monotonous decrease in HMGB1 binding to supercoiled plasmid DNA. Having assessed also the effect of Dox on the binding of the linker histone H1, known to antagonize HMGB1 binding, has led me to conclude that Dox used at small concentrations enhances HMGB1 binding by destabilizing H1 binding, while in the higher concentration range competes with HMGB1 for the DNA.

Nucleosomes emerge as major impediments of ligand binding as a result of the constraint of DNA conformation, while the extranucleosomal DNA exhibits a higher degree of conformational plasticity, allowing for a complexity of molecular interactions. Since the conformational features determining intercalation are tightly interdependent with all the other DNA conformational features, based on the powerful effect of nucleosomal constraint on intercalator binding I anticipate an analogous effect of the nucleosomal structure on any ligand binding, including that of TFs. My data also suggests that anthracycline therapy may be synergized by chemotherapeutic agents that induce DNA breaks such as topoisomerase inhibitors and bleomycin, or radiotherapy.

7. REFERENCES

1. Lee TI, Young RA. Transcriptional Regulation and Its Misregulation in Disease. *Cell*. 2013;152:1237-1251. doi:10.1016/j.cell.2013.02.014

2. Lambert SA, Jolma A, Campitelli LF, et al. The Human Transcription Factors. *Cell*. 2018;172:650-665. doi:10.1016/j.cell.2018.01.029

3. Sainsbury S, Bernecky C, Cramer P. Structural basis of transcription initiation by RNA polymerase II. *Nat Rev Mol Cell Biol*. 2015;16(3):129-143. doi:10.1038/nrm3952

4. Boyaci H, Chen J, Jansen R, Darst SA, Campbell EA. Structures of an RNA polymerase promoter melting intermediate elucidate DNA unwinding. *Nature*. 2019;565(7739):382-385. doi:10.1038/s41586-018-0840-5

5. Spitz F, Furlong EEM. Transcription factors: From enhancer binding to developmental control. *Nat Rev Genet*. 2012;13(9):613-626. doi:10.1038/nrg3207

6. Gross DS, Garrard WT. Nuclease hypersensitive sites in chromatin. *Annu Rev Biochem*. 1988;57:159-197. doi:10.1146/annurev.bi.57.070188.001111

7. Felsenfeld G, Groudine M. Controlling the double helix. *Nature*. 2003;421(6921):448-453. doi:10.1038/nature01411

8. Stalder J, Larsen A, Engel JD, Dolan M, Groudine M, Weintraub H. Tissue-specific DNA cleavages in the globin chromatin domain introduced by DNAase I. *Cell*. 1980;20(2):451-460. doi:10.1016/0092-8674(80)90631-5

9. Keene MA, Corces V, Lowenhaupt KY, Elgin SCR. DNase I hypersensitive sites in Drosophila chromatin occur at the 5’ ends of regions of transcription (chromatin structure/Drosophila melanogaser/heat shock). *Proc Natl Acad Sci USA*. 1981;78(1):143-146.

10. Wu C. The 5’ ends of drosophila heat shock genes in chromatin are hypersensitive to DNase I. *Nature*. 1980;286(5776):854-860. doi:10.1038/286854a0

11. Yuan GC, Liu YJ, Dion MF, et al. Molecular biology: Genome-scale identification of nucleosome positions in S. cerevisiae. *Science (80-).* 2005;309(5734):626-630.

doi:10.1126/science.1112178

12. Lee W, Tillo D, Bray N, et al. A high-resolution atlas of nucleosome occupancy in yeast. *Nat Genet*. 2007;39(10):1235-1244. doi:10.1038/ng2117

13. Mavrich TN, Jiang C, Ioshikhes IP, et al. Nucleosome organization in the Drosophila genome. *Nature*. 2008;453(7193):358-362. doi:10.1038/nature06929

14. Suck D. DNA Recognition by DNase I. *J Mol Recognit*. 1994;7(August 1993):65-70.

15. Campbell VW, Jackson DA. The effect of divalent cations on the mode of action of DNase I. *J Biol Chem*. 1980;255(8):3726-3735.

16. Chen A, Chen D, Chen Y. Advances of DNase-seq for mapping active gene regulatory elements across the genome in animals. *Gene*. 2018;667(May):83-94. doi:10.1016/j.gene.2018.05.033

17. Song L, Crawford GE. DNase-seq: A high-resolution technique for mapping active gene regulatory elements across the genome from mammalian cells. *Cold Spring Harb Protoc*. 2010;5(2):pdb.prot5384. doi:10.1101/pdb.prot5384

18. Boyle AP, Davis S, Shulha HP, et al. High-Resolution Mapping and Characterization of Open Chromatin across the Genome. *Cell*. 2008;132:311-322. doi:10.1016/j.cell.2007.12.014

19. He HH, Meyer CA, Hu SS, et al. Refined DNase-seq protocol and data analysis reveals intrinsic bias in transcription factor footprint identification. *Nat Methods*. 2014;11(1):73-78. doi:10.1038/nmeth.2762

20. Lazarovici A, Zhou T, Shafer A, et al. Probing DNA shape and methylation state on a genomic scale with DNase I. *Proc Natl Acad Sci U S A*. 2013;110(16):6376-6381. doi:10.1073/pnas.1216822110

21. Heddi B, Abi-Ghanem J, Lavigne M, Hartmann B. Sequence-Dependent DNA Flexibility Mediates DNase I Cleavage. *J Mol Biol*. 2010;395(1):123-133. doi:10.1016/j.jmb.2009.10.023

22. Gaulton KJ, Nammo T, Pasquali L, et al. A map of open chromatin in human pancreatic

islets. *Nat Genet*. 2010;42(3):255-259. doi:10.1038/ng.530

23. Chereji R V, Bryson TD, Henikoff S. Quantitative MNase-seq accurately maps nucleosome occupancy levels. *Genome Biol*. 2019;20(198). doi:10.1186/s13059-019-1815-z

24. Dingwall C, Lomonossoff GP, Laskey RA. High sequence specificity of micrococcal nuclease. *Nucleic Acids Res*. 1981;9(12):2659-2674. doi:10.1093/nar/9.12.2659

25. Chereji R V., Ocampo J, Clark DJ. MNase-Sensitive Complexes in Yeast: Nucleosomes and Non-histone Barriers. *Mol Cell*. 2017;65(3):565-577.e3. doi:10.1016/j.molcel.2016.12.009

26. Brahma S, Henikoff S. RSC-Associated Subnucleosomes Define MNase-Sensitive Promoters in Yeast. *Mol Cell*. 2019;73(2):238-249.e3. doi:10.1016/j.molcel.2018.10.046

27. Ivics Z, Li MA, Mátés L, et al. Transposon-mediated genome manipulation in vertebrates. *Nat Methods*. 2009;6(6):415-422. doi:10.1038/nmeth.1332

28. Buenrostro JD, Wu B, Chang HY, Greenleaf WJ. ATAC-seq: A method for assaying chromatin accessibility genome-wide. *Curr Protoc Mol Biol*. 2015;2015:21.29.1-21.29.9. doi:10.1002/0471142727.mb2129s109

29. Klein DC, Hainer SJ. Genomic methods in profiling DNA accessibility and factor localization. *Chromosome Res*. 2020;28(1):69-85. doi:10.1007/s10577-019-09619-9

30. Rhee HS, Pugh BF. Comprehensive genome-wide protein-DNA interactions detected at single-nucleotide resolution. *Cell*. 2011;147(6):1408-1419. doi:10.1016/j.cell.2011.11.013

31. He Q, Johnston J, Zeitlinger J. ChIP-nexus enables improved detection of in vivo transcription factor binding footprints. *Nat Biotechnol*. 2015;33(4):395-401. doi:10.1038/nbt.3121

32. Skene PJ, Henikoff S. An efficient targeted nuclease strategy for high-resolution mapping of DNA binding sites. *Elife*. 2017;6. doi:10.7554/eLife.21856

33. Heitz E. Das Heterochromatin der Moose. In: *Jahrbücher Für Wissenschaftliche Botanik*. Vol 69. ; 1928:762-818.

34. Verschure PJ, van der Kraan I, Manders EMM, Hoogstraten D, Houtsmuller AB, van Driel R. Condensed chromatin domains in the mammalian nucleus are accessible to large macromolecules. *EMBO Rep*. 2003;4(9):861-866. doi:10.1038/sj.embor.embor922

35. Görisch SM, Wachsmuth M, Tóth KF, Lichter P, Rippe K. Histone acetylation increases chromatin accessibility. *J Cell Sci*. 2005;118(24):5825-5834. doi:10.1242/jcs.02689

36. Dross N, Spriet C, Zwerger M, Muller G, Waldeck W, Langowski J. Mapping eGFP Oligomer Mobility in Living Cell Nuclei. *PLoS One*. 2009;4(4):5041. doi:10.1371/journal.pone.0005041

37. Grünwald D, Martin RM, Buschmann V, et al. Probing intranuclear environments at the single-molecule level. *Biophys J*. 2008;94(7):2847-2858. doi:10.1529/biophysj.107.115014

38. Marshall WF, Straight A, Marko JF, et al. Interphase chromosomes undergo constrained diffusional motion in living cells. *Curr Biol*. 1997;7(12):930-939. doi:10.1016/S0960-9822(06)00412-X

39. Hihara S, Pack CG, Kaizu K, et al. Local Nucleosome Dynamics Facilitate Chromatin Accessibility in Living Mammalian Cells. *Cell Rep*. 2012;2(6):1645-1656. doi:10.1016/j.celrep.2012.11.008

40. Maeshima K, Kaizu K, Tamura S. The physical size of transcription factors is key to transcriptional regulation in chromatin domains. *J Phys Condens Matter*. 2015;27(6). doi:10.1088/0953-8984/27/6/064116

41. Zaret KS, Carroll JS. Pioneer transcription factors: Establishing competence for gene expression. *Genes Dev*. 2011;25(21):2227-2241. doi:10.1101/gad.176826.111

42. Lee CK, Shibata Y, Rao B, Strahl BD, Lieb JD. Evidence for nucleosome depletion at active regulatory regions genome-wide. *Nat Genet*. 2004;36(8):900-905. doi:10.1038/ng1400

43. Berger MF, Bulyk ML. Universal protein-binding microarrays for the comprehensive characterization of the dna-binding specificities of transcription factors. *Nat Protoc*. 2009;4(3):393-411. doi:10.1038/nprot.2008.195

44. Rohs R, West SM, Sosinsky A, Liu P, Mann RS, Honig B. The role of DNA shape in protein-DNA recognition. *Nature*. 2009;461. doi:10.1038/nature08473

45. Rohs R, Jin X, West SM, Joshi R, Honig B, Mann RS. Origins of specificity in protein-DNA recognition. *Annu Rev Biochem*. 2010;79:233. doi:10.1146/ANNUREV-BIOCHEM-060408-091030

46. Li J, Sagendorf JM, Chiu TP, Pasi M, Perez A, Rohs R. Expanding the repertoire of DNA shape features for genome-scale studies of transcription factor binding. *Nucleic Acids Res*. 2017;45(22):12877-12887. doi:10.1093/nar/gkx1145

47. Calladine CR, Drew HR, Luisi BF, Travers AA. *Understanding DNA: The Molecule and How It Works: Third Edition*.; 2004. doi:10.1016/B978-0-12-155089-9.X5000-5

48. Olson WK, Bansal M, Burley SK, et al. A Standard Reference Frame for the Description of Nucleic Acid Base-pair Geometry. *J Mol Biol*. 2001;313:229-237. doi:10.1006/jmbi.2001.4987

49. Heinemann U, Roske Y. Symmetry in nucleic-acid double helices. *Symmetry (Basel)*. 2020;12(5). doi:10.3390/SYM12050737

50. Liebl K, Drsata T, Lankas F, Lipfert J, Zacharias M. Explaining the striking difference in twist-stretch coupling between DNA and RNA: A comparative molecular dynamics analysis. *Nucleic Acids Res*. 2015;43(21):10143-10156. doi:10.1093/nar/gkv1028

51. Afek A, Shi H, Rangadurai A, et al. DNA mismatches reveal conformational penalties in protein–DNA recognition. *Nature*. 2020;587(7833):291-296. doi:10.1038/s41586-020-2843-2

52. Bhaduri S, Ranjan N, Arya DP. An overview of recent advances in duplex DNA recognition by small molecules. *Beilstein J Org Chem*. 2018;14:1051-1086. doi:10.3762/bjoc.14.93

53. Blackburn GM, Grait MJ, Loakes D, Williams DM, eds. *Nucleic Acid in Chemistry and Biology*. Third. Cambridge: The Royal Society of Chemistry; 2006.

54. Strekowski L, Wilson B. Noncovalent interactions with DNA: An overview. *Mutat Res - Fundam Mol Mech Mutagen*. 2007;623(1-2):3-13. doi:10.1016/j.mrfmmm.2007.03.008

55. Wang JG. The degree of unwinding of the DNA helix by ethidium. *J Mol Biol*. 1974;89(4):783-801. doi:10.1016/0022-2836(74)90053-9

56. Günther K, Mertig M, Seidel R. Mechanical and structural properties of YOYO-1 complexed DNA. *Nucleic Acids Res*. 2010;38(19):6526-6532. doi:10.1093/nar/gkq434

57. Dikic J, Seidel R. Anticooperative Binding Governs the Mechanics of Ethidium-Complexed DNA. *Biophys J*. 2019;116(8):1394-1405. doi:10.1016/j.bpj.2019.03.005

58. Heller DP, Greenstock CL. Fluorescence lifetime analysis of DNA intercalated ethidium bromide and quenching by free dye. *Biophys Chem*. 1994;50(3):305-312. doi:10.1016/0301-4622(93)E0101-A

59. Bauer W, Vinograd J. The interaction of closed circular DNA with intercalative dyes. I. The superhelix density of SV40 DNA in the presence and absence of dye. *J Mol Biol*. 1968;33(1):141-171. doi:10.1016/0022-2836(68)90286-6

60. Silva EF, Bazoni RF, Ramos EB, Rocha MS. DNA-doxorubicin interaction: New insights and peculiarities. *Biopolymers*. 2017;107(3):e22998. doi:10.1002/bip.22998

61. Frederick CA, Williams LD, Ughetto G, et al. Structural Comparison of Anticancer Drug-DNA Complexes: Adriamycin and Daunomycin. *Biochemistry*. 1990;29(10):2538-2549. doi:10.1021/bi00462a016

62. Olmsted J, Kearns DR. Mechanism of Ethidium Bromide Fluorescence Enhancement on Binding to Nucleic Acids. *Biochemistry*. 1977;16(16):3647-3654. doi:10.1021/bi00635a022

63. Chen X, Jiang G, Wang Z, et al. DNA sequence-dependent fluorescence of doxorubicin for turn-on detection of biothiols in human serum. *Anal Bioanal Chem 2015 4083*.

2015;408(3):683-693. doi:10.1007/S00216-015-9168-2

64. DuVernay VH, Pachter JA, Crooke ST. Deoxyribonucleic Acid Binding Studies on Several New Anthracycline Antitumor Antibiotics. Sequence Preference and Structure-Activity Relationships of Marcellomycin and Its Analogues as Compared to Adriamycin. *Biochemistry*. 1979;18(18):4024-4030. doi:10.1021/bi00585a028

65. Almutawa F, Alnomair N, Wang Y, Hamzavi I, Lim HW. Systematic Review of UV-Based Therapy for Psoriasis. *Am J Clin Dermatol*. 2013;14:87-109. doi:10.1007/S40257-013-0015-Y

66. Singh F, Lebwohl MG. Cutaneous T-cell lymphoma treatment using bexarotene and PUVA: A case series. *J Am Acad Dermatol*. 2004;51(4):570-573. doi:10.1016/J.JAAD.2003.05.010

67. Couvé-Privat S, Macé G, Rosselli F, Saparbaev MK. Psoralen-induced DNA adducts are substrates for the base excision repair pathway in human cells. *Nucleic Acids Res*. 2007;35(17):5672. doi:10.1093/NAR/GKM592

68. Verma SC, Qian Z, Adhya SL. Architecture of the Escherichia coli nucleoid. *PLoS Genet*. 2019;15(12):e1008456. doi:10.1371/journal.pgen.1008456

69. Keller W. Determination of the number of superhelical turns in simian virus 40 DNA by gel electrophoresis. *Proc Nati Acad Sci USA*. 1975;72(12):4876-4880.

70. Simpson RT, Thoma F, Brubaker JM. Chromatin reconstituted from tandemly repeated cloned DNA fragments and core histones: A model system for study of higher order structure. *Cell*. 1985;42(3):799-808. doi:10.1016/0092-8674(85)90276-4

71. Luger K, Mäder AW, Richmond RK, Sargent DF, Richmond TJ. Crystal structure of the nucleosome core particle at 2.8 Å resolution. *Nature*. 1997;389(6648):251-260. doi:10.1038/38444

72. Hayes JJ, Tulliust TD, Wolffe AP. *The Structure of DNA in a Nucleosome*. Vol 87.; 1990.

73. White JH, Bauer WR. The helical repeat of nucleosome-wrapped DNA. *Cell*.

1989;56(1):9-10. doi:10.1016/0092-8674(89)90977-X

74. White JH, Cozzarelli NR, Bauer WR. Helical repeat and linking number of surface-wrapped DNA. *Science (80-).* 1988;241(4863):323-327. doi:10.1126/science.3388041

75. Drew HR, Travers AA. DNA bending and its relation to nucleosome positioning. *J Mol Biol*. 1985;186(4):773-790. doi:10.1016/0022-2836(85)90396-1

76. Nikitina T, Norouzi D, Grigoryev SA, Zhurkin VB. DNA topology in chromatin is defined by nucleosome spacing. *Sci Adv*. 2017;3(10):1-9. doi:10.1126/sciadv.1700957

77. Bass M V, Nikitina T, Norouzi D, Zhurkin VB, Grigoryev SA. Nucleosome spacing periodically modulates nucleosome chain folding and DNA topology in circular nucleosome arrays. *J Biol Chem*. 2019. doi:10.1074/jbc.RA118.006412

78. Grigoryev SA. Chromatin Higher-Order Folding: A Perspective with Linker DNA Angles. *Biophys J*. 2018;114(10):2290-2297. doi:10.1016/j.bpj.2018.03.009

79. Risca VI, Denny SK, Straight AF, Greenleaf WJ. Variable chromatin structure revealed by in situ spatially correlated DNA cleavage mapping. *Nat 2017 5417636*. 2016;541(7636):237-241. doi:10.1038/nature20781

80. Angelov D, Vitolo JM, Mutskov V, Dimitrov S, Hayes JJ. Preferential interaction of the core histone tail domains with linker DNA. *Proc Natl Acad Sci U S A*. 2001;98(12):6599-6604. doi:10.1073/pnas.121171498

81. Ausio J, Dong F, van Holde KE. Use of selectively trypsinized nucleosome core particles to analyze the role of the histone "tails" in the stabilization of the nucleosome. *J Mol Biol*. 1989;206(3):451-463. doi:10.1016/0022-2836(89)90493-2

82. Polach KJ, Lowary PT, Widom J. Effects of core histone tail domains the equilibrium constants for dynamic DNA site accessibility in nucleosomes. *J Mol Biol*. 2000;298(2):211-223. doi:10.1006/jmbi.2000.3644

83. Pepenella S, Murphy KJ, Hayes JJ. Intra-and inter-nucleosome interactions of the core histone tail domains in higher-order chromatin structure. *Chromosoma*. 2014;123:3-13. doi:10.1007/s00412-013-0435-8

84. McGinty RK, Tan S. Nucleosome structure and function. *Chem Rev*. 2015;115(6):2255-2273. doi:10.1021/cr500373h

85. Richmond TJ, Davey CA. The structure of DNA in the nucleosome core. *Nature*. 2003;423(6936):145-150. doi:10.1038/nature01595

86. Davey CA, Sargent DF, Luger K, Maeder AW, Richmond TJ. Solvent mediated interactions in the structure of the nucleosome core particle at 1.9 Å resolution. *J Mol Biol*. 2002;319(5):1097-1113. doi:10.1016/S0022-2836(02)00386-8

87. Murphy IV F V., Churchill ME. Nonsequence-specific DNA recognition: A structural perspective. *Structure*. 2000;8(4):R83-R89. doi:10.1016/S0969-2126(00)00126-X

88. Li G, Levitus M, Bustamante C, Widom J. Rapid spontaneous accessibility of nucleosomal DNA. *Nat Struct Mol Biol*. 2005;12(1):46-53. doi:10.1038/nsmb869

89. Finch JT, Klug A. Solenoidal model for superstructure in chromatin. *Biochemistry*. 1976;73(6):1897-1901.

90. Woodcock CLF, Frado LLY, B RJ. The Higher-order Structure of Chromatin : Evidence for a Helical Ribbon Arrangement. *J Cell Biol*. 1984;99:42-52.

91. Dorigo B, Schalch T, Kulangara A, Duda S, Schroeder RR, Richmond TJ. Nucleosome arrays reveal the two-start organization of the chromatin fiber. *Science (80-)*. 2004;306(5701):1571-1573. doi:10.1126/SCIENCE.1103124

92. Correll SJ, Schubert MH, Grigoryev SA. Short nucleosome repeats impose rotational modulations on chromatin fibre folding. *EMBO J*. 2012;31:2416-2426. doi:10.1038/emboj.2012.80

93. Garcia-Ramirez M, Dong F, Ausio J. Role of the histone “tails” in the folding of oligonucleosomes depleted of histone H1. *J Biol Chem*. 1992;267(27):19587-19595. doi:10.1016/s0021-9258(18)41815-7

94. Tse C, Hansen JC. Hybrid trypsinized nucleosomal arrays: Identification of multiple functional roles of the H2A/H2B and H3/H4 N-termini in chromatin fiber compaction. *Biochemistry*. 1997;36(38):11381-11388. doi:10.1021/bi970801n

95. Dorigo B, Schalch T, Bystricky K, Richmond TJ. Chromatin fiber folding: Requirement for the histone H4 N-terminal tail. *J Mol Biol*. 2003;327(1):85-96. doi:10.1016/S0022-2836(03)00025-1

96. Bajpai G, Jain I, Inamdar MM, Das D, Padinhateeri R. Binding of DNA-bending non-histone proteins destabilizes regular 30-nm chromatin structure. Morozov A V, ed. *PLOS Comput Biol*. 2017;13(1):e1005365. doi:10.1371/journal.pcbi.1005365

97. Eltsov M, MacLellan KM, Maeshima K, Frangakis AS, Dubochet J. Analysis of cryo-electron microscopy images does not support the existence of 30-nm chromatin fibers in mitotic chromosomes in situ. *Proc Natl Acad Sci U S A*. 2008;105(50):19732-19737. doi:10.1073/pnas.0810057105

98. Dixon JR, Selvaraj S, Yue F, et al. Topological domains in mammalian genomes identified by analysis of chromatin interactions. *Nature*. 2012. doi:10.1038/nature11082

99. Nuebler J, Fudenberg G, Imakaev M, Abdennur N, Mirny LA. Chromatin organization by an interplay of loop extrusion and compartmental segregation. *Proc Nati Acad Sci USA*. 2018;115(29):6697-6706. doi:10.1073/pnas.1717730115

100. Racko D, Benedetti F, Dorier J, Stasiak A. Transcription-induced supercoiling as the driving force of chromatin loop extrusion during formation of TADs in interphase chromosomes. *Nucleic Acids Res*. 2018;46(4):1648-1660. doi:10.1093/nar/gkx1123

101. Rao SSP, Huntley MH, Durand NC, et al. A 3D map of the human genome at kilobase resolution reveals principles of chromatin looping. *Cell*. 2014;159(7):1665-1680. doi:10.1016/j.cell.2014.11.021

102. Tedeschi A, Wutz G, Huet S, et al. Wapl is an essential regulator of chromatin structure and chromosome segregation. *Nature*. 2013;501(7468):564-568. doi:10.1038/nature12471

103. Sanyal A, Lajoie BR, Jain G, Dekker J. The long-range interaction landscape of gene promoters. *Nature*. 2012;489(7414):109-113. doi:10.1038/nature11279

104. Jin F, Li Y, Dixon JR, et al. A high-resolution map of the three-dimensional chromatin interactome in human cells. *Nature*. 2013;503(7475):290-294. doi:10.1038/nature12644

105. Mescher AL. *Junqueira's Basic Histology: Text and Atlas*. 12th ed. (Weitz M, Kearns B, eds.). McGraw-Hill education; 2013.

106. Stevens TJ, Lando D, Basu S, et al. 3D structures of individual mammalian genomes studied by single-cell Hi-C. *Nature*. 2017;544(7648):59-64. doi:10.1038/nature21429

107. Bolzer A, Kreth G, Solovei I, et al. Three-dimensional maps of all chromosomes in human male fibroblast nuclei and prometaphase rosettes. *PLoS Biol*. 2005;3(5):0826-0842. doi:10.1371/journal.pbio.0030157

108. Gassler J, Brandão HB, Imakaev M, et al. A mechanism of cohesin-dependent loop extrusion organizes zygotic genome architecture. *EMBO J*. 2017;36(24):3600-3618. doi:10.15252/embj.201798083

109. Sogo JM, Stahl H, Koller T, Knippers R. Structure of replicating simian virus 40 minichromosomes: The replication fork, core histone segregation and terminal structures. *J Mol Biol*. 1986;189(1):189-204. doi:10.1016/0022-2836(86)90390-6

110. Muskhelishvili G, Travers A. The regulatory role of DNA supercoiling in nucleoprotein complex assembly and genetic activity. *Biophys Rev*. 2016;8:5-22. doi:10.1007/s12551-016-0237-3

111. Liu LF, Wang JC. *Supercoiling of the DNA Template during Transcription*. Vol 84.; 1987.

112. Yu H, Dröge P. Replication-induced supercoiling: A neglected DNA transaction regulator? *Trends Biochem Sci*. 2014;39(5):219-220. doi:10.1016/j.tibs.2014.02.009

113. Gartenberg MR, Wang JC. Positive supercoiling of DNA greatly diminishes mRNA synthesis in yeast. *Proc Natl Acad Sci U S A*. 1992;89(23):11461-11465. doi:10.1073/pnas.89.23.11461

114. Kouzine F, Gupta A, Baranello L, et al. Transcription dependent dynamic supercoiling is a short-range genomic force. *Nat Struct Mol Biol*. 2013;20(3):396-403. doi:10.1038/nsmb.2517

115. Gupta P, Zlatanova J, Tomschik M. Nucleosome assembly depends on the torsion in the

DNA molecule: a magnetic tweezers study. *Biophys J*. 2009;97(12):3150-3157. doi:10.1016/j.bpj.2009.09.032

116. Teves SS, Henikoff S. Transcription-generated torsional stress destabilizes nucleosomes. *Nat Struct Mol Biol*. 2014;21(1):88-94. doi:10.1038/nsmb.2723

117. Sheinin MY, Li M, Soltani M, Luger K, Wang MD. Torque modulates nucleosome stability and facilitates H2A/H2B dimer loss. *Nat Commun*. 2013;4(2579):1-8. doi:10.1038/ncomms3579

118. Joshi RS, Piña B, Roca J. Positional dependence of transcriptional inhibition by DNA torsional stress in yeast chromosomes. *EMBO J*. 2010;29(4):740-748. doi:10.1038/emboj.2009.391

119. Churchill MEA, Klass J, Zoetewey DL. Structural Analysis of HMGD-DNA Complexes Reveals Influence of Intercalation on Sequence Selectivity and DNA Bending. *J Mol Biol*. 2010;403(1):88-102. doi:10.1016/j.jmb.2010.08.031

120. Yen YM, Wong B, Johnson RC. Determinants of DNA binding and bending by the Saccharomyces cerevisiae high mobility group protein NHP6A that are important for its biological activities. Role of the unique N terminus and putative intercalating methionine. *J Biol Chem*. 1998;273(8):4424-4435. doi:10.1074/jbc.273.8.4424

121. Kasai N, Tsunaka Y, Ohki I, Hirose S, Morikawa K, Tate S-I. Solution structure of the HMG-box domain in the SSRP1 subunit of FACT. *J Biomol NMR*. 2005;32:83-88. doi:10.1007/s10858-005-3662-3

122. Ngo HB, Lovely GA, Phillips R, Chan DC. Distinct structural features of TFAM drive mitochondrial DNA packaging versus transcriptional activation. *Nat Commun*. 2014;5(1):1-12. doi:10.1038/ncomms4077

123. Kamachi Y, Kondoh H. Sox proteins: Regulators of cell fate specification and differentiation. *Dev*. 2013;140(20):4129-4144. doi:10.1242/dev.091793

124. Starr DB, Hoopes BC, Hawley DK. DNA bending is an important component of site-specific recognition by the TATA binding protein. *J Mol Biol*. 1995;250(4):434-446. doi:10.1006/jmbi.1995.0388

125. Klass J, Murphy IV F V., Fouts S, et al. The role of intercalating residues in chromosomal high-mobility-group protein DNA binding, bending and specificity. *Nucleic Acids Res*. 2003;31(11):2852-2864. doi:10.1093/nar/gkg389

126. Sandmann A, Sticht H. Probing the role of intercalating protein sidechains for kink formation in DNA. 2018. doi:10.1371/journal.pone.0192605

127. Agresti A, Scaffidi P, Riva A, Caiolfa VR, Bianchi ME. GR and HMGB1 Interact Only within Chromatin and Influence Each Other's Residence Time. *Mol Cell*. 2005;18(1):109-121. doi:10.1016/J.MOLCEL.2005.03.005

128. Štros M. HMGB proteins: Interactions with DNA and chromatin. *Biochim Biophys Acta - Gene Regul Mech*. 2010;1799(1-2):101-113. doi:10.1016/j.bbagrm.2009.09.008

129. Hergeth SP, Schneider R. The H1 linker histones: multifunctional proteins beyond the nucleosomal core particle. *EMBO Rep*. 2015;16(11):1439-1453. doi:10.15252/embr.201540749

130. Agresti A, Bianchi ME. HMGB proteins and gene expression. *Curr Opin Genet Dev*. 2003;13(2):170-178. doi:10.1016/S0959-437X(03)00023-6

131. Bonaldi T, Talamo F, Scaffidi P, et al. Monocytic cells hyperacetylate chromatin protein HMGB1 to redirect it towards secretion. *EMBO J*. 2003;22(20):5551-5560. doi:10.1093/emboj/cdg516

132. Wang H, Bloom O, Zhang M, et al. HMG-1 as a Late Mediator of Endotoxin Lethality in Mice. *Science (80-)*. 1999;285(5425):248-251. doi:10.1126/SCIENCE.285.5425.248

133. Scaffidi P, Misteli T, Bianchi ME. Release of chromatin protein HMGB1 by necrotic cells triggers inflammation. *Nat 2002 4186894*. 2002;418(6894):191-195. doi:10.1038/nature00858

134. Blair RH, Horn AE, Pazhani Y, Grado L, Goodrich JA, Kugel JF. The HMGB1 C-terminal tail regulates DNA bending. *J Mol Biol*. 2016;428(20):4060-4072. doi:10.1016/j.jmb.2016.08.018. The

135. Watson M, Stott K, Thomas JO. Mapping Intramolecular Interactions between Domains

in HMGB1 using a Tail-truncation Approach. *J Mol Biol*. 2007;374(5):1286-1297. doi:10.1016/J.JMB.2007.09.075

136. Stott K, Watson M, Howe FS, Grossmann JG, Thomas JO. Tail-Mediated Collapse of HMGB1 Is Dynamic and Occurs via Differential Binding of the Acidic Tail to the A and B Domains. *J Mol Biol*. 2010;403(5):706-722. doi:10.1016/J.JMB.2010.07.045

137. Youn JH, Shin J-S. Nucleocytoplasmic Shuttling of HMGB1 Is Regulated by Phosphorylation That Redirects It toward Secretion. *J Immunol*. 2006;177(11):7889-7897. doi:10.4049/JIMMUNOL.177.11.7889

138. Wang L, He L, Bao G, He X, Fan S, Wang H. Ionizing Radiation Induces HMGB1 Cytoplasmic Translocation and Extracellular Release. *Guo ji fang she yi xue he yi xue za zhi = Int J Radiat Med Nucl Med*. 2016;40(2):91.

139. Chikhirzhina E, Starkova T, Beljajev A, Polyanichko A, Tomilin A. Functional Diversity of Non-Histone Chromosomal Protein HmgB1. *Int J Mol Sci*. 2020;21(21):1-29. doi:10.3390/IJMS21217948

140. Ueda T, Yoshida M. HMGB proteins and transcriptional regulation. *Biochim Biophys Acta - Gene Regul Mech*. 2010;1799(1-2):114-118. doi:10.1016/j.bbagrm.2009.11.005

141. Bonaldi T, Längst G, Strohner R, Becker PB, Bianchi ME. The DNA chaperone HMGB1 facilitates ACF/CHRAC-dependent nucleosome sliding. *EMBO J*. 2002;21(24):6865. doi:10.1093/EMBOJ/CDF692

142. Joshi SR, Sarpong YC, Peterson RC, Scovell WM. Nucleosome dynamics: HMGB1 relaxes canonical nucleosome structure to facilitate estrogen receptor binding. *Nucleic Acids Res*. 2012;40(20):10161. doi:10.1093/NAR/GKS815

143. McKinney K, Prives C. Efficient Specific DNA Binding by p53 Requires both Its Central and C-Terminal Domains as Revealed by Studies with High-Mobility Group 1 Protein. *Mol Cell Biol*. 2002;22(19):6797-6808. doi:10.1128/MCB.22.19.6797-6808.2002

144. Agresti A, Scaffidi P, Riva A, Caiolfa VR, Bianchi ME. GR and HMGB1 Interact Only within Chromatin and Influence Each Other's Residence Time. *Mol Cell*. 2005;18(1):109-121. doi:10.1016/J.MOLCEL.2005.03.005

145. Lange SS, Vasquez KM. HMGB1: The Jack-of-all-Trades Protein is a Master DNA Repair Mechanic. *Mol Carcinog*. 2009;48(7):571-580. doi:10.1002/mc.20544

146. Böyum A. No TitleIsolation of mononuclear cells and granulocytes from human blood. Isolation of monuclear cells by one centrifugation, and of granulocytes by combining centrifugation and sedimentation at 1 g. *Scand J Clin Lab Invest Suppl*. 1968;97:77-89.

147. Varga T, Szilágyi I, Szabó G. Single-Strand Breaks in Agarose-Embedded Chromatin of Nonapoptotic Cells. *Biochem Biophys Res Commun*. 1999;264(2):388-394. doi:10.1006/bbrc.1999.1470

148. Brazda P, Krieger J, Daniel B, et al. Ligand Binding Shifts Highly Mobile Retinoid X Receptor to the Chromatin-Bound State in a Coactivator-Dependent Manner, as Revealed by Single-Cell Imaging. *Mol Cell Biol*. 2014;34(7):1234-1245. doi:10.1128/mcb.01097-13

149. McMurray CT, Van Holde K. E. Binding of ethidium bromide causes dissociation of the nucleosome core particle. *Proc Natl Acad Sci U S A*. 1986;83(November):8472-8476.

150. Imre L, Simándi Z, Horváth A, et al. Nucleosome stability measured in situ by automated quantitative imaging. *Sci Rep*. 2017;7(12734):1-15. doi:10.1038/s41598-017-12608-9

151. Banerjee A, Majumder P, Sanyal S, et al. The DNA intercalators ethidium bromide and propidium iodide also bind to core histones. *FEBS Open Bio*. 2014;4(1):251-259. doi:10.1016/j.fob.2014.02.006

152. Bosire R, Nánási P, Imre L, et al. Intercalation of small molecules into DNA in chromatin is primarily controlled by superhelical constraint. Hancock R, ed. *PLoS One*. 2019;14(11):e0224936. doi:10.1371/journal.pone.0224936

153. Štros M, Polanská E, Kučírek M, Pospíšilová Š. Histone H1 Differentially Inhibits DNA Bending by Reduced and Oxidized HMGB1 Protein. Wu Q, ed. *PLoS One*. 2015;10(9):e0138774. doi:10.1371/journal.pone.0138774

154. Catez F, Yang H, Tracey KJ, Reeves R, Misteli T, Bustin M. Network of Dynamic Interactions between Histone H1 and High-Mobility-Group Proteins in Chromatin. *Mol Cell Biol*. 2004;24(10):4321-4328. doi:10.1128/mcb.24.10.4321-4328.2004

155. Wójcik K, Zarebski M, Cossarizza A, Dobrucki JW. Daunomycin, an antitumor DNA intercalator, influences histone-DNA interactions. *Cancer Biol Ther*. 2013;14(9):823-832. doi:10.4161/cbt.25328

156. Zarębski M, Bosire R, Wesołowska J, et al. Translocation of chromatin proteins to nucleoli—The influence of protein dynamics on post-fixation localization. *Cytom Part A*. June 2021:cyto.a.24464. doi:10.1002/cyto.a.24464

157. Huebinger J, Spindler J, Holl KJ, Koos B. Quantification of protein mobility and associated reshuffling of cytoplasm during chemical fixation. *Sci Rep*. 2018;8(1):1-11. doi:10.1038/s41598-018-36112-w

158. Aeschbacher M, Reinhardt CA, Zbinden G. A rapid cell membrane permeability test using flourescent dyes and flow cytometry. *Cell Biol Toxicol*. 1986;2(2):247-255. doi:10.1007/BF00122693

159. Ellwart JW, Kremer J-P, Dörmer P. Drug Testing in Established Cell Lines by Flow Cytometric Vitality Measurements versus Clonogenic Assay. *Cancer Res*. 1988;48(20).

160. Boltz RCD, Fischer PA, Wicker LS, Peterson LB. Single UV excitation of hoechst 33342 and ethidium bromide for simultaneous cell cycle analysis and viability determinations on in vitro cultures of murine B lymphocytes. *Cytometry*. 1994;15(1):28-34. doi:10.1002/cyto.990150106

161. Tramier M, Kemnitz K, Durieux C, et al. Restrained torsional dynamics of nuclear DNA in living proliferative mammalian cells. *Biophys J*. 2000;78(5):2614-2627. doi:10.1016/S0006-3495(00)76806-8

162. McMurray CT, van Holde KE. Binding of Ethidium to the Nucleosome Core Particle. 1. Binding and Dissociation Reactions. *Biochemistry*. 1991;30(23):5631-5643. doi:10.1021/bi00237a001

163. Erard M, Das GC, De Murcia G, et al. Ethidium bromide binding to core particle: comparison with native chromatin. *Nucleic Acids Res*. 1979;6(10):3231-3253.

164. Vergani L, Gavazzo P, Mascetti G, Nicolini C. Ethidium bromide intercalation and chromatin structure: a spectropolarimetric analysis. *Biochemistry*. 1994;33(21):6578-

6585.

165. Paoletti J, Magee BB, Magee PT. The structure of chromatin: interaction of ethidium bromide with native and denatured chromatin. *Biochemistry*. 1977;16(3):351-357.

166. Yager TD, McMurray CT, Van Holde KE. Salt-induced release of DNA from nucleosome core particles. *Biochemistry*. 1989;28(5):2271-2281. doi:10.1021/bi00431a045

167. McMurray CT, Small EW, van Holde KE. Binding of Ethidium to the Nucleosome Core Particle. 2. Internal and External Binding Modes. *Biochemistry*. 1991;30(23):5644-5652. doi:10.1021/bi00237a002

168. Mukherjee A, Lavery R, Bagchi B, Hynes JT. On the molecular mechanism of drug intercalation into DNA: A simulation study of the intercalation pathway, free energy, and DNA structural changes. *J Am Chem Soc*. 2008;130(30):9747-9755. doi:10.1021/ja8001666

169. Luger K, Richmond TJ. DNA binding within the nucleosome core. *Curr Opin Struct Biol*. 1998;(8):33-40. doi:10.1016/S0959-440X(98)80007-9

170. Polach KJ, Widom J. Mechanism of protein access to specific DNA sequences in chromatin: A dynamic equilibrium model for gene regulation. *J Mol Biol*. 1995;254(2):130-149. doi:10.1006/jmbi.1995.0606

171. Tims HS, Gurunathan K, Levitus M, Widom J. Dynamics of nucleosome invasion by DNA binding proteins. *J Mol Biol*. 2011;411(2):430-448. doi:10.1016/j.jmb.2011.05.044

172. Li G, Widom J. Nucleosomes facilitate their own invasion. *Nat Struct Mol Biol*. 2004;11(8):763-769. doi:10.1038/nsmb801

173. Anderson JD, Thåström A, Widom J. Spontaneous Access of Proteins to Buried Nucleosomal DNA Target Sites Occurs via a Mechanism That Is Distinct from Nucleosome Translocation. *Mol Cell Biol*. 2002;22(20):7147-7157. doi:10.1128/mcb.22.20.7147-7157.2002

174. McGrath RA, Williams RW. Reconstruction in vivo of irradiated Escherichia coli deoxyribonucleic acid; The rejoining of broken pieces. *Nature*. 1966;212(5061):534-535. doi:10.1038/212534a0

175. Ljungman M, Hanawalt PC. Localized torsional tension in the DNA of human cells. *Proc Nadl Acad Sci USA*. 1992;89:6055-6059.

176. Sinden RR, Carlson JO, Pettijohn DE. Torsional tension in the DNA double helix measured with trimethylpsoralen in living E. coli cells: Analogous measurements in insect and human cells. *Cell*. 1980;21(3):773-783. doi:10.1016/0092-8674(80)90440-7

177. Naughton C, Avlonitis N, Corless S, et al. Transcription forms and remodels supercoiling domains unfolding large-scale chromatin structures. *Nat Struct Mol Biol*. 2013;20(3):387-395. doi:10.1038/nsmb.2509

178. Madabhushi R, Gao F, Pfenning AR, et al. Activity-Induced DNA Breaks Govern the Expression of Neuronal Early-Response Genes. *Cell*. 2015;161(7):1592-1605. doi:10.1016/j.cell.2015.05.032

179. Haffner MC, De Marzo AM, Meeker AK, Nelson WG, Yegnasubramanian S. Transcription-induced DNA double strand breaks: Both oncogenic force and potential therapeutic target? *Clin Cancer Res*. 2011;17(12):3858-3864. doi:10.1158/1078-0432.CCR-10-2044

180. Puc J, Kozbial P, Li W, et al. Ligand-dependent enhancer activation regulated by topoisomerase-I activity. *Cell*. 2015;160(3):367-380. doi:10.1016/j.cell.2014.12.023

181. Pommier Y, Sun Y, Huang SYN, Nitiss JL. Roles of eukaryotic topoisomerases in transcription, replication and genomic stability. *Nat Rev Mol Cell Biol*. 2016;17(11):703-721. doi:10.1038/nrm.2016.111

182. Puc J, Aggarwal AK, Rosenfeld MG. Physiological functions of programmed DNA breaks in signal-induced transcription. *Nat Rev Mol Cell Biol*. 2017;18(8):471-476. doi:10.1038/nrm.2017.43

183. Wang JC. Cellular roles of DNA topoisomerases: A molecular perspective. *Nat Rev Mol Cell Biol*. 2002;3(6):430-440. doi:10.1038/nrm831

184. Pommier Y, Leo E, Zhang H, Marchand C. Chemistry & Biology Review DNA Topoisomerases and Their Poisoning by Anticancer and Antibacterial Drugs. *Chem Biol*. 2010:421-433. doi:10.1016/j.chembiol.2010.04.012

185. Pang B, Qiao X, Janssen L, et al. Drug-induced histone eviction from open chromatin contributes to the chemotherapeutic effects of doxorubicin. *Nat Commun*. 2013;4(May):1908-1913. doi:10.1038/ncomms2921

186. Nánási P, Imre L, Niaki EF, et al. Doxorubicin induces large-scale and differential H2A and H2B redistribution in live cells. *PLoS One*. 2020;15(4). doi:10.1371/journal.pone.0231223

187. Malarkey CS, Churchill MEA. The high mobility group box: The ultimate utility player of a cell. *Trends Biochem Sci*. 2012;37(12):553-562. doi:10.1016/j.tibs.2012.09.003

188. Dahm-Daphi J, Saß C, Alberti W. Comparison of biological effects of DNA damage induced by ionizing radiation and hydrogen peroxide in CHO cells. *Int J Radiat Biol*. 2000;76(1):67-75. doi:10.1080/095530000139023

189. Caldecott KW. Single-strand break repair and genetic disease. *Nat Rev Genet*. 2008;9(8):619-631. doi:10.1038/nrg2380

190. Wang L, He L, Bao G, He X, Fan S, Wang H. Ionizing Radiation Induces HMGB1 Cytoplasmic Translocation and Extracellular Release. *Int J Radiat Med Nucl Med*. 2016;40(2):91-99.

191. Tang D, Shi Y, Kang R, et al. Hydrogen peroxide stimulates macrophages and monocytes to actively release HMGB1. *J Leukoc Biol*. 2007;81(3):741-747. doi:10.1189/jlb.0806540

192. Michael AK, Grand RS, Isbel L, et al. Mechanisms of OCT4-SOX2 motif readout on nucleosomes. *Science (80-).* 2020;368(6498):1460-1465. doi:10.1126/SCIENCE.ABB0074

193. Richter KN, Revelo NH, Seitz KJ, et al. Glyoxal as an alternative fixative to formaldehyde in immunostaining and super-resolution microscopy. *EMBO J*. 2018;37(1):139-159. doi:10.15252/embj.201695709

8. PUBLICATION LIST

UNIVERSITY of DEBRECEN

UNIVERSITY AND NATIONAL LIBRARY
UNIVERSITY OF DEBRECEN
H-4002 Egyetem tér 1, Debrecen
Phone: +3652/410-443, email: publikaciok@lib.unideb.hu

Registry number: DEENK/363/2021.PL
Subject: PhD Publication List

Candidate: Rosevalentine Bosire
Doctoral School: Doctoral School of Molecular Cell and Immune Biology

List of publications related to the dissertation

1. Zarębski, M.*, **Bosire, R.***, Wesołowska, J., Szelest, O., Eatmann, A., Jasińska-Konior, K., Kepp, O., Kroemer, G., Szabó, G., Dobrucki, J. W.: Translocation of chromatin proteins to nucleoli: the influence of protein dynamics on post-fixation localization.
Cytom. Part A. [Epub ahead of print], 2021.
DOI: http://dx.doi.org/10.1002/cyto.a.24464
* These authors contributed equally this work.
IF: 3.124 (2019)

2. **Bosire, R.**, Nánási, P. P. i., Imre, L., Dienes, B., Szöőr, Á., Türk-Mázló, A., Kovács, A., Seidel, R., Vámosi, G., Szabó, G.: Intercalation of small molecules into DNA in chromatin is primarily controlled by superhelical constraint.
PLoS One. 14 (11), 1-18, 2019.
DOI: https://doi.org/10.1371/journal.pone.0224936
IF: 2.74

UNIVERSITY AND NATIONAL LIBRARY
UNIVERSITY OF DEBRECEN
H-4002 Egyetem tér 1, Debrecen
Phone: +3652/410-443, email: publikaciok@lib.unideb.hu

List of other publications

3. Nánási, P. P. i., Imre, L., Firouzi Niaki, E., **Bosire, R.**, Mocsár, G., Türk-Mázló, A., Ausio, J., Szabó, G.: Doxorubicin induces large-scale and differential H2A and H2B redistribution in live cells.
PLoS One. 15 (4), e0231223-, 2020.
DOI: http://dx.doi.org/10.1371/journal.pone.0231223
IF: 2.74 (2019)

Total IF of journals (all publications): 8,604
Total IF of journals (publications related to the dissertation): 5,864

The Candidate's publication data submitted to the iDEa Tudóstér have been validated by DEENK on the basis of the Journal Citation Report (Impact Factor) database.

15 June, 2021

9. KEYWORDS

Accessibility, DNA shape, constrained superhelicity, HMGB1, intercalators

10. ACKNOWLEDGEMENTS

A Ph.D. is the culmination of years of learning. I thank God for the gift of life &well-being, for provision and for His unmerited favour that enabled me to come this far and achieve this much.

Through the journey I have encountered several people who gave me direction, made known opportunities to me and motivated me to stay on course. It is practically impossible to name each one of them here, but to all who have contributed to my success, I say thank you.

I appreciate my supervisor, Prof. Gábor Szabó for opening the doors of his lab for me. Through the five years the door of his office has also remained open for consultation and guidance. Thank you for going far and beyond to ensure my well-being during my stay in Debrecen. A well-deserved appreciation to my co-supervisor Dr. György Vámosi who especially helped understand many of the biophysical techniques. Thank for your availability for numerous consultations.

Much gratitude to my colleagues, Dr. László Imre, Dr. Péter Nánási, Dr. Erfaneh Firouzi Niaki and Dr. Szabolcs Tarapcsák. I learnt many techniques from you and greatly benefited from random discussions with you. Working alongside you in the lab was great moral support. In the same breath, I thank our lab assistant Ms. Adél Nagy Vezendiné for always making sure I had all materials required for the experiments.

I thank my friends who made my stay in Debrecen worthwhile. Dr. Lina Fadel, Dr. Bernard Bogonko, Anthony Mucheru, Timea Hajdu, Kuljeet Singh, Ndidi Omosigho and Michael Suja. You were a family away from home.

I am immensely grateful to our collaborators who either shared their knowledge or materials to make my research complete. They include Prof. Jurek Dobrucki (Jagiellonian University, Kraków), Jennifer Kugel (University of Colorado Boulder), Ralf Seidel (Universität Leipzig), Dr. Guido Kroemer & Dr. Oliver Kepp (Centre de Recherche des Cordeliers, Paris) and Prof. Nick Gilbert (University of Edinburgh).

A big thank you to Prof. Isaac Orina of the Technical University of Kenya, for drawing my attention to the scholarship and for his guidance through the application process. I have also greatly benefited from your motivation and guidance during the course of my research.

I am grateful to the Tempus foundation that offered me the scholarship and the Technical University of Kenya for granting me study leave.

Much gratitude to my family for their prayers and support though out this PhD program. Thank you for your high expectations of me that motivated me to keep going in my academic journey. Special thanks to my mum who sacrificially invested in my education and has been a support to lean on through the years, my grandmother, Aska Nyaboke who from a young age ensured I learnt the alphabet and the numerals well setting the right foundation for my academic journey and my aunt Fridah who has always been looking out for me.

11. APPENDIX